REPORT DOCUMENTATION PAGE			Form Approved OMB No. 0704-0188

Public reporting burden for this collection of information is estimated to average 1 hour per response, including the time for reviewing instructions, searching existing data sources, gathering and maintaining the data needed, and completing and reviewing the collection of information. Send comments regarding this burden estimate or any other aspect of this collection of information, including suggestions for reducing this burden, to Washington Headquarters Services, Directorate for Information Operations and Reports, 1215 Jefferson Davis Highway, Suite 1204, Arlington, VA 22202-4302, and to the Office of Management and Budget, Paperwork Reduction Project (0704-0188), Washington, DC 20503.

1. AGENCY USE ONLY *(Leave blank)*	2. REPORT DATE	3. REPORT TYPE AND DATES COVERED
	8.Feb.99	DISSERTATION

4. TITLE AND SUBTITLE
INVESTIGATION OF EFFECTS OF SURFACE ROUGHNESS ON SYMMETRIC AIRFOIL LIFT AND LIFT-TO-DRAG RATIO

5. FUNDING NUMBERS

6. AUTHOR(S)
MAJ BEIERLE MARK T

7. PERFORMING ORGANIZATION NAME(S) AND ADDRESS(ES)
UNIVERSITY OF MARYLAND COLLEGE PARK

8. PERFORMING ORGANIZATION REPORT NUMBER

9. SPONSORING/MONITORING AGENCY NAME(S) AND ADDRESS(ES)
THE DEPARTMENT OF THE AIR FORCE
AFIT/CIA, BLDG 125
2950 P STREET
WPAFB OH 45433

10. SPONSORING/MONITORING AGENCY REPORT NUMBER
FY99-75

11. SUPPLEMENTARY NOTES

12a. DISTRIBUTION AVAILABILITY STATEMENT
Unlimited distribution
In Accordance With AFI 35-205/AFIT Sup 1

12b. DISTRIBUTION CODE

13. ABSTRACT *(Maximum 200 words)*

19990219129

14. SUBJECT TERMS			15. NUMBER OF PAGES
			16. PRICE CODE
17. SECURITY CLASSIFICATION OF REPORT	18. SECURITY CLASSIFICATION OF THIS PAGE	19. SECURITY CLASSIFICATION OF ABSTRACT	20. LIMITATION OF ABSTRACT

ABSTRACT

Title of Dissertation: INVESTIGATION OF EFFECTS OF SURFACE ROUGHNESS ON SYMMETRIC AIRFOIL LIFT AND LIFT-TO-DRAG RATIO

Mark Thomas Beierle, Doctor of Philosophy, 1998

Dissertation Directed By: Professor John D. Anderson, Jr.
Department of Aerospace Engineering

This research investigated the effects of surface roughness in the form of protuberances on the lift and lift-to-drag ratio of an airfoil with a NACA 0015 profile. Russian researchers first recorded the positive effect on lift from naturally formed surface protuberances in 1984 and reported on their research in 1991. Based on experimental studies, the Russian researchers identified a protuberance geometry on a low aspect ratio wing which created both additional lift and an improved lift-to-drag ratio for a given angle-of-attack over the low to moderate angle-of-attack region.

The primary objective of this research was to develop a phenomenological understanding of the flow physics related to the effects of surface roughness on the lift and lift-to-drag ratio of a symmetric airfoil. Two wind tunnel experiments were conducted at the University of Maryland's Glenn L. Martin Wind Tunnel to investigate the effect of protuberance coverage, size, and density. A two-dimensional

computational experiment studied the effect of protuberance location, geometry, and spacing using the OVERFLOW Navier-Stokes flow solver.

Results indicated that the variation of the aerodynamic lift and the lift-to-drag ratio for symmetric airfoils and wings populated with protuberances is due to the increased pressure induced by a recirculation region downstream of the protuberance. An alternative understanding based on changes in the effective camber and thickness of the airfoil was developed. Wind tunnel and computational results qualitatively validated the lift enhancement on symmetric airfoils due to surface roughness. Results indicated that the magnitude of the lift increment was strongly dependent on airfoil angle-of-attack and protuberance height and had a weak dependence on protuberance width and spacing. Just one configuration, based on a wind tunnel test of a wing with protuberances, generated a larger lift-to-drag ratio compared to a smooth wing. This research concluded that surface protuberances located on the lower surface of a symmetric airfoil are a lift generating mechanism at low to moderate angles-of-attack.

INVESTIGATION OF EFFECTS OF SURFACE ROUGHNESS ON SYMMETRIC AIRFOIL LIFT AND LIFT-TO-DRAG RATIO

by

Mark Thomas Beierle

Dissertation submitted to the Faculty of the Graduate School of the
University of Maryland at College Park in partial fulfillment
of the requirements for the degree of
Doctor of Philosophy
1998

Advisory Committee:
Professor John D. Anderson, Jr., Chair
Professor James D. Baeder
Professor Jewel B. Barlow
Dr. Anthanassios A. Dimas
Professor James H. Duncan
Dr. Robert C. Ranzenbach

© Copyright by

Mark Thomas Beierle

1998

DEDICATION

To The Beierle Boys

Jacob Aaron
Thomas James
Peter Joseph

ACKNOWLEDGEMENTS

I would like to thank the Department of Aeronautics of the United States Air Force Academy and Colonel Michael L. Smith for the opportunity to pursue this degree and for their continued support.

I am indebted to Dr. Pieter Buning and Dr. Ahmed Hassan for their technical assistance. I would like to thank these gentlemen for being so generous with their time and their experience.

I would like to thank Dr. Jewel Barlow and the Staff of the Glenn L. Martin Wind Tunnel for their support in conducting the two wind tunnel experiments and for giving me a campus home.

I would like to thank my Dissertation Examining Committee for their guidance during my tenure at the University of Maryland. In particular, I very much appreciated the daily interactions with Dr. Robert Ranzenbach and the insight shared. I have a special thank you for Dr. John D. Anderson, Jr., my Advisor -- he taught me much more than just engineering. I shall miss our frequent and far-ranging conversations.

I would like to recognize and thank my family and friends. To the Wind Tunnel Posse of Chris Mairs, Rick Harris, and Rui Guterres, thanks for your spirit and humor. Thanks to Colonel Dale O. Condit for his constant encouragement and steadfast friendship. Most importantly, I would like to thank my parents, my father-in-law, my sons, and my wife -- they are my greatest source of strength and energy.

TABLE OF CONTENTS

LIST OF TABLES

LIST OF FIGURES

NOMENCLATURE

c	Chord Length
C_y	Wing Lift Coefficient (Vorobiev)
C_x	Wing Drag Coefficient (Vorobiev)
K	Lift-to-Drag Ratio (Vorobiev)
h	Protuberance Height (c)
λ	Protuberance Width (c)
C_l	Airfoil Lift Coefficient
C_d	Airfoil Drag Coefficient
L/D	Lift-to-Drag Ratio
C_L	Wing Lift Coefficient
C_D	Wing Drag Coefficient
C_P	Pressure Coefficient
α	Angle-of-Attack (Degrees)
t	Maximum Airfoil Thickness (c)
x	Chord Position (c)
y_t	Airfoil Thickness (c)
y	Protuberance Height at Chord Position x (c)
Re_∞	Freestream Reynolds Number

y^+	Sub-Layer Scaled Distance (Non-Dimensional)
L	Reference Length (Chord Length)
U_∞	Freestream Velocity
(x,y)	Cartesian Coordinate System (Coordinates Non-Dimensionalized by L)
(u,v)	Velocity Components (Non-Dimensionalized by U_∞)
t	Time (Non-Dimensionalized by U_∞/L)
$\vec{V}$	Total Velocity Vector, Components (u.v)
ρ	Density (Non-Dimensionalized by Freestream Density)
P	Pressure (Non-Dimensionalized by Freestream Pressure)
M_∞	Freestream Mach Number
γ	Ratio of Specific Heats
τ_{ij}	Shear Stresses
$\overline{\rho u''^2}$	Reynolds Stresses
$\overline{\rho v''^2}$	
$\overline{\rho uv}$	
Q_i	Flux Variables
$C_{d,o}$	Minimum Airfoil Drag Coefficient
δ_1	Displacement Thickness (c)

CHAPTER 1 INTRODUCTION

This research continues the long history of investigations studying the effects of small surface perturbations on the well-defined National Advisory Committee for Aeronautics (NACA) 4-digit airfoils. The present work expands the existing base through an investigation of a relatively unstudied family of surface roughness for which claims of enhanced aerodynamic lift and improved lift-to-drag ratio have been made. This chapter details the background which motivated this effort, outlines the research objectives and the plan designed to achieve them, discusses the unique challenges of this problem, and lists the potential contributions of this investigation to the field of aerodynamics.

1.1 MOTIVATION

In 1984, the commanding officer of a Soviet VICTOR III class attack nuclear submarine reported that the vessel was unable to maintain level motion with aft control surfaces within allowable trim angles.[1,2] The submarine moved to surface from a horizontal attitude with the large horizontal stern planes at zero degrees setting. To avoid surfacing, the large horizontal stern planes had to be set at 8 to 9 degrees of dive. Because of the excessive angle required on the large horizontal stern planes, the usual method of controlling the ship at high speeds using the ship's small horizontal stern planes could not be used because these small surfaces could not generate enough

control authority. The large horizontal stern planes had a 20% thick, symmetric NACA profile.

Because a similar, and yet unexplained, incident occurred on a submarine of the same class three years earlier, a special investigative team, including the hydrodynamicist Nikolai Vorobiev, formed to identify and understand the problem. The group conducted extensive sea trials to analyze the ship's maneuverability and balancing parameters in conditions ranging from 2 to 27 knots. The trials identified an inherent trim moment that required 8 to 11 degrees of deflection by the large horizontal stern planes. While this further defined the problem, it did not establish a cause. A parallel underwater survey of the ship showed no damage nor any deviations in the hull and appendage shapes.

During an inspection of the upper surfaces of the large horizontal stern planes in dry dock, researchers found "acorn-like, horny-like (with sharp edges) foulage, with heights of 8-10 millimeters in amounts of 10-15 per square decimeter, and above them covered by green, soft slime-like seaweeds."[2] This was a relative height of approximately 0.002c. The lower surface, which had been properly protected against natural elements with anti-fouling paint, had no such foulage. When the top of the control surface was cleaned and treated with anti-fouling paint, the submarine maneuvered normally and returned to active service.

The researchers concluded that the difference in surface roughness between the upper and lower surfaces of the large horizontal stern planes caused the force imbalance. They reasoned that the natural protuberances affect the nature of the flow past the roughened surface by slowing down the flow and thus increasing the pressure

and producing a force directed toward the surface. Detailed discussion of subsequent testing by Vorobiev [1] is presented in Chapter 2.

1.2 CHALLENGE OF PROBLEM

Research on protuberance and surface roughness to date can be separated into four concentrations. The NACA expanded the study of distributed surface roughness as related to the surface condition through its investigations of what is now identified as standard leading edge roughness. This work focused on the aerodynamic drag resulting from perturbations of a smooth surface as determined by grit and small grains of carborundum. The second area of concentration continues to study the influence of ice accretion on the performance of aerodynamic bodies. This type of protuberance is inherently a leading edge modification. The third area of concentration is the use of protuberances as transition devices, tripping laminar flow into turbulent flow for a desired aerodynamic outcome. The emphasis of this work is to influence the quality and character of the flow to achieve a desired effect.The final concentration area relates to the original protuberance studies. This work studied the aerodynamic effect of surface variations introduced mainly by manufacturing processes. The earliest examples were the surface waves in cloth wings and the required stitching. This area later expanded to include irregularities such as sheet metal joints and more classic protuberances such as rivet heads and screw sets. The clear aerodynamic focus of these studies was the impact on total drag.

The present work most nearly matches the concentration of the last area, with a more expansive focus. The protuberances studied are not a leading edge phenomena

like ice, their height exceeds the local boundary layer thickness unlike the NACA standard leading edge roughness, and the use of these protuberances as a potential means to enhance aerodynamic performance through increased lift and lift-to-drag ratio is unique compared to transition devices and previous drag-centered studies. The challenge of the present research was to study surface roughness with the potential to enhance aerodynamic performance given that the earlier reported results appeared to contradict traditional aerodynamic predictions for surface roughness.

1.3 RESEARCH OBJECTIVE

To address the challenges of this problem, an investigation of the fundamental aerodynamics of this surface roughness was planned and executed. The primary objective of this dissertation research was to study and identify the phenomenological basis of the flow physics related to the effects of surface roughness on symmetric airfoil lift and lift-to-drag ratio. The secondary objectives were to potentially validate the results of the Russian research and to develop either a quantitative or qualitative predictive capability based on the understanding of the factors which dominate the changes in lift and lift-to-drag ratio.

The established procedure to achieve the stated objectives used the two phase approach of a wind tunnel experiment followed by a computational study. The wind tunnel test was designed to first replicate the Russian results and then to study the dominant factors in changing the lift and lift-to-drag ratio of an airfoil. Based on the results of the first wind tunnel experiment, a second wind tunnel experiment was added with the identical focus using a wing baseline. The purpose of the

computational experiments was to obtain detailed insight into the flow field from which to develop a phenomenological understanding of the changes in the lift and lift-to-drag ratio.

The next chapter describes the work of Vorobiev and other related, previous research efforts. The two experimental investigations of this phenomena that were conducted in the Glenn L. Martin Wind Tunnel (GLMWT) at the University of Maryland are detailed in Chapter 3. Chapter 4 outlines the computational method and the theoretical basis for the computational experiments. Chapter 5 presents the results of computational experiments performed using a NACA 0015 airfoil for the baseline configuration. Included are sections outlining the results of investigations into the effects of changing airfoil angle-of-attack, protuberance size, protuberance shape, protuberance location, and protuberance spacing. In Chapter 6, the results of the experimental and the numerical investigations are integrated, and additional analysis is reported. Chapter 7 presents the conclusions of this research effort and lists recommendations for further study.

1.4 CONTRIBUTIONS TO AERODYNAMICS

Achieving the stated objectives would contribute to the field of aerodynamics in the following key ways:

1. Replicate and potentially validate the positive lift increment and enhanced lift-to-drag ratio reported by Russian researchers for symmetric airfoils with protuberances on the lower surface;

2. Develop a phenomenological understanding of the flow physics related to the lift and lift-to-drag ratio changes;
3. Develop an understanding capable of predicting the change in aerodynamic performance based on the flow physics.

The true benefit of this research might be in beginning a new understanding of a practical application using protuberances as a means to create control surface-like inputs in aerodynamic designs, an example being the use of protuberances on an unmanned air vehicle to replace or augment control surface inputs.

CHAPTER 2 PREVIOUS WORK

Researchers have conducted extensive experiments on the aerodynamic effects of surface roughness and surface irregularities on airfoil and wing performance over the past 60 years. There have been three general types of surface roughness studied: distributed roughness such as grit, two-dimensional isolated elements such as a two-dimensional trip wire, and three-dimensional isolated elements such as a circular cylinder. The common goal of these studies was either the influence of the modified surface on drag or the influence of the surface roughness on transition. Few investigators reported data or commented on the influence of the modified airfoil or wing surface on the lift or lift-to-drag ratio. Another common feature of the research conducted to date, with the exception of Vorobiev's work and the study of ice accretion on airfoils, was that the work focused on roughness whose height was less than the local boundary layer thickness. This chapter highlights the work conducted by the Russian researcher Vorobiev, whose reports inspired the present effort, and then reviews related research associated with distributed surface roughness, two- and three-dimensional surface protuberances, surface shape changes, and zero-mass 'synthetic' jets.

2.1 RUSSIAN RESEARCH

Subsequent to the investigation of the surface roughness related lift enhancement on the Soviet submarine, Vorobiev [1] conducted wind tunnel testing of

this effect at the Central Shipbuilding Krylov's Institute. The test used a three-dimensional wing with an aspect ratio of 0.9 and a 16.6% thick, symmetric profile. Cusp-edged protuberances extended above the lower surface of the wing. Figure 2-1 shows a representative sample of the protuberances used by Vorobiev and Figure 2-2 shows a representative configuration used by Vorobiev.[3] Note that there is no scientific shape nor regularity to the protuberances and their distribution. The protuberances in the Russian experiment varied according to the following properties:

- Density: 1,694 or 4,840 protuberances/c^2;
- Height: 0.0027c or 0.0036c;
- Width: 0.0055c or 0.0073c;
- Coverage: Leading edge aft to a maximum station at 0.9091c.

Figure 2-3 and Figure 2-4 detail the results reported by Vorobiev.[1] Figure 2-3 shows the wing lift coefficient (C_y) and wing drag coefficient (C_x) as a function of angle-of-attack and Figure 2-4 shows the lift-to-drag ratio (K) as a function of angle-of-attack. For both plots, Configuration #1 was the smooth wing and Configurations #2 through #4 included surface protuberances. Based on these results, the following observations were made:

1. Increased lift due to the presence of protuberances extending from zero through 10 degrees angle-of-attack;
2. Positive lift force at zero degrees angle-of-attack;
3. Maximum lift coefficient increase of 0.084;

4. Lift-to-Drag ratio equal to, or exceeding that of, the clean configuration from zero through 10 degrees angle-of-attack;
5. Strong effect of protuberance size, density, and surface coverage in increasing the lift.

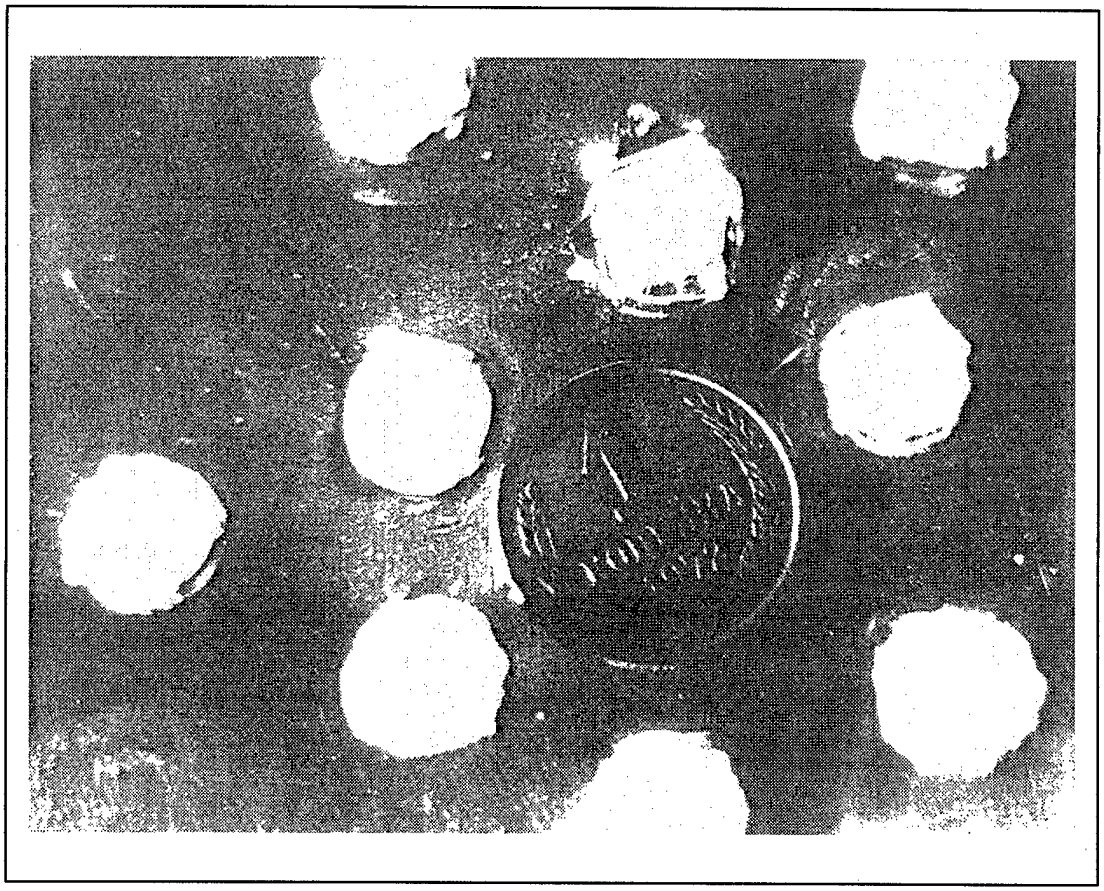

Figure 2-1. Cusp-Edged Protuberances (Vorobiev)

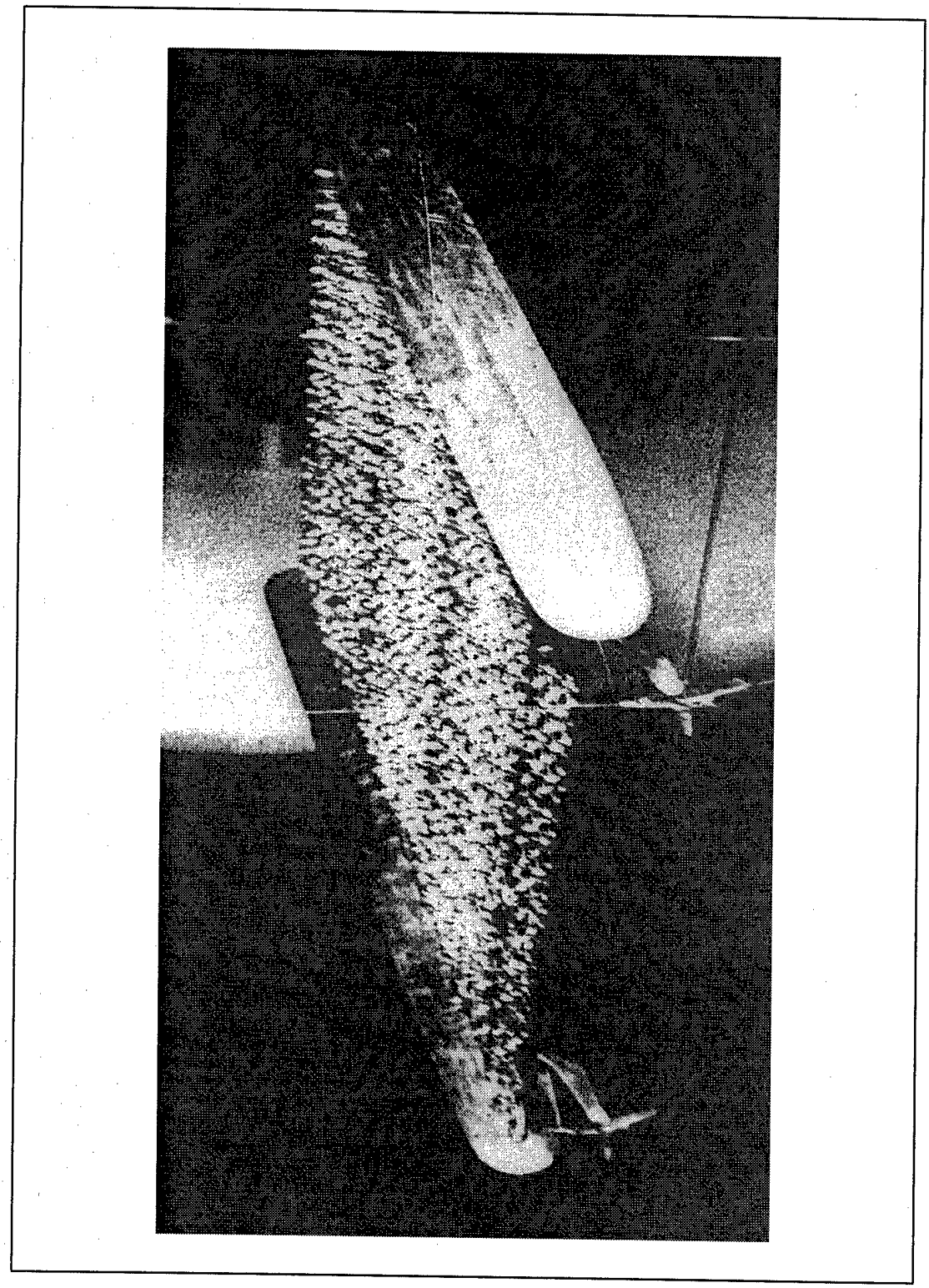

Figure 2-2. Representative Configuration with Protuberances (Vorobiev)

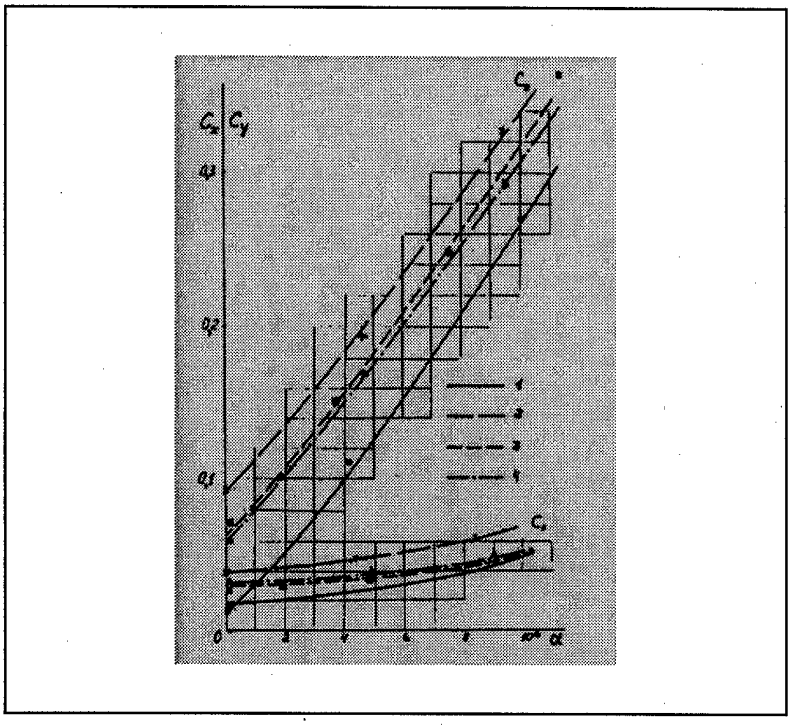

Figure 2-3. Lift and Drag Coefficient Versus Angle-of-Attack (Vorobiev)

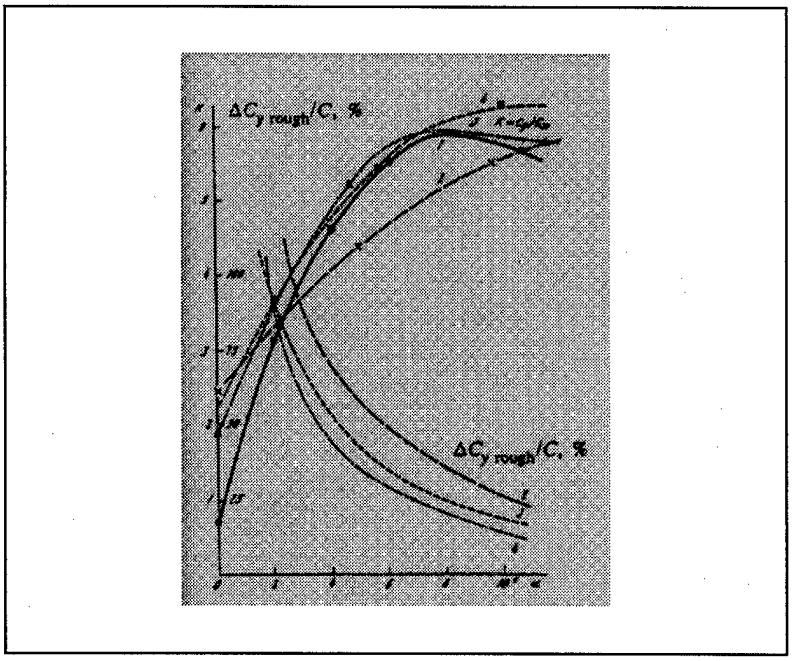

Figure 2-4. Lift-to-Drag Ratio Versus Angle-of-Attack (Vorobiev)

2.2 DISTRIBUTED SURFACE ROUGHNESS

As early as 1927, Warner [4] considered the potential of increased lift due to distributed surface roughness: "frictional retardation of that flow on the lower surface would appear likely to strengthen the circulation around the wing and so increase the lift."[4] Based on experiments using sand to create the roughness on the lower surface, Warner reported that the maximum lift coefficient remained unchanged or decreased, the lift-to-drag ratio decreased up to 20%, and the minimum drag increased by up to 50%. He concluded the "results on the whole unfavorable."[4] Warner also reported on an experiment using sand to create equivalent roughness over 60% of the upper surface starting at 0.1c aft of the leading edge. For this test, there was an approximate 5% increase in the maximum lift-to-drag ratio and a 3% increase in maximum lift. Warner concluded that this limited data set suggested a potential benefit could be gained by varying surface texture.

Wood [5] focused on the drag rise associated with the construction and fielding of airfoils and other aerodynamic bodies with surface imperfections. He experimentally investigated the aerodynamic effects of surface roughness by testing airfoils with surfaces of plywood, unpainted metal, painted metal, and two different configurations of corrugated metal, with corrugation peaks running chordwise. Wood concluded that small surface variations produced negligible aerodynamic effects. The corrugated surfaces produced the same or less lift as compared with the smooth airfoil except for a small, positive increment near stall. The lift-to-drag ratio for the corrugated airfoils was smaller than that of the smooth airfoil throughout the angle-of-attack range.

In order to systematically study roughness near the leading edge, the NACA conducted a series of experiments with a defined standard roughness. The NACA standard leading edge roughness consisted of 0.011 inch carborundum grains thinly spread to cover 5 to 10 per cent of the area from the leading edge aft to 0.08c along both surfaces of the 24 inch chord models.[6] For comparison with other work, this equates to a protuberance height of 0.00046c. In summarizing the NACA results, Abbott and von Doenhoff [6] reported that the standard leading edge roughness had no effect on the lift curve slope for airfoils with less than 18% thickness, did not effect the angle-of-attack for zero lift, and decreased maximum airfoil lift with increased roughness. Standard leading edge roughness significantly increased airfoil drag. For a NACA 0015 airfoil with standard leading edge roughness, the minimum drag coefficient increased 63% compared to a smooth airfoil; the drag coefficient changed from 0.0063 to 0.0103.

2.3 SURFACE PROTUBERANCES

Jacobs [7] conducted an extensive study in the NACA Variable-Density Tunnel of the drag and interference caused by a protuberance on the surface of an airfoil. Single protuberances extending across the entire span (two-dimensional protuberance) of an airfoil with a NACA 0012 section at a freestream Reynolds number of 3.1 million were tested for varying protuberance position, size, and shape. The protuberances tested ranged in height from 0.0004c to 0.0125c and were placed on either the upper or lower surfaces at stations ranging from the leading edge to 0.65c aft of the leading edge. For the largest protuberance at all lower surface positions, the lift

increased slightly at low angles-of-attack (<6 degrees). At higher angles-of-attack, the protuberance had no apparent effect on the lift, including the maximum lift. Smaller protuberances produced similar results, but had less of an effect, in general. Jacobs found that protuberances drastically increased drag compared to a smooth airfoil for all protuberance positions and airfoil attitudes. Drag increased 100% to over 200% for the largest protuberance positioned along the lower surface. The smallest drag increases occurred for protuberances at the leading edge at low angles-of-attack and at the lower surface positions aft of the leading edge at higher angles-of-attack. The report concluded that the drag increase could be estimated for unfaired protuberances as the product of the freestream dynamic pressure and the frontal area of the protuberance. In this test, Jacobs also studied the effect of fairing the protuberances and found that fairings limited the drag increase, but caused the lift to match or fall below the baseline airfoil performance. There is no indication that the investigator pursued the positive lift increment findings of this report.

It is known that surface roughness can cause premature transition. Schlichting [8] describes three goals in understanding the influence of roughness on transition:

1. Determining the critical height of roughness elements required to influence transition;
2. Determining the limiting height of roughness elements which cause transition to occur at the element;
3. Describing the transition point in the range between these limits.

The experiments conducted to address these goals have investigated the effect of roughness size and location on the transition location for an airfoil or have studied

the instability mechanisms generated by roughness which contribute to transition. According to Kerho and Bragg,[9] most of these studies reported on experiments applied to surface roughness with a height less than the local boundary layer thickness and on a flat plate with zero pressure gradient. The work of Klebanoff, Schubauer and Tidstrom [10] and that of Smith and Clutter [11] are examples of this research. With regards to the present research, the studies focusing on transition provide little insight; in the present study the flow is primarily turbulent and the protuberance height exceeds the local boundary layer thickness.

2.4 SURFACE SHAPE CHANGES

Hood [12] studied the effects of rib stitching and surface waviness on wing drag at Reynolds numbers from 4 to 17 million in the NACA 8-foot high-speed wind tunnel. Drag increased for all surface irregularities tested. However, in his study of surface waviness, Hood noted that specific wave geometries and wave locations produced significantly smaller drag increases. First, Hood showed that the magnitude of the drag increment was proportional to the increase in the ratio of wave height, h, to wave width, λ. Based on skin friction calculations, Hood concluded that the increased drag with increasing h/λ was due to increasing pressure drag. Second, Hood's results showed that surface waviness of $h/\lambda = 0.016$ with $h = 0.002c$ or $0.0008c$ over the rear 67% of both surfaces of the wing produced a 1% drag increase compared to a 10% drag rise when covering the rear 92% of the wing surfaces. Hood concluded that waviness should not be present forward of the smooth wing transition point to avoid drag due to premature transition. Finally, Hood showed that a single wave of $h/\lambda =$

0.04 with h = 0.002c centered at 0.105c from the leading edge of the upper surface produced more than twice the drag increase than an identically placed wave on the lower surface for small angles-of attack.

Roughness due to ice accretion is characterized by its location very close to the leading edge and by its height which is equal to or greater than the local boundary layer thickness. The study of the aerodynamic effect of ice formation dates to the experiment of Gulick [13] and remains an active field through the work of Bragg and his collaborators.[14] The presence of ice on an airfoil or wing leads to decreased lift, including maximum lift, and increased drag. Beyond the degraded lift-to-drag ratio performance, the drop in maximum lift raises stall speed, hence creating significant safety issues. The primary difference between ice accretion and the present research is the leading edge location of the ice and its negative impact on lift.

2.5 ZERO-MASS 'SYNTHETIC' JETS

Hassan and JanakiRam [15] conducted the first known computational study of the beneficial aerodynamic effects of an array of zero-mass "synthetic" jets on a NACA 0012 airfoil. Originally conceptualized to alter effective leading edge geometry and camber of a helicopter blade to alleviate blade-vortex interactions, these investigators noted that the combined use of blowing and suction with an array of these jets created effective changes in blade camber which resulted in an increase in the lift capability of the symmetric airfoil section. Based on computational experiments using the ARC2D Navier-Stokes flow solver at a freestream Reynolds number of 3 million and a freestream Mach number of 0.6, the researchers reported

that a jet array located on the lower surface of the airfoil between 0.13c to 0.23c created a positive increment in the airfoil lift at both zero and 5 degrees angle-of-attack. Airfoil lift decreased proportionately with the jet array located on the upper surface between the same chord stations. The researchers also studied the effect of peak jet velocity and oscillation frequency and found positive correlations between increased peak jet velocity and increased lift, and increased oscillation frequency and increased lift. Accompanying the increased lift was an increase in the airfoil's mean drag, where mean drag is the time-averaged total drag for this unsteady flow. One example configuration resulted in a 175% increase in the mean airfoil drag, with drag decreasing with lower peak jet velocity and higher jet oscillation frequency. Subsequently, Hassan [16] investigated the effects of freestream Mach number. Over the freestream Mach number range of 0.15 to 0.65, Hassan reported that increased Mach number resulted in increased lift for a set configuration. The reported lift enhancement for an array of zero mass "synthetic" jets on the lower surface of a symmetric airfoil is strikingly similar to that obtained for an airfoil populated with protuberances.

2.6 SYNOPSIS

With the exception of Vorobiev, previous research of surface roughness has focused on the drag penalty of using such a surface modification or the relationship of surface roughness and transition. The current work benefited from the previous work and, in conjunction with the work of Vorobiev, expanded beyond this base by investigating the following unique combination of surface roughness characteristics:

- Protuberance height exceeded that of local boundary layer thickness.
- Protuberance location started at least 0.05c aft of the leading edge.
- Roughness configurations described as distributed surface roughness and isolated two- and three-dimensional protuberances were studied.
- Potential aerodynamic performance improvement through increased lift and lift-to-drag ratio was predicted and investigated.

The remainder of this report details the process and results of wind tunnel and computational experiments centered on this form of surface roughness and its effect on the aerodynamics of a symmetric airfoil.

CHAPTER 3 WIND TUNNEL EXPERIMENTS

The first step was to replicate the results of Vorobiev and then to vary the configuration parameters to study their effect on the expected aerodynamic performance improvement. Wind tunnel experiments were selected because of the ease of quickly changing protuberance configurations and the speed at which force coefficient results could be generated and interpreted. This chapter reports on the separate wind tunnel tests conducted using surface protuberances on the lower surface of an airfoil and a wing.

3.1 GLMWT TEST #1583

This experiment was conducted in June 1996 at the University of Maryland's Glenn L. Martin Wind Tunnel. This was an experiment using a two-dimensional airfoil model with two- and three-dimensional protuberances.

3.1.1 OBJECTIVE

The primary objective of this investigation was to verify the lift and lift-to-drag ratio improvement reported by the Russian researchers using an airfoil baseline. If observed, the secondary objective was to investigate the factors required to achieve the noted increases and identify those which positively influence the magnitude of this effect.

3.1.2 EXPERIMENT DESIGN

3.1.2.1 Experimental Method

The GLMWT is a closed, single return, atmospheric type facility. The test section measures 7.88 m^2 and the maximum speed is 107.3 m/s. The turbulence factor is 1.05 as measured by the sphere test and the turbulence intensity is 0.21% as measured by hot wire.

This experiment used the two-dimensional insert, a rig composed of two parallel wall plates which span the entire height of the test section. At midsection, there are circular mounting plates on the interior walls which can rotate to pitch a model 360 degrees. The model was mounted with the quarter-chord aligned with the center of the mounting disk, the rotation center.

The uncertainty of the balance measurements is evaluated by computing the precision of the mean of the force and moment components through statistical analysis and comparing these values against user specified levels of acceptable error. This process works by sampling each of the six balance components at a typical rate of 8 Hz during every internal loop of the balance data acquisition process. After eight data points have been sampled, the mean balance component and the precision of each mean is computed and compared to preset target levels. If the computed precision of the mean is below the target levels on all six components, the mean value of each component, the precision of the mean, and the number of data points required is recorded. If the precision of the mean has not reached its target value, then more

sampled data is acquired, and the process continues until the target precision levels are met or the operator overrides the system.

For this experiment, the target precisions of the mean lift and drag were set to 0.001 and 0.0006, respectively, in coefficient form.

3.1.2.2 Airfoil Model

The rectangular airfoil, mounted in the two-dimensional insert, had a chord of 457.2 mm and a span of 609.6 mm. The airfoil had a constant NACA 0015 section across its span. The leading edge, the trailing edge, and the upper surface of the airfoil were constructed of wood and attached to a 25.4 mm thick aluminum core. The original wood section for the lower surface was removed and the surface was shaped with clay to approximate the airfoil section. Cylindrical protuberances and rectangular spanwise strips were made of clay and were attached to the lower surface of the airfoil using spray adhesive.

3.1.2.3 Test Matrix

Based on a review of the Russian results, it was decided to hold tunnel conditions fixed for this test at a freestream Reynolds number equal to 1.5 million and a freestream velocity of 44.7 m/s. The angle-of-attack was varied through sweeps extending from -4 to +20 degrees at 2 degree increments.

The cylindrical protuberances with a diameter of 0.0088c and a height of 0.0044c were used based on the recommendations of the Russian report. Protuberance density was held constant at $835/c^2$. Protuberance coverage, as measured from the leading edge, varied as:

- 0.056c to 0.28c;
- 0.056c to 0.56c;
- 0.056c to 0.82c.

The raised strips stretched across the entire airfoil span and were sized to be consistent with the protuberances. The strips were 0.0088c wide and had a height of 0.0044c. This modification was pursued as a means to isolate and study the effect of purely two-dimensional flow in producing the performance changes and as a way to investigate the potential of achieving the effect with a more reproducible geometry. Two different strip spacings were tested, the baseline spacing of 0.05c and the wide spacing of 0.10c. Strip coverage varied as follows, as measured from the leading edge:

- 0.10c to 0.35c (equates to 4 strips at baseline spacing);
- 0.10c to 0.50c (equates to 8 strips at baseline spacing);
- 0.10c to 0.78c (equates to 15 strips at baseline spacing).

It is important to note that the present investigation focused on the effect of protuberances using mathematically well-defined, reproducible shapes in contrast to the irregular, cusp-edged protuberances of Vorobiev. Figure 3-1 depicts a representative cylindrical protuberance configuration where the coverage extended from 0.056c to 0.82c at a density of $835/c^2$. Figure 3-2 shows a representative strip protuberance configuration in the two-dimensional test insert rig where the strip coverage extended from 0.10c to 0.78c at the baseline spacing of 0.05c.

The performance baseline for all cases presented was the experimentally measured results from the smooth airfoil.

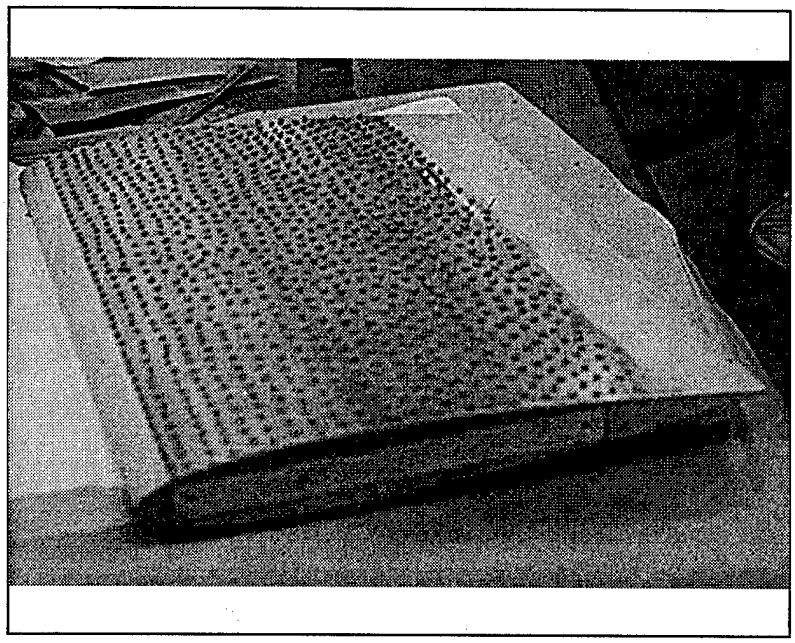

Figure 3-1. Representative Cylindrical Protuberance Configuration

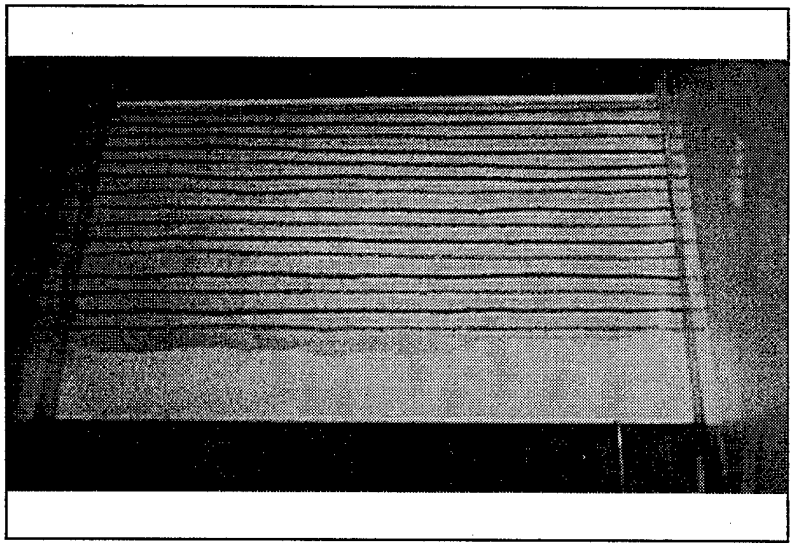

Figure 3-2. Representative Strip Protuberance Configuration

3.1.3 RESULTS

3.1.3.1 Protuberance Modification

The first experiments were conducted to replicate the results reported by the Russian researchers and to investigate the influence of cylindrical protuberance coverage on the lift and lift-to-drag ratio of a NACA 0015 airfoil. The configuration varied protuberance coverage using the clay cylindrical shapes in a random pattern at a density of $835/c^2$.

As evident in Figure 3-3, additional lift was generated at low to moderate angles-of-attack for all protuberance coverage configurations. The general shape of the enhanced lift coefficient curve matched that of the expected baseline case. Note, the generation of positive lift at zero degrees angle-of-attack suggests the baseline airfoil was not symmetric as intended or that the model angle-of-attack was not correctly zeroed. Given the reasonable testing precautions to ensure the correct attitude, the baseline airfoil was assumed asymmetric due to the clay shaped to replicate the lower surface. No correction was made to the data as the quality of the asymmetry was not characterized.

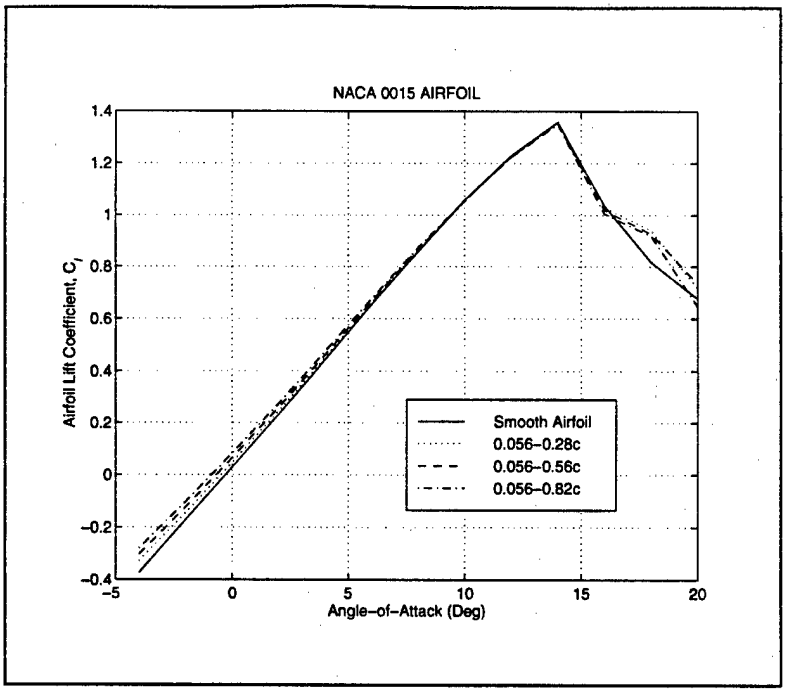

Figure 3-3. Lift as a Function of Protuberance Coverage

Figure 3-4 more clearly shows the positive lift increment, including positive lift at zero degrees angle-of-attack for the configurations populated with protuberances. The positive lift increment washed out with angle-of-attack and approached zero near 10 degrees angle-of-attack, just prior to stall. From Figure 3-4, there was a positive correlation between increased protuberance coverage and increased lift through moderate angles-of-attack. There was an interesting post-stall event at 18 degrees angle-of-attack which was not further investigated as either a unique feature to that angle-of-attack or a trend over a broader angle-of-attack range.

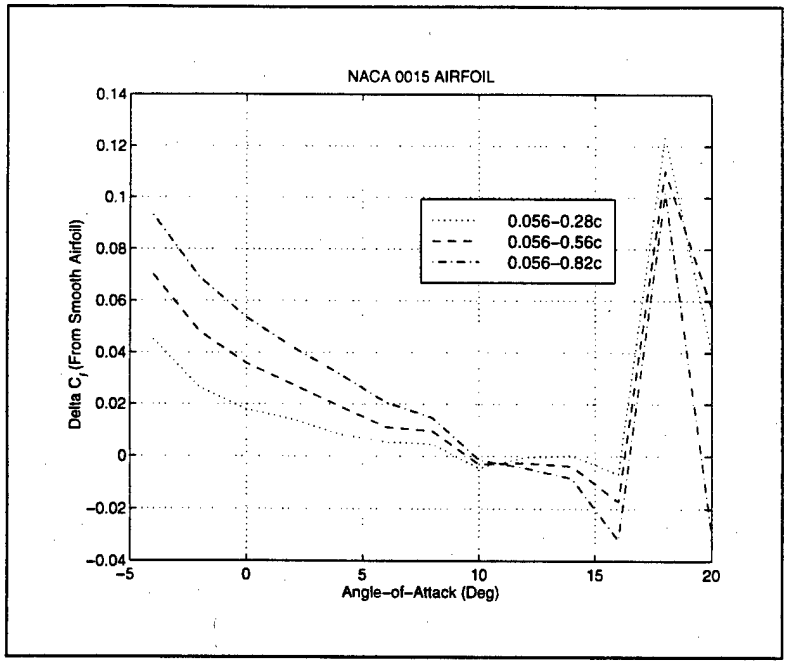

Figure 3-4. Lift Increment as a Function of Protuberance Coverage

Figure 3-5 shows that increasing the region of protuberance coverage reduced the lift-to-drag ratio. In addition to this negative correlation between protuberance coverage and the lift-to-drag ratio, the protuberance modified configurations never exceeded nor equaled the lift-to-drag ratio performance of the baseline airfoil. Finally, note that in the post-stall region, the lift-to-drag ratios for all configurations collapsed to a common performance.

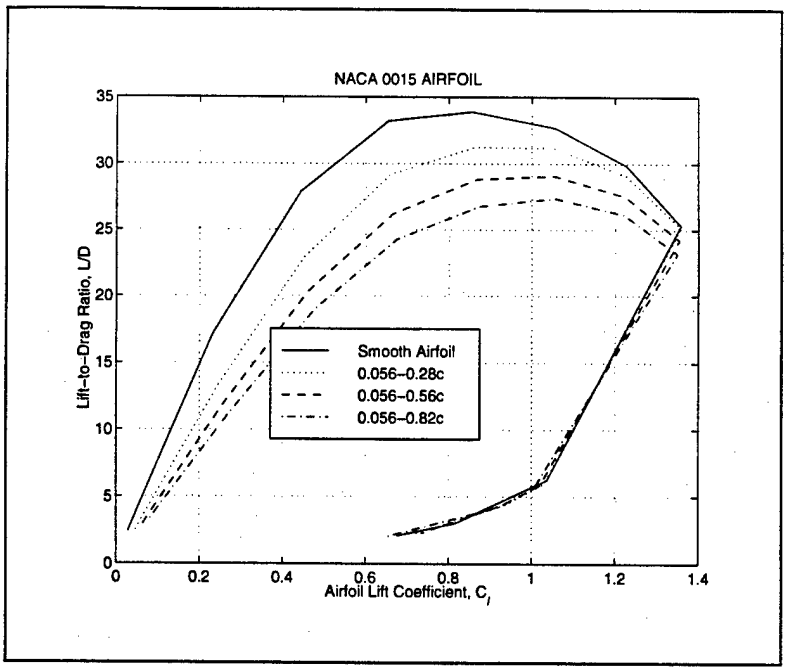

Figure 3-5. Lift-to-Drag Ratio as a Function of Protuberance Coverage

3.1.3.2 Raised Strip Modification

The second series of testing in this experiment replaced the cylindrical protuberances with span-wise strips and investigated the effect of coverage and strip spacing on lift and lift-to-drag ratio performance.

Strip Coverage. For these tests, the NACA 0015 airfoil was populated with the clay strips over varying surface coverages at the baseline spacing of 0.05c. Figure 3-6 indicates a positive correlation between increased strip coverage and increased lift. There was a positive lift increment at zero degrees angle-of-attack which continued to near 10 degrees angle-of-attack where it washed out. The post-stall feature noted in the protuberance testing reoccurred at the same angle-of-attack with the strips. Note,

Figure 3-4 and Figure 3-6 show that the magnitude of the lift increment is comparable between the protuberance and the strip configurations for the same surface area coverage.

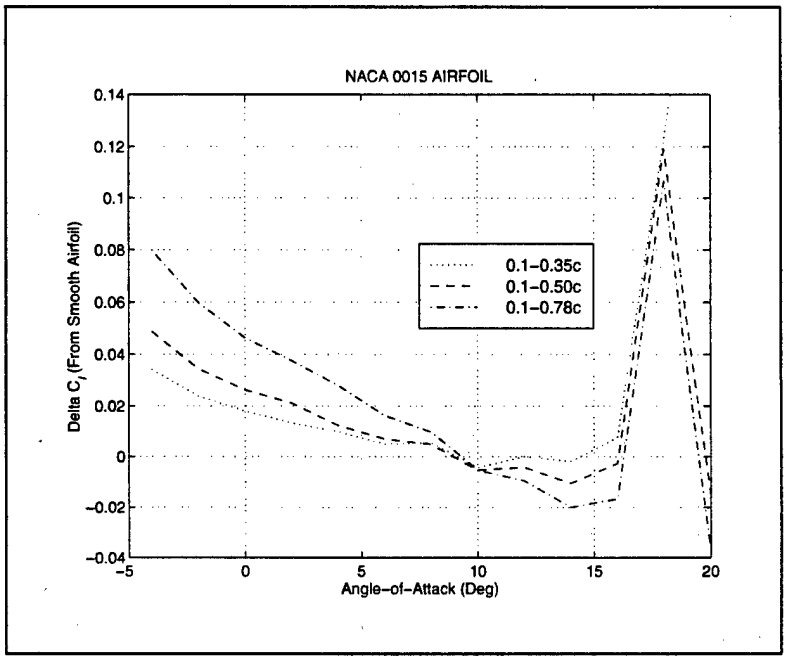

Figure 3-6. Lift Increment as a Function of Strip Coverage

In Figure 3-7, the performance trend identified for protuberance coverage persisted, an increase in strip coverage resulted in a lower lift-to-drag ratio for all configurations tested at all angles-of-attack. The magnitude of the lift-to-drag ratio for the protuberance coverage in Figure 3-5 appear comparable to similar strip coverage regions as shown in Figure 3-7. Again, the lift-to-drag ratios for all configurations collapsed to one performance curve in the post-stall region.

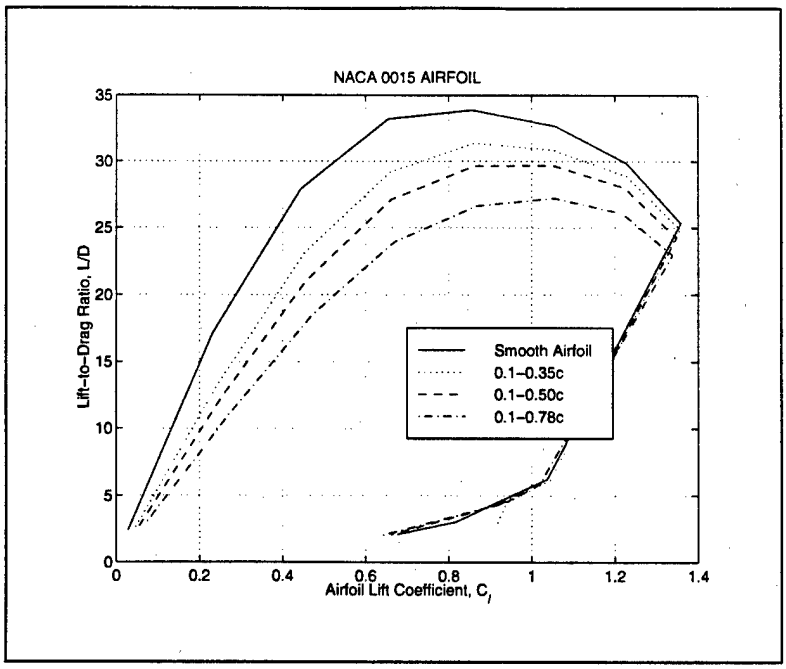

Figure 3-7. Lift-to-Drag Ratio as a Function of Strip Coverage

Strip Spacing. The effect of strip spacing on lift and lift-to-drag ratio was studied using the NACA 0015 airfoil with surface coverage from 0.1c to 0.78c. The baseline spacing included 15 strips and the wide spacing of 0.10c incorporated 8 strips. This test was the equivalent of studying protuberance density.

A positive lift increment at zero degrees angle-of-attack was produced and continued until it washed out near 10 degrees angle-of-attack as seen in Figure 3-8. There was a positive correlation between closer spaced strips and increased lift until the relationship inverts at 6 degrees angle-of-attack. The magnitude of the lift increment remained comparable to the previous strip and protuberance coverage testing and the interesting result in the post-stall region reoccurred.

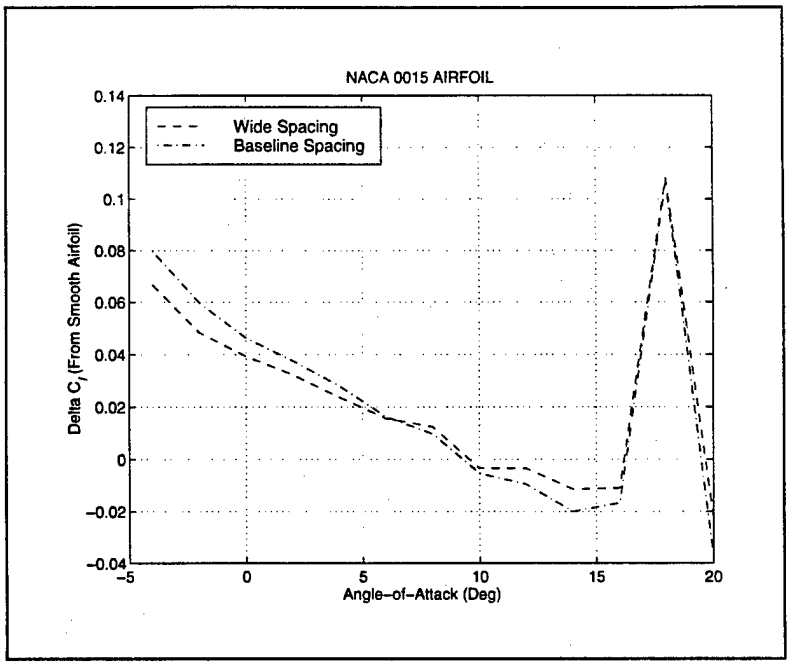

Figure 3-8. Lift Increment as a Function of Strip Spacing at Constant Coverage

Figure 3-9 shows that there was a negative correlation between closer spaced strips and an increase in the lift-to-drag ratio. For all configurations tested, none equaled nor exceeded the lift-to-drag ratio performance of the baseline airfoil. The magnitude of the lift-to-drag ratio for the rough airfoil was consistent with the previous airfoil results. As previously seen in Figure 3-5 and Figure 3-7, the performance converged to a common curve in the post-stall region in Figure 3-9. Note, despite the inversion of the relationship between strip spacing and lift near 6 degrees angle-of-attack, there was not a similar event in the lift-to-drag ratio.

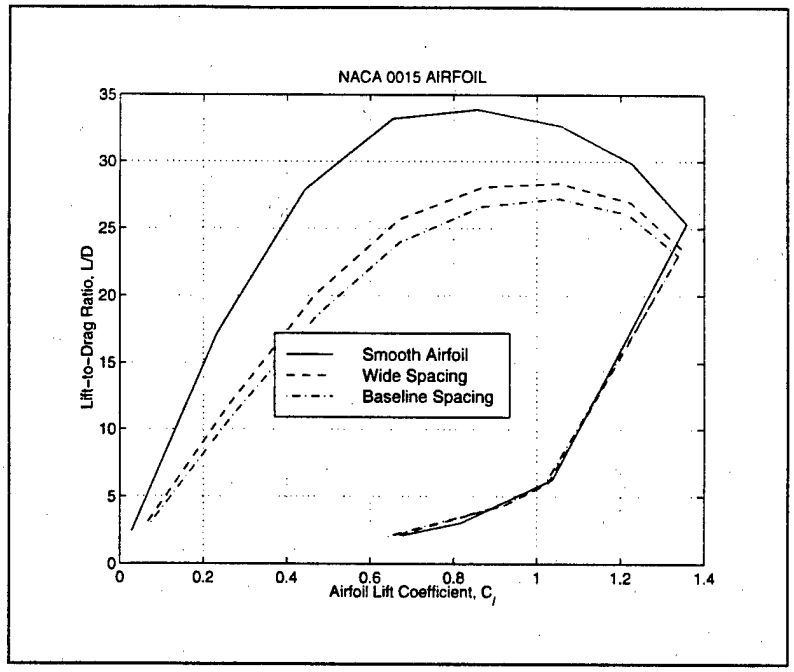

Figure 3-9. Lift-to-Drag Ratio as a Function of Strip Spacing at Constant Coverage

The effect of strip spacing on lift and lift-to-drag ratio was studied using the NACA 0015 airfoil with a constant 8 strips. The resulting coverage was from 0.10c to 0.5c for the baseline spacing and from 0.10c to 0.78c for the wide spacing.

For a constant number of strips, Figure 3-10 shows that there was a positive correlation between increased coverage and increased lift. There was a positive lift increment for zero degrees angle-of-attack and this persisted until washing out near 10 degrees angle-of-attack. These results included the abrupt increase to a large, positive lift increment at 18 degrees angle-of-attack seen throughout all results in this test.

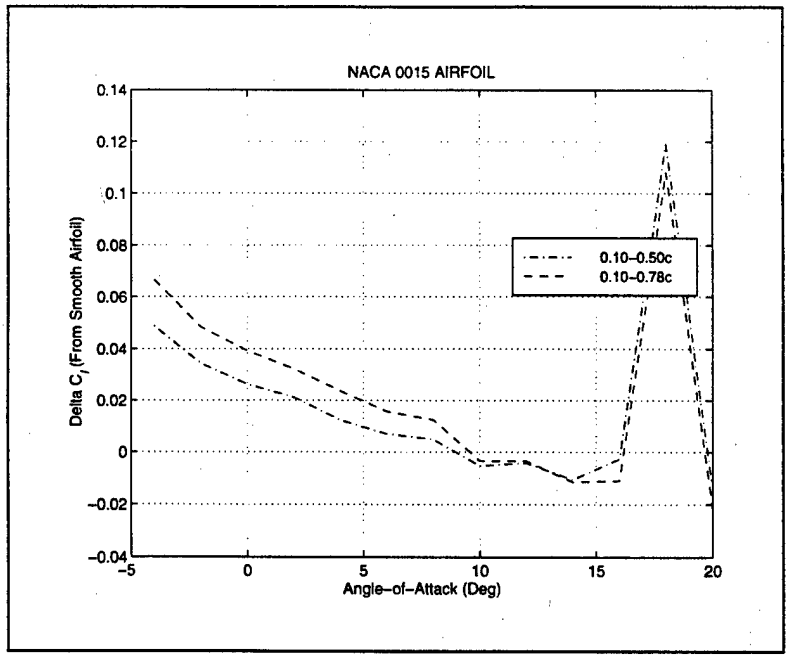

Figure 3-10. Lift Increment as a Function of Strip Spacing Using 8 Strips

As strip coverage increased while maintaining a constant number of strips, the lift-to-drag ratio decreased. Figure 3-11 shows this negative correlation and that the strip modified airfoils never exceeded nor equaled the lift-to-drag ratio performance of the baseline airfoil. The post-stall collapse of all configurations to a single performance curve is seen in Figure 3-11.

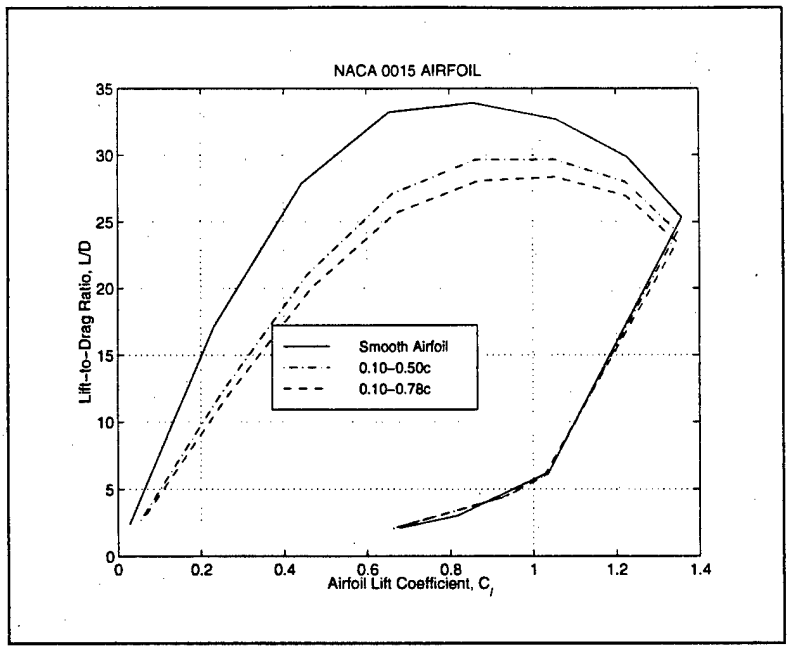

Figure 3-11. Lift-to-Drag Ratio as a Function of Strip Spacing Using 8 Strips

3.2 GLMWT TEST #1616

Because the previous wind tunnel experiment achieved only a positive lift increment and not an accompanying lift-to-drag ratio improvement, a second experiment was designed to explore the potential influence of three-dimensional flow about a wing in the creation and promotion of the flow field which produces the results reported by Vorobiev. In this experiment, a wing was employed and the protuberances assumed a cylindrical, three-dimensional form to create a problem completely defined by three-dimensional effects.

The experiment was conducted in the Glenn L. Martin Wind Tunnel in January 1997 and the results were reported to the American Institute of Aeronautics and Astronautics' (AIAA) 15th Applied Aerodynamics Conference in June 1997.[17]

3.2.1 OBJECTIVE

The primary objective of this experiment was to characterize the roughness related lift enhancement phenomena reported by the Russian researchers using a wing baseline. The specific case studied was a low aspect ratio NACA 0015 wing mounted perpendicular to the wind tunnel floor at high Reynolds number with the roughness simulated by cylindrical protuberances of varying coverage, size, and density.

3.2.2 EXPERIMENT DESIGN

3.2.2.1 Experimental Method

The experiment was conducted in the GLMWT at the University of Maryland. The wing was mounted perpendicular to the wind tunnel floor at the center of a 0.45 m round mounting disk that was attached to the main tunnel balance. Angle-of-attack variation was achieved through the rotation of the mounting plate.

For this experiment, the target precisions of the mean lift and drag were set to 0.001 and 0.0006, respectively, in coefficient form.

3.2.2.2 Wing Model

The rectangular wing had a chord of 0.45 m and a span of 0.61 m for an aspect ratio of 1.33. The NACA 0015 section profile extended across the entire span except near the wing tip which was a smoothed, half-round shape. The wing was constructed of foam with a fiberglass exterior surface. Pressure taps were installed chordwise at mid-span. Protuberances were constructed of cylindrical plastic beads and attached directly to the wing's fiberglass surface using hot glue.

3.2.2.3 Test Matrix

The wind tunnel conditions were set to a freestream Reynolds number of 1.5 million based on wing chord. The angle-of-attack for the wing was varied from -4 degrees to 30 degrees in 2 degree increments.

The following three protuberance parameters were selected for investigation based on the Russian reporting:

- Protuberance coverage of one side of the wing surface as measured aft of the leading edge;
- Protuberance size as measured by the ratio of protuberance height to wing chord, h/c;
- Protuberance density as measured by the number of protuberances per chord length squared.

Based upon the recommendations of the Russian report, the protuberance size and density selected for this experiment are shown in Table 3-1.

ID	Diameter (mm)	Height (mm)	Size (h/c)	Density ($\#/c^2$)
Small	2.5	1.65	0.0036	835 and 418
Large	4.4	2.75	0.0060	835, 418, 292

Table 3-1. Protuberance Test Parameters

Studied using small protuberances, coverage as measured from the leading edge varied as:

- 0.1c to 0.17c;

- 0.1c to 0.28c;
- 0.1c to 0.40c;
- 0.1c to 0.57c;
- 0.1c to 1.00c.

Recall that the present investigation focused on the effect of protuberances using mathematically well-defined, reproducible shapes in contrast to the irregular protuberances used by Vorobiev. Figure 3-12 shows a sample configuration where the coverage of small protuberances extended from 0.1c to 1.00c at a density of $835/c^2$.

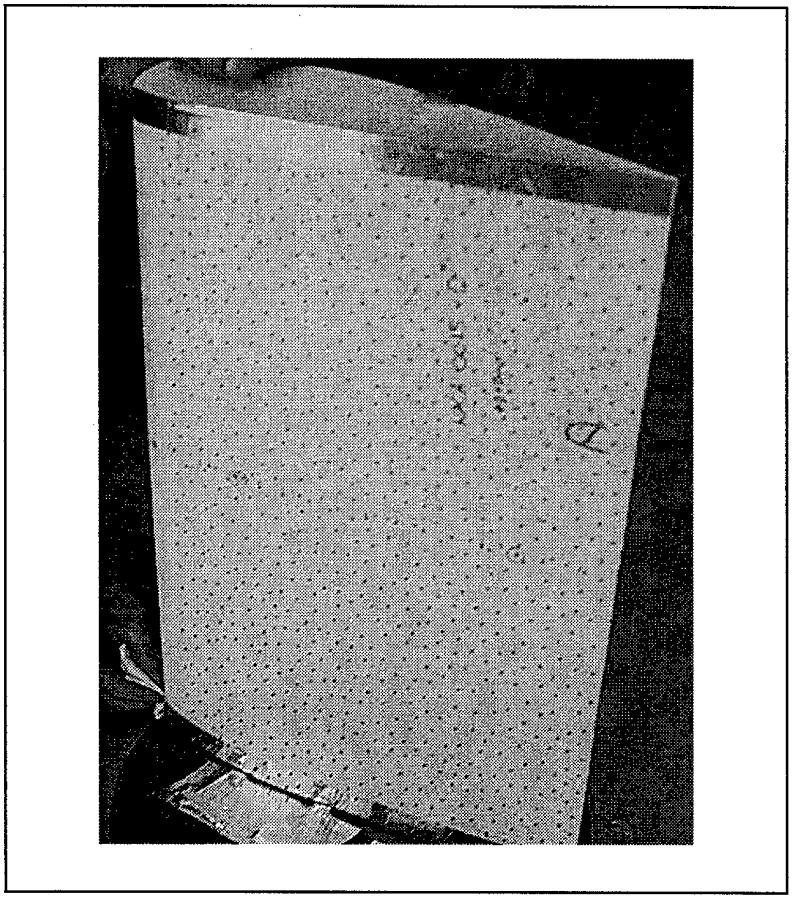

Figure 3-12. Representative Cylindrical Protuberance Configuration

The baseline for all cases presented was the experimentally measured results from the smooth wing.

3.2.3 RESULTS

3.2.3.1 Lift and Lift-to-Drag Ratio

Experimental results of wing performance as measured by the wing lift coefficient, C_L, as a function of angle-of-attack and lift-to-drag ratio as a function of C_L are presented for varying protuberance coverage, size, and density.

Coverage. Comparison plots of experimental results of wing performance for varying coverage of small protuberances at a density of $835/c^2$ are shown in Figure 3-13 and Figure 3-14.

The data shown in Figure 3-13 indicate that the wing lift coefficient with varying protuberance coverage increased relative to the baseline for all cases until stall, which occurred at approximately 22 degrees angle-of-attack. The positive lift increment was greatest at low angles-of-attack and diminished as lift approached stall. There was a positive correlation between increased surface coverage and increased lift in the pre-stall region. Note that there was a positive lift coefficient at zero degrees angles-of-attack for a symmetric wing. The results also show that the presence of the protuberances degraded lift in the post-stall region.

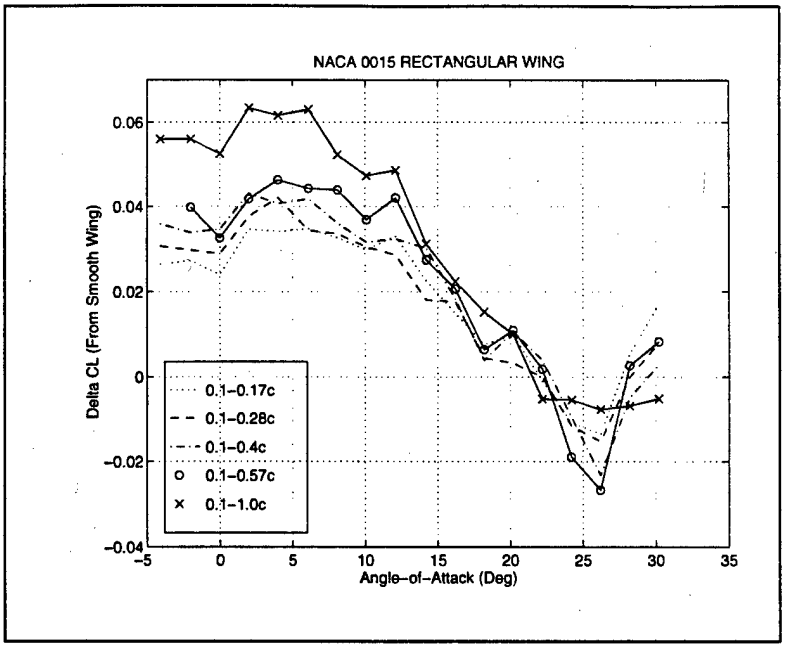

Figure 3-13. Lift Increment as a Function of Protuberance Coverage

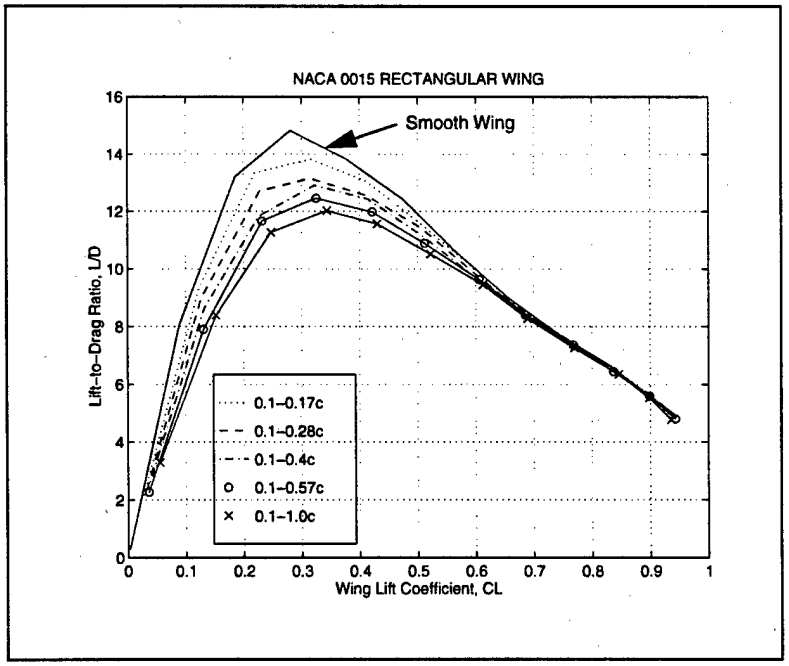

Figure 3-14. Lift-to-Drag Ratio as a Function of Protuberance Coverage

The results shown in Figure 3-14 indicate that for all modified configurations tested, the lift-to-drag ratio decreased with the presence of protuberances. There was a negative correlation between the surface covered by protuberances and the lift-to-drag ratio, i.e. increased surface coverage resulted in decreased lift-to-drag ratio performance.

A protuberance field located from 0.156c to 0.34c using the small protuberances at the same density was investigated. The lift increment and the lift-to-drag ratio for this configuration were nearly identical to those presented for the 0.1c to 0.28c coverage. Note that these two protuberance fields covered approximately the same surface area but over two different chord stations.

Size. Experimental results comparing wing performance for varying protuberance size are shown in Figure 3-15 and Figure 3-16. The configuration for this testing used a baseline coverage from 0.1c to 0.28c at a density of $835/c^2$.

The results in Figure 3-15 indicate a positive lift increment for the configurations tested at all angles-of-attack until approximately reaching stall. There was a positive lift coefficient at zero degrees angle-of-attack and the magnitude of the increment decreased with increased angle-of-attack. There was a positive correlation between increased protuberance size and increased lift. Results in the post-stall region indicate a decrease in lift over most attitudes tested.

From Figure 3-16, the results show a negative correlation between increased protuberance size and lift-to-drag ratio, i.e. larger protuberances produced smaller lift-

to-drag ratios. For all protuberance populations tested, none produced a lift-to-drag ratio greater than the baseline wing.

Results for other surface coverage areas were similar to those presented here.

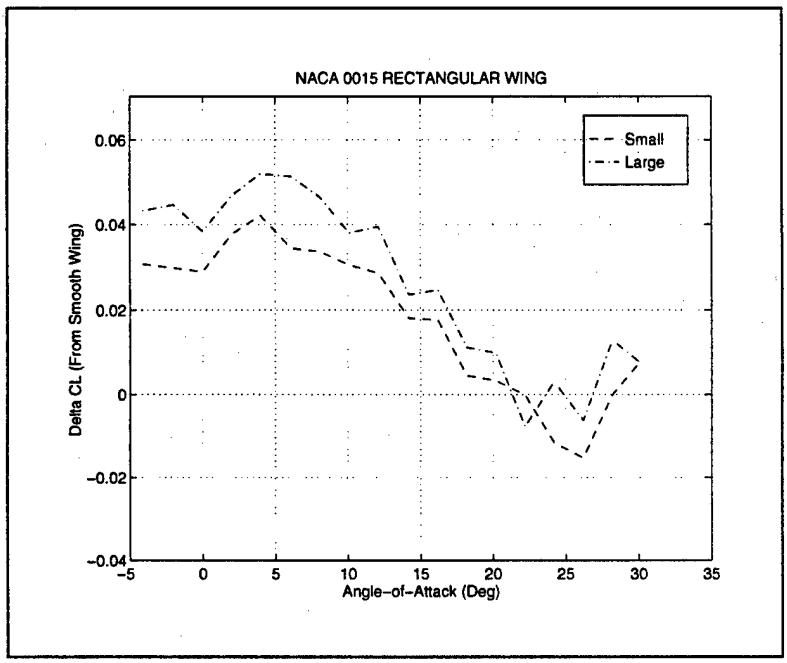

Figure 3-15. Lift Increment as a Function of Protuberance Size

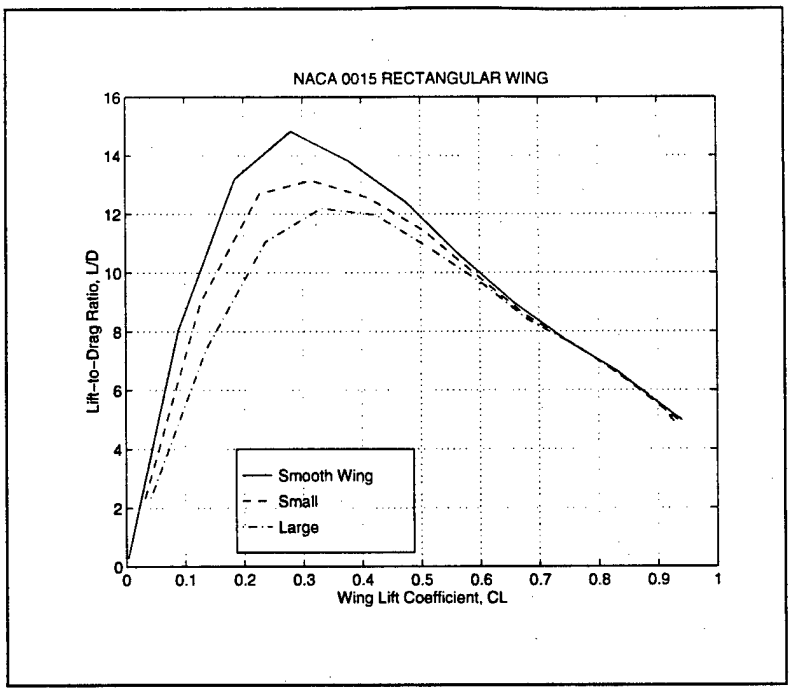

Figure 3-16. Lift-to-Drag Ratio as a Function of Protuberance Size

Density. Results comparing the performance of the NACA 0015 airfoil with varying protuberance density are shown in Figure 3-17 and Figure 3-18. The configuration used large protuberances with coverage from 0.1c to 0.28c.

The data presented in Figure 3-17 suggest that there was a positive correlation between increased protuberance density and lift production, i.e. increased density resulted in additional lift. There was positive lift generated at zero degrees angle-of-attack and the positive increment continued until near stall attitudes for all modified configurations. Results indicate that the presence of protuberances during post-stall attitudes decreased lift.

From Figure 3-18, no modified configuration at any angle-of-attack exceeded the lift-to-drag ratio generated by the smooth wing. There was a negative correlation

between protuberance density and the magnitude of the lift-to-drag ratio, i.e. increased protuberance density resulted in larger decreases in the lift-to-drag ratio.

Density variation was not performed for any other protuberance coverage, though identical trends were observed for small protuberances over the 0.1c to 0.28c coverage region.

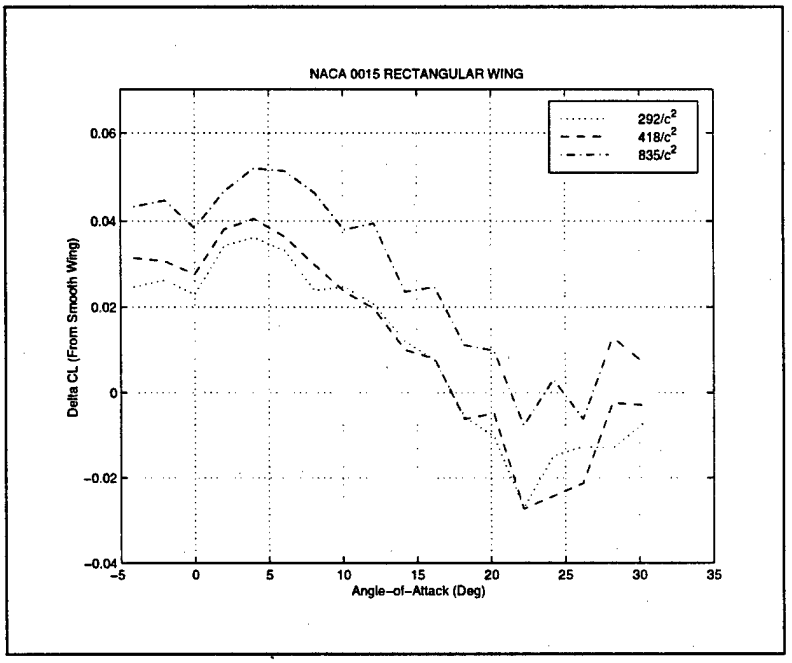

Figure 3-17. Lift Increment as a Function of Protuberance Density

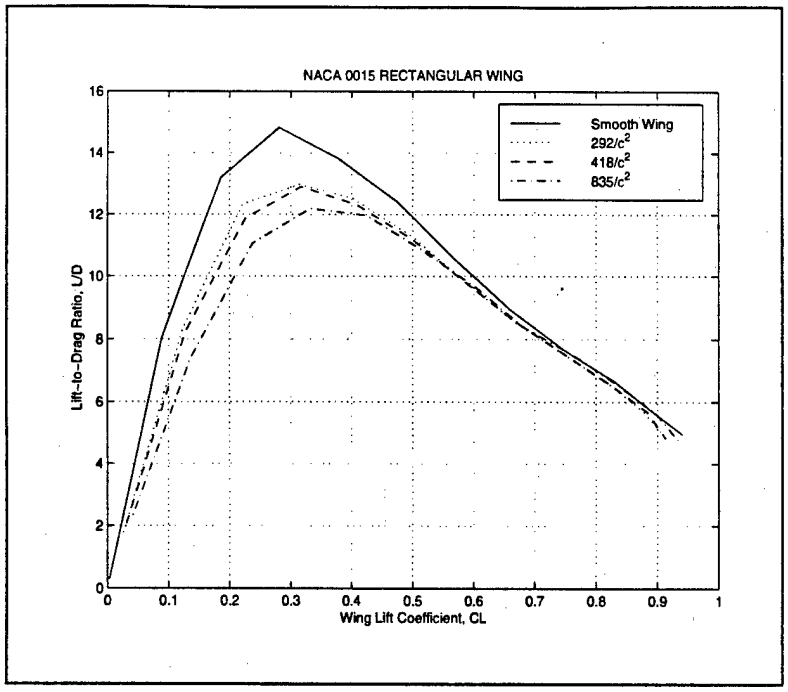

Figure 3-18. Lift-to-Drag Ratio as a Function of Protuberance Density

Wavy Wing. During the conduct of the experiment, the baseline configuration was repeatedly tested to ensure no changes were introduced during the application and removal of the protuberances. The final baseline check produced unexpected results. The application of heat used during the removal of the last set of protuberances caused the foam under the wing's fiberglass skin to detach. This created a wavy surface of irregularly shaped bumps not exceeding one inch across and which protruded above the original surface. These bumps were concentrated in the region from 0.28c to 0.57c.

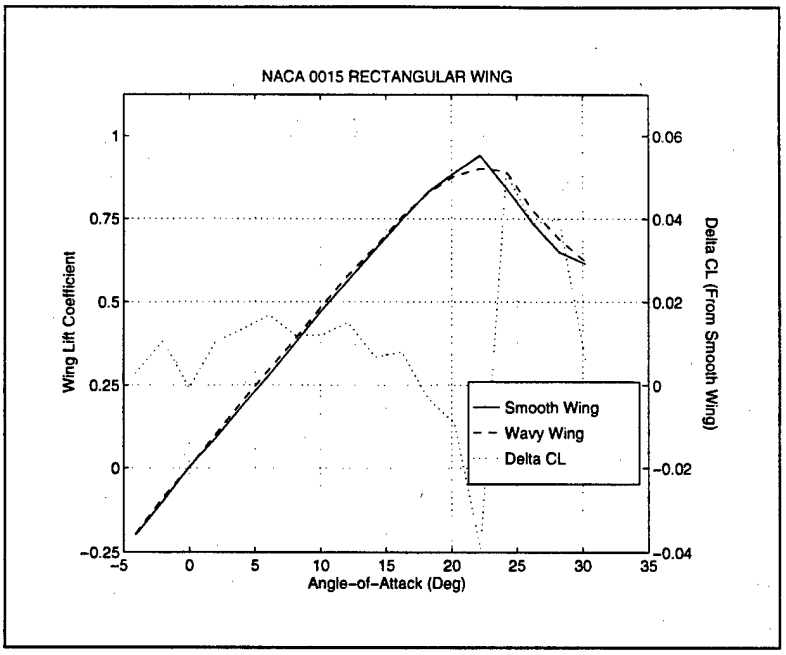

Figure 3-19. Lift and Lift Increment for the Wavy Wing

The results from Figure 3-19 indicate that the wavy wing produced a positive lift increment which continued until near the stall region. In contrast to the other configurations tested, note that the wavy wing did not produce a positive lift at zero degrees angle-of-attack.

The results in Figure 3-20 show that in the pre-stall region, the lift-to-drag ratio of the wavy wing exceeded that of the baseline wing. The maximum value of lift-to-drag occurred at 6 degrees angle-of-attack and was nearly 4% larger than that of the smooth wing.

The wavy wing was the only configuration tested which qualitatively matched the reported Russian results by generating a higher lift-to-drag ratio compared to the smooth wing.

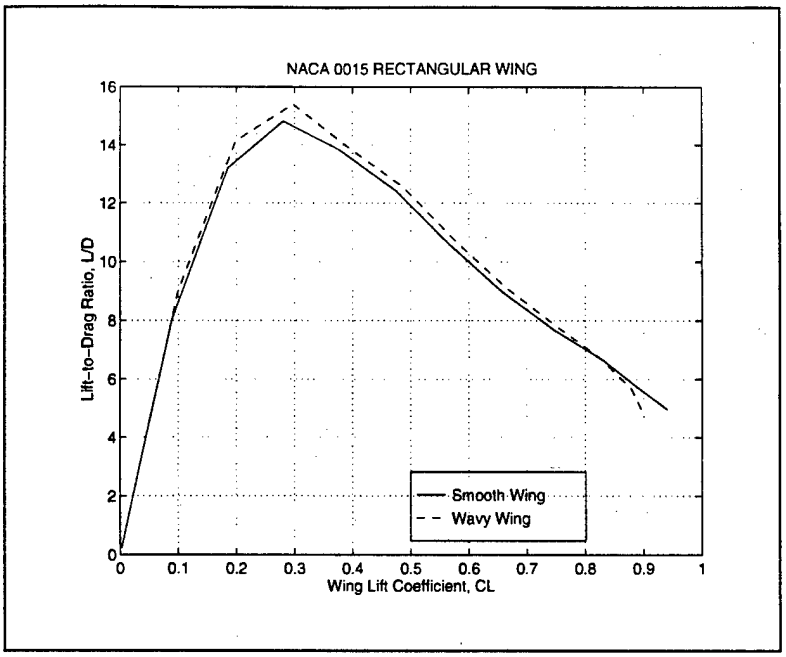

Figure 3-20. Lift-to-Drag Ratio for the Wavy Wing

3.2.3.2 Pressure Measurements

Pressure measurement results for the wing with large protuberances covering the region from 0.1c to 0.28c and a density of $835/c^2$ are shown in Figure 3-21 and Figure 3-22. An angle-of-attack of 6 degrees corresponds to the experimentally measured angle of maximum lift-to-drag.

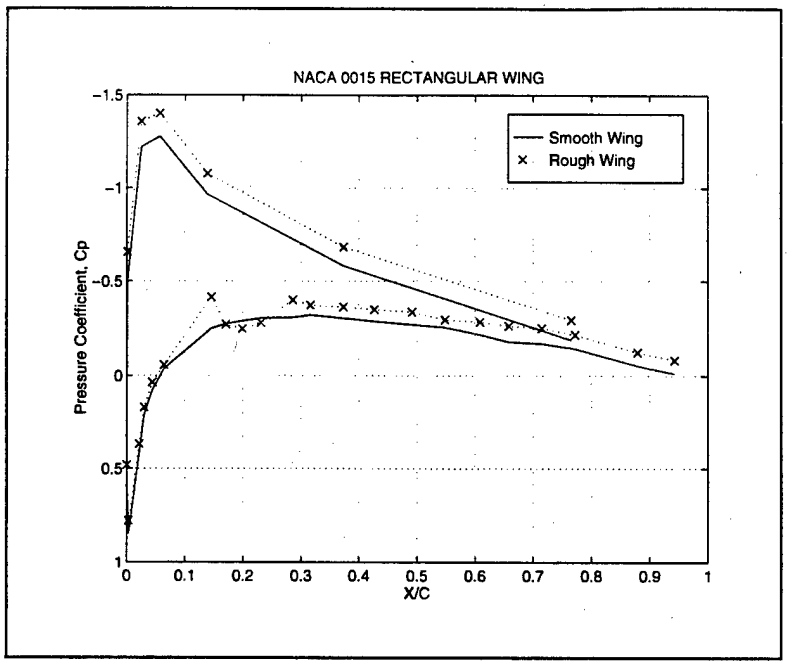

Figure 3-21. Pressure Coefficient Comparison Plot (α=6^o)

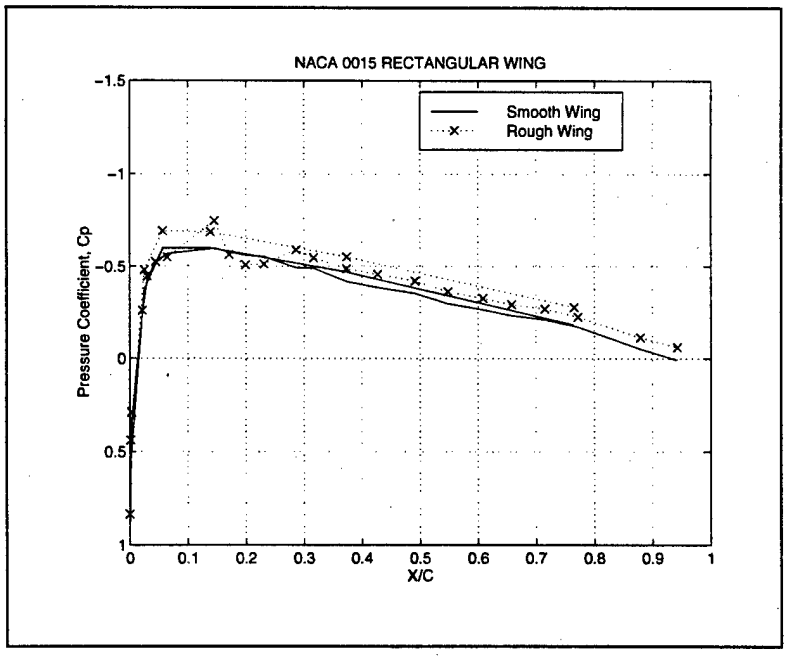

Figure 3-22. Pressure Coefficient Comparison Plot (α=0^o)

The shape of the pressure coefficient, C_P, curve for the protuberance populated wing deviates from the smooth wing in two important ways. First, the pressure was lower, in general, over much of the roughened wing as indicated by the upward shift in the C_P curve. This is seen clearly at both zero degrees angle-of-attack in Figure 3-22 and at 6 degrees angle-of-attack in Figure 3-21. Second, there was a localized pressure effect in the vicinity of the protuberance covered region. This effect was present at both angles-of-attack shown, but was more distinct at 6 degrees angle-of-attack. It appears that the flow accelerated slightly upstream of the region covered by the protuberances as evidenced by the pressure drop that begins near 0.05c and ends near 0.15c. From 0.15c to 0.20c, the flow decelerated and partially recovered from the initial pressure drop. Finally, near 0.2c, the flow again accelerated until 0.28c, the end of the region covered with protuberances. This pressure variation and its attendant velocity distribution suggest that the leading protuberances created a venturi effect and accelerated the flow. This effect was reversed after the flow penetrated into the protuberance populated region a critical distance or impacted a critical number of protuberances and a blockage effect slowed the flow and increased pressure. As the flow neared the rear edge of the protuberance region, the flow again accelerated based on the venturi effect.

Pressure measurements at other angles-of attack, including the stall and post-stall regions, produced qualitatively identical characteristics.

3.3 SYNOPSIS

This section summarizes the results of the wind tunnel investigations, highlights conclusions noted, develops preliminary explanations of the flow phenomena, and details the rationale for the ensuing computational experiments.

3.3.1 SUMMARY OF EXPERIMENTAL RESULTS

3.3.1.1 Airfoil Test

Study of the experimental force data for a NACA 0015 airfoil with cylindrical surface protuberances attached on a single side led to the following observations:

- The presence of protuberances produced an incremental lifting force in a transverse direction to the surface. This effect included the generation of lift at zero degrees angle-of-attack. The effect occurred at low and moderate angles-of-attack and diminished to zero near stall.
- Increasing surface area covered by the protuberances increased the lift generated and decreased the lift-to-drag ratio.

Study of the experimental force data for a NACA 0015 airfoil with strips attached on a single side led to the following observations:

- The presence of strips produced an incremental lifting force in a transverse direction to the surface. This effect included the generation of lift at zero degrees angle-of-attack. The effect occurred at low and moderate angles-of-attack and diminished to zero near stall.
- Increasing surface area covered by the strips increased the lift generated and decreased the lift-to-drag ratio.

- Decreasing the spacing between the strips increased the lift generated and decreased the lift-to-drag ratio.

Study of the airfoil test results for cylindrical protuberances and strips compared to the results reported by Vorobiev for cusp-like protuberances led to the following observation:

- All configurations tested produced a similar increase in lift, but none achieved an equal or greater lift-to-drag ratio compared to a smooth, baseline airfoil.

3.3.1.2 Wing Test

Study of the experimental force data for a NACA 0015 wing with cylindrical surface protuberances attached on a single side led to the following observations:

- The presence of protuberances produced an incremental lifting force in a transverse direction to the surface. This effect included the generation of lift at zero degrees angle-of-attack. The effect occurred at low and moderate angles-of-attack and diminished to zero near stall.
- Increasing surface area covered by the protuberances increased the lift generated and decreased the lift-to-drag ratio.
- Increasing the protuberance size, as measured by the ratio of protuberance height to wing chord, increased the lift generated and decreased the lift-to-drag ratio.
- Increasing the density of the protuberances in the covered region increased the lift generated and decreased the lift-to-drag ratio.

Study of the wing test results for cylindrical protuberances compared to the results reported by Vorobiev for cusp-like protuberances led to the following observation:

- All configurations tested produced a similar increase in lift, but none achieved an equal or greater lift-to-drag ratio compared to a smooth, baseline wing.

Study of the pressure distribution over a NACA 0015 wing with cylindrical surface protuberances attached on a single side led to the following observation:

- The presence of the protuberances significantly altered the pressure distribution about much of the wing and specifically in the region populated with protuberances.

3.3.1.3 Wavy Wing Test

Study of the force data for a NACA 0015 wing with a wavy-like surface on a single side led to the following observations:

- The presence of the wavy surface produced an incremental lifting force in a transverse direction to the surface. The effect occurred at low and moderate angles-of-attack and diminished to zero near stall. Unlike the cases for cylindrical protuberances and strips, no incremental lift was generated at zero degrees angle-of-attack.
- The presence of the wavy surface produced an increase in the lift-to-drag ratio over a significant portion of the pre-stall region.

3.3.2 CONCLUSIONS FROM EXPERIMENTAL RESULTS

The airfoil and wing experimental results do not support any conclusions regarding the necessity of a two-dimensional airfoil body versus a three-dimensional wing and their distinct flow fields in achieving the desired performance effect. In addition, the airfoil experimental results do not support any conclusions regarding the necessity of a two-dimensional strip versus a three-dimensional protuberance to achieve the desired performance improvement. Only a preliminary conclusion can be made suggesting that a three-dimensional body coupled with a three-dimensional protuberance is required to produce the roughness related lift enhancement phenomena.

The inability of the cylindrical protuberances and the strips to produce an increase in the lift-to-drag similar to that reported by Vorobiev using cusp-like protuberances implies that geometry details of the surface roughness are critical to the roughness related lift enhancement phenomena. This conclusion is strengthened by the demonstrated increase in the lift-to-drag ratio for the wavy wing.

The influence of the protuberances on the pressure distribution of the wing was demonstrated. These results suggest that a significant source of the roughness related lift enhancement phenomena is pressure related.

3.3.3 POTENTIAL EXPLANATIONS OF PHENOMENA

Upon completion of the wind tunnel experiments, potential explanations of the experimental results and the Russian results were developed. This section presents three concepts considered at that time.

3.3.3.1 Increased Circulation

This concept is based entirely on the Circulation Theory of Lift and the direct relationship between an increase in vorticity and an increase in lift. In this thinking, the protuberances generate more vorticity compared to the flow about a wing with no protuberances. The increase in vorticity produces an increase in circulation. Using the Kutta-Jouwkowski Theorem, the increased circulation predicts a increase in lift.

This approach is appealing because it provides a direct cause and effect link, at least in theory. However, it is not satisfactory considering the directional nature of vorticity and given the unresolved debate on the importance of two-dimensional versus three-dimensional flow fields. In addition, if this concept proves accurate, it still is inadequate in explaining the fundamental nature of the aerodynamic effect.

3.3.3.2 Surface Shape Modification

This explanation was inspired by the work of Amity, Smith, and Glezer [18] on synthetic jets applied to two-dimensional, blunt body cylinders. In their work, the researchers describe how the jets create a region of recirculation immediately downstream of the oscillating jet. The effect on the flow is to trap this region between ends which remain attached. The investigators hypothesize that the flow now acts such that the outer edge of the recirculation region, that is the edge parallel to the original surface and now in contact with the freestream flow, becomes the effective body surface and that the noted increase in lift and decrease in drag are directly related to this boundary change. The researchers present this idea with no substantiative research to support the explanation. This concept is very appealing because it offers a very

physical explanation of the aerodynamic effect. In essence, this concept attributes the change in aerodynamic performance to changes in the thickness and/or camber of the wing or airfoil.

Based on the airfoil experiments reported by Abbott and von Doenhoff, [6] the aerodynamic effects reported by Vorobiev for a wing covered by protuberances could be explained as an increase in camber alone as there is no observed evidence of thickness related effects. The primary effect of increasing thickness are a slight decrease in the lift curve slope for NACA 4- and 5-digit airfoils, a slight increase in the lift curve slope for 6x-series airfoils, and an increase in the maximum lift coefficient for both. An increase in airfoil thickness has little effect on the angle-of-attack for zero lift. In contrast, an increase in camber decreases the angle-of-attack for zero lift without change in the lift curve slope. Again, there is an increase in the maximum lift coefficient. With regards to minimum drag, increasing thickness strongly increases drag while increasing camber has little effect on drag, especially for NACA 4- and 5-digit airfoils. This evidence suggests the potential increase in effective camber as a means to support this concept.

3.3.3.3 Mini Vortex Generators

This explanation is very similar to that described in the Surface Shape Modification Section (see Section 3.3.3.2) except that the focus is narrowed to the effect on the surface pressures. As described by Bragg and Gregorek [19] in their study on adding vortex generators to the upper surface of the wing on the Voyager aircraft, the purpose of adding the vortex generators was to keep the flow attached

when the boundary layer prematurely separated near the leading edge. The researchers identified a vortex generator geometry which accomplished this objective. The vortex generator was delta shaped and had a height of 0.0182c. This protuberance is similar to the protuberance under study as its height exceeded the local boundary layer thickness. In the Voyager wing program, the vortex generator created a recirculation region immediately downstream of its location and maintained the surface static pressure value measured at the most forward point in the region. On the upper surface at approximately a mid-chord location, this means that a lower pressure is maintained over a greater portion of the airfoil with a resulting increase in lift. If this concept were now transferred to the lower surface where properly positioned protuberances might act like vortex generators, a recirculation region could be created immediately downstream of the protuberances. If this region could hold the initial high pressure of the region, the net effect could be a resulting increase in lift.

Apparent evidence supporting this concept can be seen in Figure 3-21. The surface static pressure in the region covered by protuberances is higher and appears nearly constant in the region. This evidence suggests the potential validity of this concept. What is not adequately explained for the pressure distribution using this concept is the gross decrease in pressure about the wing.

3.3.4 RESEARCH DIRECTION

Thus far, wind tunnel experiments of surface protuberances on the lower surface of an airfoil and a wing have demonstrated increased lift potential with decreased lift-to-drag ratio performance. These results, with the exception of the wavy

wing, do not match the performance reported by Vorobiev. It was decided at this point to shift the approach of this research project to a computational study of this effect. Results from the computational experiments should provide greater insight into the flow field and its properties because the solution is based on relatively fine grid scales and the computational experiments better allow a systematic study of the apparent critical parameters defining protuberance geometry. The next two chapters detail the approach and results of the computational experiments.

CHAPTER 4 COMPUTATIONAL PROCEDURE

4.1 SOLUTION PROCEDURE

An investigation was performed of a NACA 0015 airfoil with protuberances using the OVERFLOW Navier-Stokes flow solver as a two-dimensional Reynolds-Averaged Navier-Stokes (RANS) code at a freestream Mach number of 0.15 and a freestream Reynolds number of 1.5 million based on airfoil chord. Results of these computational experiments are presented in Chapter 5. This chapter details the necessary theory and the solution procedure to achieve computational results for the given geometries and flow conditions, as outlined below:

1. Define body surface lines (see Section 4.2.1);
   - Define NACA 0015 airfoil surface;
   - Define protuberance surface;
   - Define wake cut "surface";
2. Generate volume grids (see Section 4.2.2);
   - Generate volume grids for the airfoil, protuberance, and wake cut;
   - Generate volume grid for far field boundaries;
   - Integrate volume grids into a single, chimera grid;
3. Execute OVERFLOW solver (see Section 4.3.3);
4. Terminate OVERFLOW using convergence criteria (see Section 4.3.4);
5. Analyze solution results (see Section 4.4).

4.2 GRID GENERATION

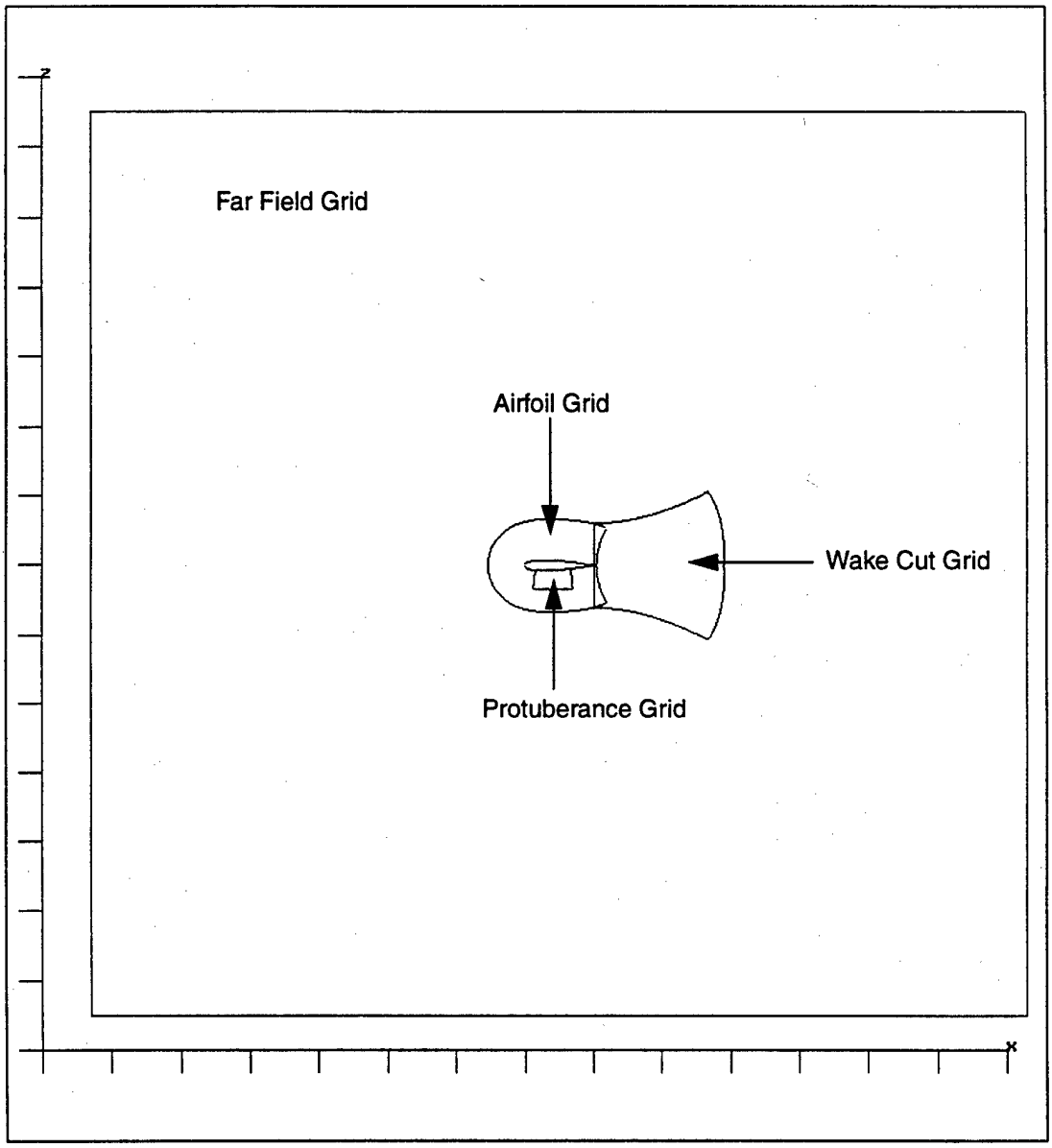

Figure 4-1. Individual Grid Boundary Outlines Used in Chimera Scheme

Surface grids were defined for the airfoil, protuberance, and the wake cut geometries. Once set, these grids were discretized and volume grids were generated. These computational experiments utilized chimera or overset grids. This section

details the surface grid development and the generation and integration of the airfoil, protuberance, wake cut, and far field volume grids. As an introduction to the grid structure, Figure 4-1 shows the grid boundaries for the individual volume grids.

4.2.1 SURFACE GRID GENERATION

Individual surface grid components were defined for the airfoil, the protuberance geometries, and the wake cut. The hyperbolic tangent spacing scheme of Vinokur [20] was used to discretize each grid. One-sided and two-sided functions were utilized as appropriate to concentrate the surface discritization based on body curvature and expected, high gradient regions.

4.2.1.1 Airfoil Surface Grid Definition

The thickness distribution for the NACA 4-digit airfoil series was defined by Abbott and von Doenhoff,[6] where t is the maximum thickness as a fraction of chord, x is defined as the non-dimensional chord position, and y_t is the corresponding thickness as a fraction of chord and set perpendicular to the chord:

$$\pm y_t = (t/0.20)(0.29690\sqrt{x} - 0.12600x - 0.39160x^2 + 0.28430x^3 - 0.10150x^4) \quad (4.1)$$

The thickness distribution equation did not generate a closed surface at the trailing edge. Three techniques to create a closed airfoil surface were considered:

- Create a blunt, backward facing step at the trailing edge;
- Create a chisel point trailing edge;
- Scale the airfoil thickness based on the chord position.

The third option was selected and the airfoil was reduced in scale by a factor of 1.008930411365. This scaling resulted in a closed surface with a smooth surface free of any discontinuities and a zero thickness at the trailing edge.

No modification was made to the leading-edge radius.

The airfoil surface was discretized using a two-sided hyperbolic tangent spacing function from the leading and trailing edges. Initial spacing along the airfoil surface from these anchor points was selected based on previous RANS computational studies:[21]

- Leading-Edge Spacing = 0.001c;
- Trailing-Edge Spacing = 0.002c.

4.2.1.2 Protuberance Surface Grid Definition

The goal of simulating the cusp-like protuberances of Vorobiev competed against the desire to use smooth, continuous surfaces in computational modeling. The selected shape met the desirable computational qualities, yet provided for a relatively sharp protuberance peak. The protuberance definition was taken from Masad and Iyer.[22] This surface was discretized using a two-sided hyperbolic tangent spacing schemes between the leading edge and the protuberance peak with the rear, symmetric side replicated as a mirror image. The surface of the protuberance was defined by:

$$y = h(1 - 3(x(2/\lambda))^2 + 2|x(2/\lambda)|^3), \text{ where } |x| \leq (\lambda/2). \qquad (4.2)$$

Where, h is the maximum protuberance height, λ is the protuberance width, x is the chordwise position of the protuberance, and y is the corresponding protuberance

height at the specified x station. All parameters are non-dimensionalized with chord length.

Figure 4-2 depicts three variations of protuberance geometries. While the shape differs, the baseline protuberance has identical dimensions to the "large" protuberance in the wind tunnel testing using the wing baseline, h = 0.006c and λ = 0.01c. The second geometry has the smallest height tested, h = 0.002c and λ = 0.0055c. The third geometry is the tallest and narrowest geometry tested, h = 0.006c and λ = 0.002c.

The surface upstream and downstream of the protuberance were extended away from the protuberance using a one-sided hyperbolic tangent spacing scheme. For the single protuberance studies, the surface extended 0.12c upstream and 0.4c downstream from the centerline of the protuberance. For multiple protuberance configurations, the surface extended 0.12c upstream and 0.3c downstream.

To this point, the entire protuberance grid has used a linear base. For these computational experiments, the protuberance surface grid was projected on to the airfoil surface grid using the program PROGRD. PROGRD, a component of the NASA-Ames developed Chimera Grid Tools,[23,24] projects a user-defined set of points on to another surface grid or a panel network of multiple grid surfaces.

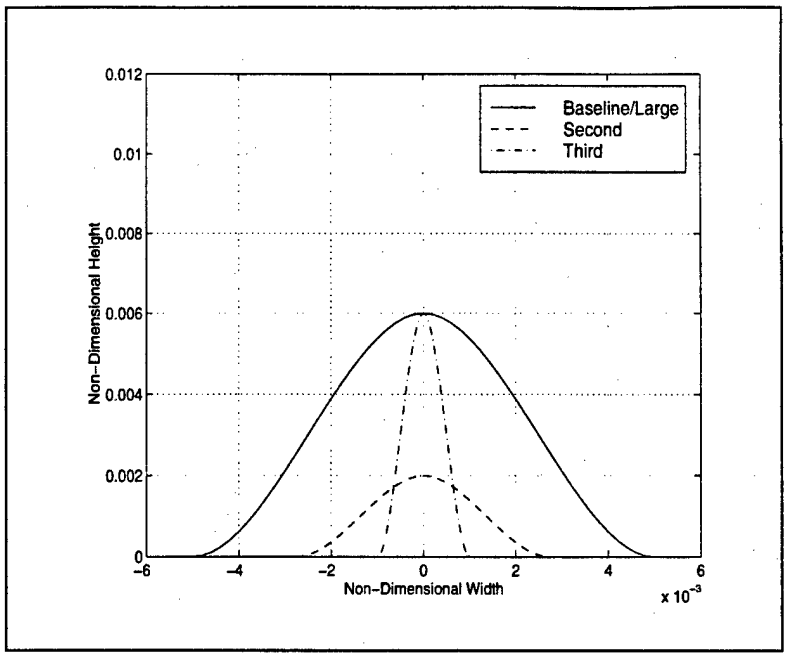

Figure 4-2. Sample of Protuberance Geometries

4.2.1.3 Wake Cut Definition

A separate wake cut grid was generated to expand the boundary layer spacing of the airfoil grid in a region expected to have smaller gradients. This was intended to reduce the overall grid size and to improve convergence.

The wake cut "surface" was specified as a line perpendicular to the extended airfoil chord centered 0.02c aft of the trailing edge and extending 0.6c away from the extended chord in both directions. One-sided hyperbolic tangent spacing was used expanding the node distribution from the center of the wake cut "surface." The upper and lower halves of the "surface" are mirror images.

4.2.2 VOLUME GRID GENERATION

Volume grids were generated from the individual component surface grids and then integrated into a single, combined grid file. A hyperbolic grid generator, HYPGEN, constructed the volume grids for the airfoil, protuberance, and wake cut elements. The far field volume grid was generated directly from a cartesian box grid program, BOXGR. The volume grids consisted of 3 identical, parallel two-dimensional grids offset in the direction normal to the planar grids.

4.2.2.1 Hyperbolic Grid Generation

Hyperbolic grid generation was used to create the volume grids for the airfoil, the protuberance, and the wake cut elements. Chan and Steger [25] detail the theoretical development of hyperbolic grid generation. According to Chan and Steger, and Hoffman,[26] hyperbolic grid generation schemes produce orthogonal grids in two-dimensions and nearly orthogonal grids in three-dimensions, have excellent clustering and spacing control through cell area and arc-length functions, and require one to two orders of magnitude less computational time compared to elliptic grid generators because hyperbolic grid generators use a marching scheme rather than the iterative schemes required for elliptic grid generators. The primary disadvantage of hyperbolic grid generators is an inability to specify the outer boundary, a consideration not restrictive for these computational experiments which involve external flows and use chimera grid schemes.

NASA-Ames developed the hyperbolic grid generator, HYPGEN, and its graphical interface, HGUI, specifically for use in developing chimera grids.[27]

HYPGEN generated the airfoil, the protuberance, and the wake volume grids from their respective surface grids using the key parameters specified in Table 4-1.

Element	Initial Spacing	Number of Points	Marching Distance
Airfoil	$5 \times 10^{-6}c$	50	0.60c
Protuberance	$5 \times 10^{-6}c$	65	0.28c
Wake	$4 \times 10^{-3}c$	25	2.00c

Table 4-1. Key Volume Grid Parameters

The desire to adequately resolve the high velocity gradients near the airfoil and protuberance determined the initial spacing from these surfaces. Grid spacing at these walls should be set to $y^+ = 1$ for viscous computations. Assuming $Re_\infty = 1.5 \times 10^6$ and using the y^+ estimate from OVERFLOW, [28] initial spacing corresponding to $y^+ = 1$ is $1.6 \times 10^{-5}c$. Finer spacing was adopted to ensure the same grids could be used in higher Reynolds number simulations.

4.2.2.2 Far Field Volume Grid

In the far field, a volume grid specified using a cartesian box grid with uniform interior spacing and geometrically stretched outer layers was used to increase grid spacing in this expected low gradient region. This approach was expected to improve overall solution convergence. Combined with a reduction in the total number of grid points compared to a far field grid region based on an extended airfoil grid, this approach was expected to reduce the number of iterations required to achieve a converged solution.

NASA-Ames developed BOXGR, a component of Chimera Grid Tools,[23,29] specifically for this application. For the far field grid used in these experiments, the interior box corners were specified at -0.5c upstream of the leading edge and 0.5c downstream of the trailing edge of the airfoil and at +/-0.7c perpendicular to the airfoil chord. Interior to these vertices, the grid was specified with 0.05c uniform, square spacing. Exterior to these vertices, the grid spacing was geometrically stretched normal to the interior box faces with a constant stretching ratio of 1.21 for a minimum marching distance of 5.0c.

4.2.2.3 Chimera Grids

For these computational experiments, four separate volume grids were combined into a single, integrated grid using the chimera or overset grid approach. In this approach, independent grids are generated about individual components or for specific flow regions. These separate grids are required to overlap, though in an arbitrary manner. The chimera algorithm then constructs an interpolation scheme to control the flow of boundary data between the individual component grids during execution of the flow solver. Developed by the Air Force's Arnold Engineering Development Center, PEGSUS [30] was the chimera scheme used to integrate the airfoil, protuberance, wake cut, and far field grids into a single, overset grid and to calculate the necessary interpolation parameters.

4.2.2.4 Sample Grids

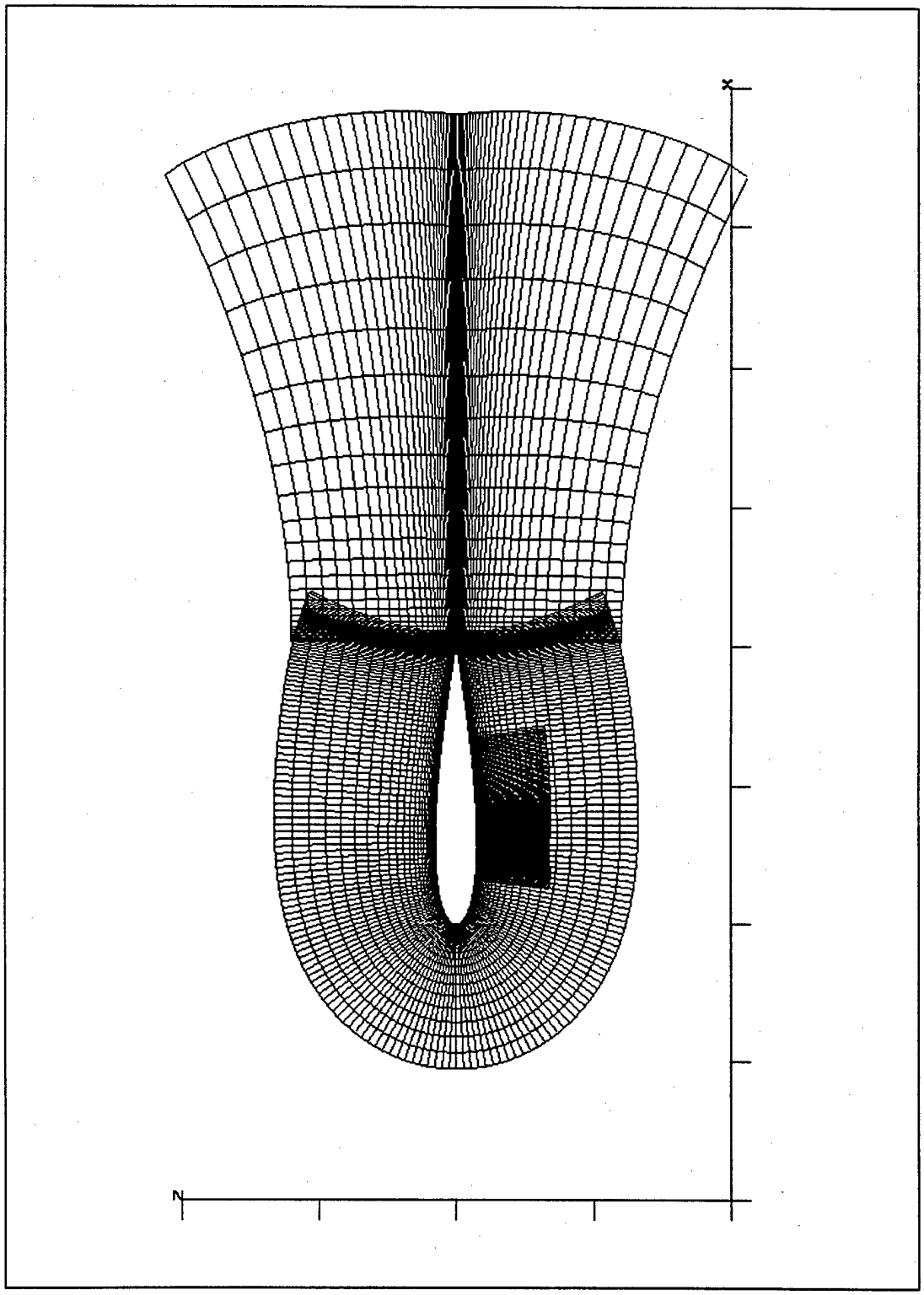

Figure 4-3. Zoom View of Airfoil, Wake Cut, and Protuberance Grids

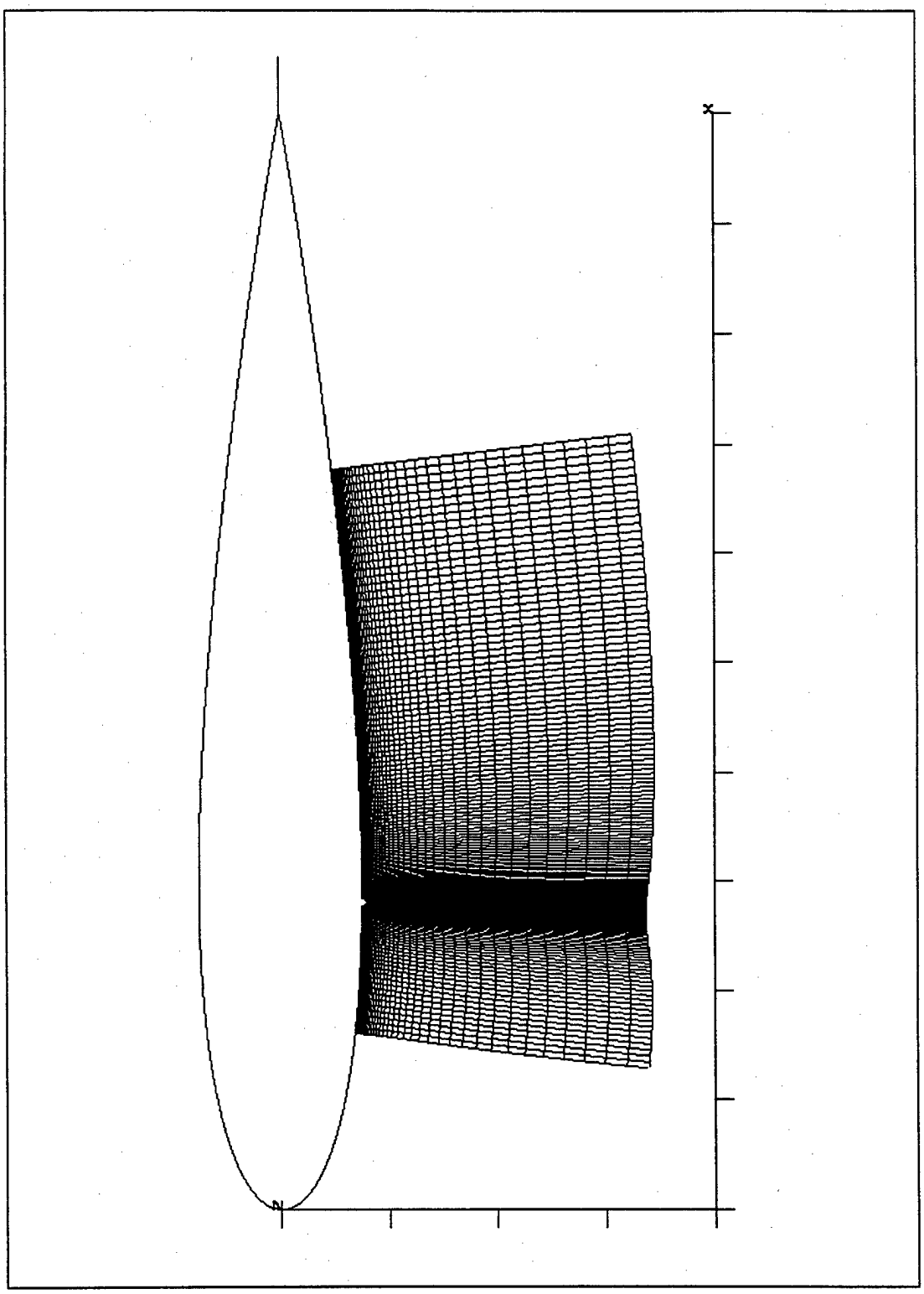

Figure 4-4. Zoom View of Protuberance Grid Along Airfoil

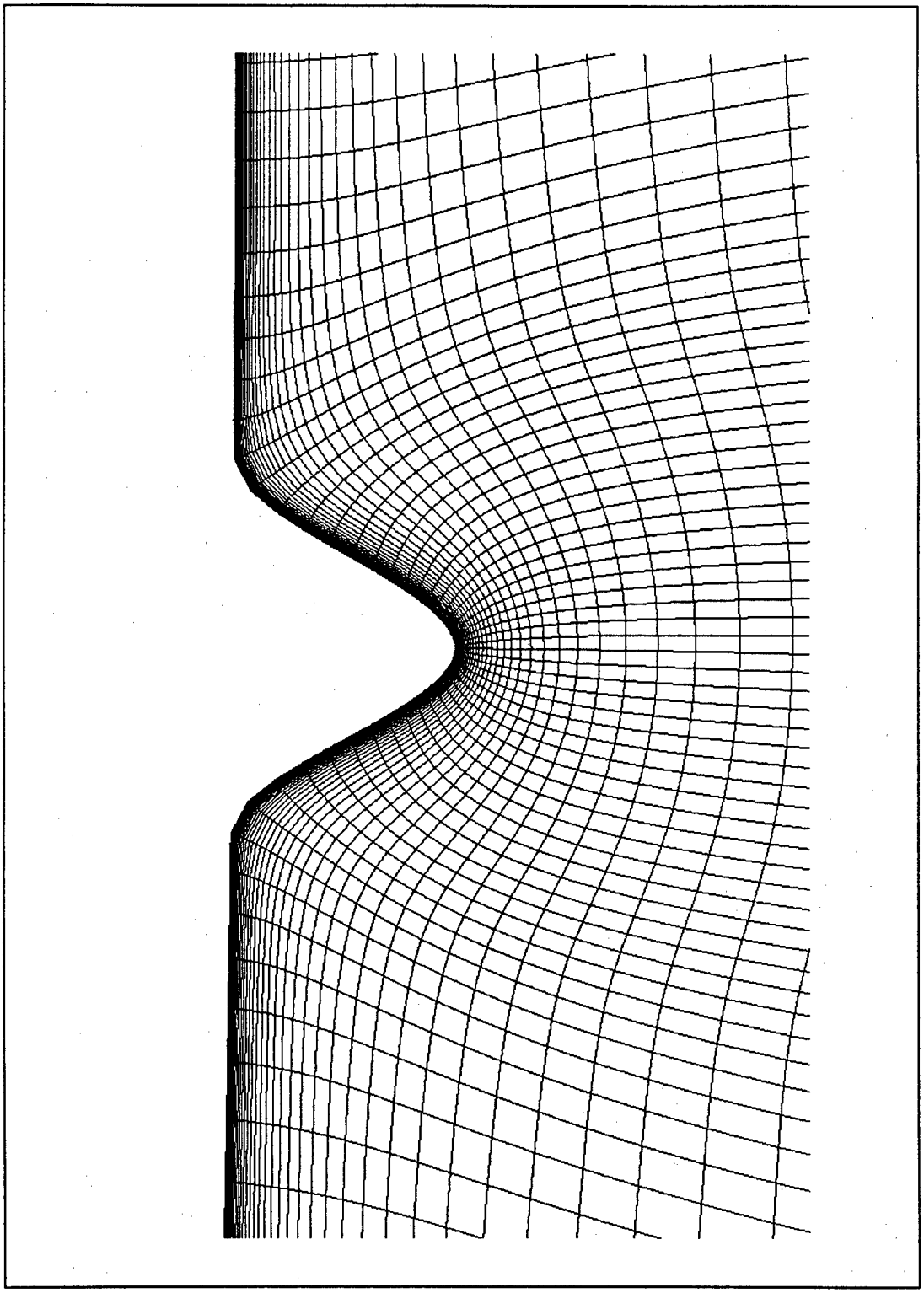

Figure 4-5. Zoom View of Protuberance Geometry in Protuberance Grid

Perspective views of the grids generated using the approach outlined are shown in Figure 4-1 and Figure 4-3 through Figure 4-5. Figure 4-1 shows the boundaries for the far field, the wake cut, the airfoil, and the protuberance grids. Figure 4-3 is a complete view of the airfoil, wake cut, and protuberance grids. Note the overlap of the grids which is required when using the chimera scheme. Figure 4-4 is a zoom view of the protuberance grid with Figure 4-5 showing the details of this grid near the protuberance.

4.3 NUMERICAL METHOD

4.3.1 FLOW MODEL

The basis of the fluid model used in these computational experiments were the Navier-Stokes equations as detailed by Schlichting.[8] In Cartesian coordinates, the non-dimensional, compressible Navier-Stokes equations in two dimensions are:

$$\frac{\partial}{\partial t}(\rho u) + \nabla\bullet(\rho u\vec{V}) = (-1/(\gamma M_\infty))\frac{\partial P}{\partial x} + (1/(Re_\infty))\left\{\frac{\partial}{\partial x}(\tau_{xx}) + \frac{\partial}{\partial y}(\tau_{yx})\right\} \tag{4.3}$$

$$\frac{\partial}{\partial t}(\rho v) + \nabla\bullet(\rho v\vec{V}) = (-1/(\gamma M_\infty))\frac{\partial P}{\partial y} + (1/(Re_\infty))\left\{\frac{\partial}{\partial x}(\tau_{xy}) + \frac{\partial}{\partial y}(\tau_{yy})\right\} \tag{4.4}$$

Here, $\vec{V}$ is the velocity vector with components (u,v), ρ is the fluid density, P is the pressure, and τ are the shear stresses. Also, $(M_\infty, Re_\infty, \gamma)$ are the freestream Mach number, the freestream Reynolds number, and ratio of specific heats, respectively.

The incorporation of turbulence was an important consideration for these experiments and was accomplished through the addition of the Reynolds stresses $(\overline{\rho u''^2}, \overline{\rho v''^2}, \overline{\rho uv})$, as detailed by Wilcox,[31] creating the Reynolds-Averaged Navier-Stokes equations. In Cartesian coordinates, the non-dimensional, compressible RANS equations in two dimensions are:

$$\frac{\partial}{\partial t}(\rho u) + \nabla\bullet(\rho u\vec{V}) = (-1/(\gamma M_\infty))\frac{\partial P}{\partial x} + (1/(Re_\infty))\left\{\frac{\partial}{\partial x}(\tau_{xx} - \overline{\rho u''^2}) + \frac{\partial}{\partial y}(\tau_{yx} - \overline{\rho u''v''})\right\} \tag{4.5}$$

$$\frac{\partial}{\partial t}(\rho v) + \nabla\bullet(\rho v\vec{V}) = (-1/(\gamma M_\infty))\frac{\partial P}{\partial y} + (1/(Re_\infty))\left\{\frac{\partial}{\partial x}(\tau_{xy} - \overline{\rho u''v''}) + \frac{\partial}{\partial y}(\tau_{yy} - \overline{\rho v''^2})\right\} \tag{4.6}$$

Predecessors of OVERFLOW, the flow solver used in these experiments, used the compressible, fully turbulent, Thin Shear Layer (TSL) Navier-Stokes equations. This model differs from the RANS equations in that the viscous derivatives in the direction normal to the body are assumed dominant and the other viscous derivatives are neglected. The TSL approximation is only valid for high Reynolds number flows. This model is included for completeness in understanding the development of OVERFLOW. The derivation of this model was detailed by Pulliam and Steger.[32] In Cartesian coordinates, the non-dimensional, compressible, fully turbulent Thin Shear Layer Navier-Stokes equations in two dimensions, assuming freestream flow in the x coordinate direction, are:

$$\frac{\partial}{\partial t}(\rho u) + \nabla\bullet(\rho u\vec{V}) = (-1/(\gamma M_\infty))\frac{\partial P}{\partial x} + (1/(Re_\infty))\left\{\mu\frac{\partial}{\partial y}u - \overline{\rho u''v''}\right\} \tag{4.7}$$

$$\frac{\partial}{\partial t}(\rho v) + \nabla\bullet(\rho v\vec{V}) = (-1/(\gamma M_\infty))\frac{\partial P}{\partial y} + (1/(Re_\infty))\left\{((4\mu)/3)\frac{\partial}{\partial y}v - \overline{\rho v''^2}\right\} \tag{4.8}$$

The version of OVERFLOW used during this investigation offered the fully integrated turbulence models of Spalart-Allmaras (1-equation model), Baldwin-Barth (1-equation model), and Baldwin-Lomax (algebraic model). Buning [33] recommended the Spalart-Allmaras model as the most appropriate and accurate for the current problem. The Spalart-Allmaras model was selected based on this recommendation. Fully turbulent flow was assumed for all computational experiments and was simulated using the 1-equation model of Spalart and Allmaras [34] except for those results used in Section 5.3.3 to identify the effect of varying the turbulence model.

4.3.2 BEAM AND WARMING SCHEME

The finite difference scheme was the implicit, approximate factorization algorithm attributed to Beam and Warming.[35,36] The implicit nature of the algorithm permitted larger time steps versus explicit schemes given the stiffness of this problem created by the small, boundary layer grid spacing used. Approximate factorization of the implicit operator reduced the complexity to a series of one-dimensional operators. Second-order, central differencing was used for spatial derivatives. The algorithm could be either first- or second-order accurate in time. For these numerical experiments, first-order time accuracy was employed, equivalent to the Euler implicit scheme.

4.3.3 OVERFLOW (VERSION 1.7V)

In the late 1970's, Steger [37] combined the implicit finite difference technique of Beam and Warming with generalized coordinate transformations to construct a compressible, two-dimensional flow solver for either the Euler equations or the Thin Shear Layer Navier-Stokes equations. The solver was applied, but not restricted to, airfoil studies. Later, Pulliam and Steger [32] expanded the work to full three-dimensional simulations over simple aerodynamic shapes. These flow solvers evolved into ARC2D and ARC3D, respectively, as detailed by Pulliam.[38] ARC2D and ARC3D used generalized coordinates and implicit finite difference schemes to solve for inviscid and viscous flows over airfoils or wings, respectively, with either time accurate or accelerated non-time accurate steady state methods. Viscous solutions were based on the Thin Shear Layer Navier-Stokes equations.

OVERFLOW [28] is the NASA developed research code which evolved, in part, from ARC3D. OVERFLOW remained, with ARC3D as its kernel, a compressible, two- or three-dimensional flow solver using implicit finite difference schemes and time accurate or accelerated, non-time accurate steady state methods. Two significant changes dramatically increased the capabilities of OVERFLOW over ARC3D. First, OVERFLOW has the ability to handle complex geometries through the use of the chimera or overset grid approach. The chimera grid scheme was used extensively in this effort (see Section 4.2.2.3). The second significant change in OVERFLOW was the incorporation of an option to include the viscous cross coupling terms. This improved the flow physics model to a full RANS simulation. This option

was used for all computational experiments in this study to ensure using the highest quality model of the subject flow field.

The most recent improvements implemented by Jespersen, Pulliam, and Buning [39] included a multigrid method, a preconditioning algorithm for faster convergence and improved solution quality at low-Mach numbers, and a matrix dissipation algorithm to improve solution quality. Multigrid is the process of systematically using finer grids to accelerate the convergence of the flow solver. The default multigrid algorithm in OVERFLOW uses 300 iterations at each of 3 grid resolution levels. Each coarser grid is constructed using every other grid node along each direction of the next finer grid. In this implementation, there are no restrictions on grid size to achieve a proper, coarser grid. After advancing the solution on the coarsest grid for a specified iteration count, the solution is interpolated to the next finer grid and again advanced. This cycle is repeated until the solution is advanced the specified number of iterations on the finest grid, which corresponds to the original, user-defined mesh. Note, the current default is to neglect the viscous terms in solving on the coarser grids. Multigrid was used extensively in these computational experiments. The low-Mach number preconditioning algorithm improves solution quality and convergence speed for steady flows, specifically those at a freestream Mach number less than 0.2. This modification was not used during these experiments to avoid any corruption of a potential unsteady result. The matrix dissipation method replaced the scalar artificial dissipation previously used with central space differencing, the differencing scheme used for these computational experiments. The non-linear scalar dissipation used second and fourth order difference operators based on the spectral radius. The matrix

dissipation method instead uses a matrix based on the absolute value of the eigenvalues. Although the computational work increases using the matrix dissipation versus the scalar dissipation, the result is improved solution accuracy in resolving boundary layer profiles. Matrix dissipation was used in all computational experiments conducted for this work.

All configurations tested during these experiments were initiated with 250 total iterations of the full multigrid method to smooth large, initial gradients. For all smooth, baseline NACA 0015 airfoil tests, the solutions were then advanced 3,000 to 4,000 iterations using the accelerated, non-time accurate steady state method. Typically, the solution was then advanced 1,000 time accurate iterations to finely resolve the flow field. After advancing through the full multigrid process, all configurations modified with protuberances were advanced using the first-order, time accurate method. The solutions required an additional 15,000 to 30,000 iterations.

4.3.4 CONVERGENCE CRITERIA

Solution convergence was determined based on the iteration history of the airfoil force coefficients and the L_2-Norm or Euclidean Norm of the flux variables, Q_i. The iteration history of these parameters was monitored through the graphical interface OVERPLOT (see Section 4.4). The L_2-Norm is defined as:

$$L_2\text{–}Norm = \sqrt{\frac{1}{NPoints}\left(\sum_{i=1}^{NPoints} (Q_{i,\,old} - Q_{i,\,new})^2\right)} \qquad (4.9)$$

For these experiments, gross convergence was assumed when the L_2-Norm of the residual of the flux variables achieved approximately constant values and final convergence was recognized when the airfoil lift and drag coefficients achieved approximately constant values. With protuberances present, the solutions required 15,000 to 30,000 iterations to converge depending on the complexity of the flow field as determined by protuberance geometry, protuberance location, and airfoil angle-of-attack.

4.4 ANALYSIS OF RESULTS

Analysis of the computational solution produced by OVERFLOW involved examining the lift and drag force data and the pressure data and the creation and study of flow visualization output.

NASA Ames created the FOMOCO Utilities [40] specifically to compute the force and moment coefficients for flow solutions utilizing overset grids. The package could be used in a stand-alone mode, but was most powerful coupled to OVERFLOW. MIXSUR, a pre-processing module, created an integrated surface grid over which to perform the surface integration. The OVERINT module calculated the force and moment coefficients. This module could be used in a stand-alone mode or it could be called by OVERFLOW at a specified iteration interval. This tool was extensively used in conjunction with OVERFLOW at the default interval of 10 iterations. The force and moment coefficient files generated by OVERINT and the residual output files created by OVERFLOW could be post-processed using two different components of FOMOCO Utilities. OVERPLOT displayed the lift, drag, side, X, Y, and Z force

coefficient iteration histories, each separated into their viscous, pressure, momentum, and total components, and the residual histories of the L_2- and L_∞-Norms of the "right hand side" of the numerical method or of the flux variables. OVERHIST created a data file of the same results which was compatible with widely available plotting routines.

Flow visualization was accomplished using PLOT3D, [41] a graphics display program designed for computational fluid dynamics and, specifically, chimera grids and the presentation of their solution files.

CHAPTER 5 COMPUTATIONAL EXPERIMENTS

5.1 OBJECTIVES

The primary purpose of the computational experiments was to further the understanding of the phenomenological explanation of the surface roughness induced lift effect. The use of numerical simulations greatly improves the ability to resolve and therefore study the details of the flow field and the resulting flow structures.

The secondary and more specific objectives were to study two-dimensional single and multiple protuberance configurations distributed along the lower surface of an otherwise smooth NACA 0015 airfoil. The single protuberance study examined the effects of airfoil angle-of-attack, protuberance location along the airfoil surface, and protuberance geometry. The multiple protuberance study investigated the effects of protuberance spacing using two protuberance configurations.

5.2 COMPUTATIONAL EXPERIMENT DESIGN

5.2.1 EXPERIMENTAL METHOD

Two-dimensional computational experiments were conducted using the OVERFLOW solver. Details of this solver and the numerical method employed were presented in Section 4.3.

5.2.2 COMPUTATIONAL MODEL

The airfoil and protuberance surfaces and the flow field were modeled using the chimera grid scheme detailed in Section 4.2.

5.2.3 TEST MATRIX

Based on the wind tunnel test conditions, the freestream flow conditions were fixed for these computational experiments at a freestream Mach number of 0.15 and a freestream Reynolds number of 1.5×10^6. A fully turbulent flow field was simulated using the Spalart-Allmaras 1-equation turbulence model.

The effect of protuberance geometry was studied using a single protuberance at 0.28c and the configurations identified in Table 5-1. The configuration of h = 0.006c and λ = 0.01c was the baseline protuberance for the computational experiments. The airfoil angle-of-attack was set at zero degrees.

Width, λ	Height, h 0.002c	0.0036c	0.006c
0.002c			X
0.0055c	X	X	X
0.01c		X	Baseline

Table 5-1. Protuberance Geometry Configurations

The effect of airfoil angle-of-attack was studied using a single, baseline protuberance centered at 0.28c on the airfoil surface. The angle-of-attack was varied as:

- 0 degrees;

- 4 degrees;
- 6 degrees;
- 8 degrees;
- 10 degrees;
- 12 degrees.

Protuberance location along the lower surface was studied using a single, baseline protuberance. The airfoil angle-of-attack was set at 6 degrees. Location varied as:

- 0.17c;
- 0.28c;
- 0.40c;
- 0.57c.

The effect of utilizing multiple protuberances and the resulting interactions was studied using the baseline protuberance. The airfoil angle-of-attack was set at 10 degrees. Two protuberance configurations were investigated with the protuberance locations specified as:

- 0.28c and 0.33c (0.05c spacing);
- 0.28c and 0.36c (0.08c spacing);
- 0.28c and 0.40c (0.12c spacing).

The performance baseline for all cases presented was the computational results for the smooth NACA 0015 airfoil.

5.3 RESULTS: BASELINE CONFIGURATION

An experiment was conducted using the baseline NACA 0015 airfoil configuration to determine a suitable grid scheme for which the calculated aerodynamic performance compared favorably with established experimental results to ensure adequate representation of known performance.

5.3.1 BASELINE AIRFOIL GRID INVESTIGATION

Numerical experiments of a NACA 0015 airfoil at 2 degrees angle-of-attack were conducted using the following grids at the baseline conditions to identify and reduce calculated aerodynamic performance dependence on grid selection:

- Baseline: Single C-grid of dimension 275x65 with 100 grid points on each surface of the airfoil and 39 points along each side of the wake cut; Initial boundary layer spacing of $5 \times 10^{-6}c$; Initial surface grid spacing at leading and trailing edges of 0.001c and 0.002c, respectively; Far field located at ~5c from airfoil surface.
- Fine Wake Spacing: Identical to Baseline grid except for doubling the number of points along each side of the wake cut to 78 for increased dimension of 353x65.
- Increased Far Field: Identical to Baseline grid except far field distance from the airfoil was increased to ~30c and extended downstream from the trailing edge to ~15c; Number of points along each side of wake cut increased to 65; Increased number of points in direction perpendicular to surface for grid dimension of 327x89.

- Fine Airfoil Spacing: Identical to Baseline grid except initial surface grid spacing at trailing edge set to 0.0001c; Increased number of points along each airfoil surface to 110 and along each side of wake cut to 45 due to finer grid spacing; New grid dimension of 307x65.
- Two Grid Baseline: Chimera grid approach integrated an airfoil grid and a wake cut grid; Airfoil grid was 227x65 and composed of 100 points along each surface of airfoil and 15 points along short wake cut of 0.1c; Airfoil grid used same initial boundary layer spacing, initial surface grid spacing, and far field boundary as Baseline grid; Wake cut grid of dimension 79x39 started 0.015c behind airfoil trailing edge and extended ~5c; Wake cut grid initial spacing perpendicular to extended chord was 1×10^{-4}c.
- Three Grid Baseline: Chimera grid approach integrated airfoil grid (221x50), wake cut grid (63x25), and far field grid (73x61); See Section 4.2.1 for surface grid definition and Section 4.2.2 for volume grid definition.
- Three Grid Extended: Identical to Three Grid Baseline except far field grid of dimension 91x79 extended to ~30c from airfoil surface in all directions.

Configuration	C_l	ΔC_l Off Baseline	C_d	ΔC_d Off Baseline	# Grid Points
Baseline	0.2043	--	0.0113	--	17,875
Fine Wake Spacing	0.2042	-0.05%	0.0113	0.00%	22,945
Increased Far Field	0.2179	6.66%	0.0111	-1.77%	29,103
Fine Airfoil Spacing	0.2009	-1.66%	0.0113	0.00%	19,955
Two Grid Baseline	0.2041	-0.10%	0.0112	-0.88%	17,836
Three Grid Baseline	0.2150	5.24%	0.0109	-3.54%	17,078
Three Grid Extended	0.2198	7.59%	0.0107	-5.31%	19,814

Table 5-2. Comparison of Computational Results with Grid Configuration

A three grid chimera approach was decided upon based on the results presented in Table 5-2 and because of the efficiency of this approach when used in combination with OVERFLOW. The three grid scheme clustered grid spacing in high gradient regions and expanded the grid in relatively low gradient regions. In doing so, this scheme was more efficient in capturing the flow field properties through its distribution of grid points and should result in fewer iterations required to achieve convergence by eliminating fine spacing in low gradient regions. No other grid generated and examined achieved a comparable distribution.

5.3.2 BASELINE AIRFOIL PERFORMANCE COMPARISON

Numerical experiments using a NACA 0015 airfoil at zero and 2 degrees angle-of-attack were conducted at the baseline conditions and were compared to existing experimental results to assess the validity of the computational results using

the three grid chimera approach. The experimental data were taken from the following:

- NACA Technical Report #460 [42]: Experimental test results from NACA Variable Density Tunnel; C_l taken at two degrees angle-of-attack; Reynolds number was 3.2×10^6.
- NACA Technical Report #824 [43]: Experimental test results from NACA Two-Dimensional Low-Turbulence Wind Tunnel; C_l taken at two degrees angle-of-attack; Reynolds number was 6×10^6.

Figure 5-1 graphically compares the computational results generated using the Three Grid Baseline with the NACA experimental data. The NACA airfoil data presented assumed a linear relationship between airfoil lift coefficient and angle-of-attack and was generated from the angle-of-attack at zero lift and the lift curve slope. The non-linear nature of the computational result was not consistent with potential theory. There was very good agreement between the computational results and the experimental results of NACA Technical Report #824. This report later formed the foundation of Abbott and von Doenhoff's Theory of Wing Sections and is a well-accepted baseline.

While the Variable Density Tunnel results were later challenged due to the suspected high freestream turbulence level of the tunnel, the results were insightful when examining the drag prediction. Table 5-3 compares quantitatively the minimum drag computed using the Three Grid Baseline and the Three Grid Extended with the NACA experimental results. The variation of the experimental drag measurements

highlight the dependence of drag on freestream turbulence levels. Although the turbulence level of the Variable Density Tunnel was never reported, [44] it is understood to have been relatively high. The Two-Dimensional Low-Turbulence Wind Tunnel was specifically designed to test airfoils at high Reynolds numbers in low turbulent flow and achieved a tunnel turbulence level on the order of a few hundredths of one percent.[43] Given the fully turbulent flow used in the computational simulation, the drag prediction was acceptable.

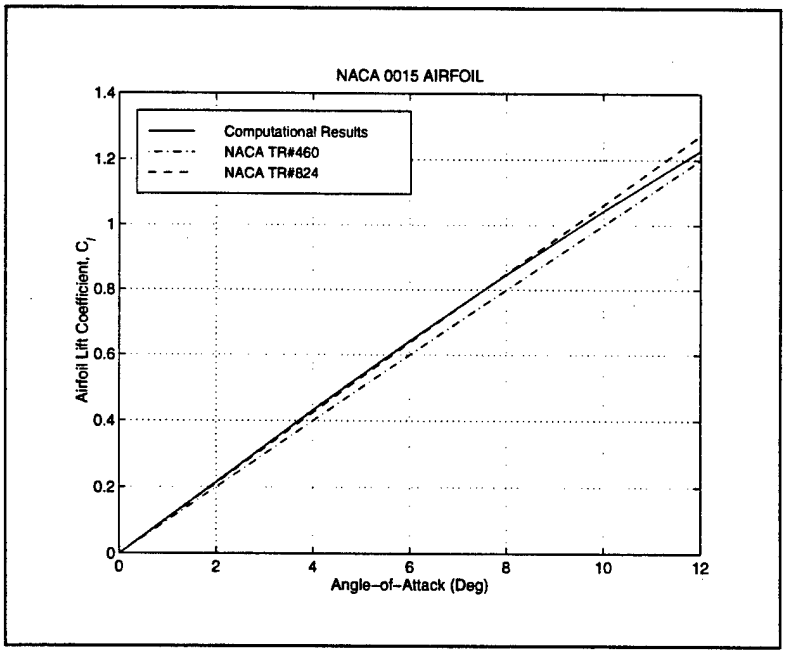

Figure 5-1. Comparison of Computed Lift Coefficient with Wind Tunnel Results

Configuration	C_l (α=2°)	$C_{d,o}$
Three Grid Baseline	0.2150	0.0105
Three Grid Extended	0.2198	0.0105
NACA TR #460	0.2000	0.0093
NACA TR #824	0.2124	0.0063

Table 5-3. Comparison of Computational Results with Wind Tunnel Results

Table 5-3 also quantitatively reinforces the very good agreement in lift coefficient for the Three Grid Baseline depicted in Figure 5-1. The variance from the NACA Technical Report #824 data was 1.22%.

Based on these findings, the Baseline Three Grid scheme was used for all computational experiments. Where appropriate, added to this was a protuberance grid. Composed of a NACA 0015 airfoil grid, a wake cut grid, and a far field cartesian grid, the geometry of the Baseline Three Grid scheme remained fixed for all computational experiments. The protuberance grid was the only grid varied as it was generated to model specific protuberance geometries.

Chord Location	Boundary Layer Thickness
0.17c	0.0024c
0.28c	0.0046c
0.40c	0.0072c
0.57c	0.0112c

Table 5-4. Calculated Boundary Layer Thickness for NACA 0015 Airfoil

The boundary layer thickness of the smooth airfoil was compared with the selected protuberance heights. Based on defining a boundary layer edge by 99% of the local freestream velocity, the boundary layer thickness was calculated for the smooth airfoil at zero degrees angle-of-attack under baseline conditions. The results, shown in Table 5-4, indicate that the protuberance heights selected matched the order of magnitude of the boundary layer thickness and were properly sized.

5.3.3 BASELINE AIRFOIL WITH PROTUBERANCE INVESTIGATION

Computational experiments using a NACA 0015 airfoil with a baseline protuberance at 0.28c were conducted at the baseline conditions to assess the adequacy of the protuberance grid and to identify the effect of the selected turbulence model.

An assessment of the adequacy of the protuberance grid was performed at zero degrees angle-of-attack. The assumed baseline grid was composed of the Three Grid Baseline combined with the protuberance grid detailed in Section 4.2. For this experiment, only the protuberance grid was modified by doubling the number of points in the direction normal to the body. The investigation was limited to the normal direction because, as will be shown in Section 5.4, large gradients occurred in that direction just downstream of the protuberance. All other parameters defining the protuberance grid remained constant. Table 5-5 compares the computational results of the finer protuberance grid with those of the baseline grid. The baseline grid proved exceptional in comparison to the finer protuberance grid based on the results shown as there was very little variation in the parameters studied. Based on these results, the baseline grid was used throughout the present work for all computational experiments.

	Baseline Grid	Fine Protuberance Grid
C_l	0.0452	0.0452
C_d	0.01653	0.01655
L/D	2.73	2.73
Re-Attachment Distance	0.0929c	0.0923c

Table 5-5. Comparison of Computational Results with Varying Protuberance Grid

The influence of the turbulence model was studied by comparing the computational results of the selected Spalart-Allmaras model with computational results using the 1-equation model of Baldwin and Barth.[45]

	$\alpha=0^o$ SA	BB	$\alpha=4^o$ SA	BB	$\alpha=10^o$ SA	BB
C_l	0.0452	0.0690	0.4568	0.4566	1.0478	1.0255
ΔC_l	0.0452	0.0690	0.0255	0.0324	0.0039	0.0035
C_d	0.0165	0.0165	0.0161	0.0162	0.0219	0.0226
L/D	2.74	4.18	28.37	28.18	47.84	45.37
Re-Attach Distance	0.0929c	0.1176c	0.0826c	0.0934c	0.0685c	0.0745c

Table 5-6. Comparison of Computational Results with Varying Turbulence Models

Computational results for the identified configuration using the Spalart-Allmaras (SA) model and the Baldwin-Barth (BB) model are presented in Table 5-6 for varying angles-of-attack. The choice of turbulence models clearly influences the magnitude of the computational results. However, the trends in aerodynamic

performance as measured by the force coefficients appear independent of the turbulence model selected. The difference in calculated lift coefficient was that the Baldwin-Barth model appeared to have a lower lift curve slope. The lift increment (ΔC_l) followed the same trend for both models. The calculated drag appeared independent of turbulence model until separation occurred near the trailing edge at higher angles-of-attack. Note, the presence of separation downstream of the protuberance did not appear to cause a variation in the drag but did cause a variation in the calculated lift. The variation in the lift-to-drag ratio can be attributed to the differences in lift. While the velocity vector field contained nearly identical structures, note that the Baldwin-Barth model consistently predicted a larger recirculation region as measured by the re-attachment distance. Detailed results of the force data are presented in Section 5.4.1.

A comparison of the calculated pressure distributions for the two turbulence models is shown in Figure 5-2. The two models produced nearly identical pressure distributions with two notable exceptions. First, the results differed slightly in the region near the protuberance. The Spalart-Allmaras model predicted larger pressure fluctuations over the protuberance and a smaller recirculation region. The second observation was also demonstrated by the re-attachment distance data presented in Table 5-6. Second, the models did not match in capturing the flow details near the trailing edge of the airfoil. These differences persisted for all angles-of-attack studied. Detailed results of the pressure data are presented in Section 5.4.2.

The effect of the selected turbulence model has been identified. The magnitude of the individual parameter results do vary in magnitude based on the turbulence model, but the aerodynamic performance trends appear consistent between models.

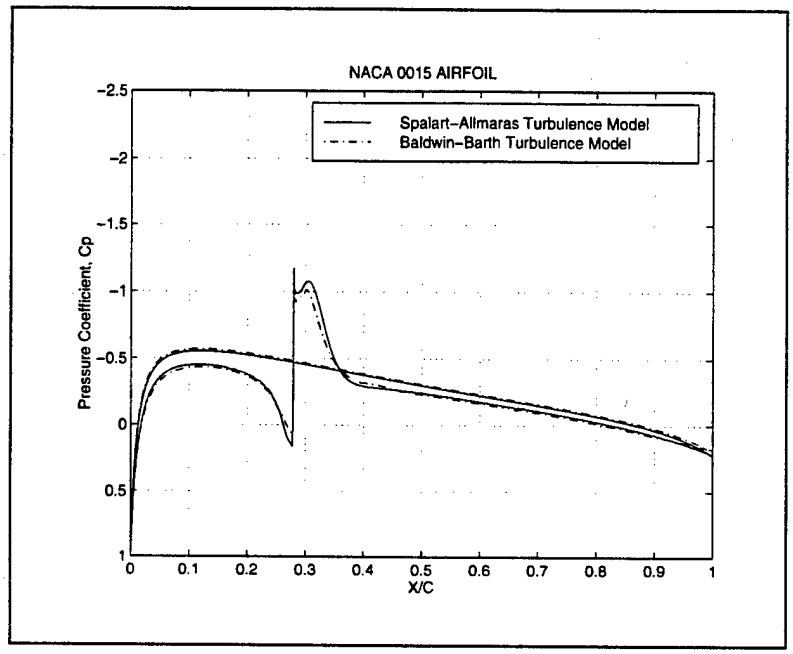

Figure 5-2. Effect of Turbulence Models on Pressure Distributions (α=0^o)

5.4 RESULTS: SINGLE PROTUBERANCE

Computational experiments of a NACA 0015 airfoil were conducted at the baseline conditions to investigate the effect of a single protuberance on the aerodynamic performance of the airfoil. The results presented were based on an analysis of the force data, the pressure data, and the visualization of the flow field properties.

5.4.1 FORCE DATA

Computational results of airfoil performance as measured by lift, drag, and the lift-to-drag ratio are presented for varying airfoil angle-of-attack, protuberance location, and protuberance geometry.

Angle-of-Attack. Comparison plots of computational results with varying airfoil angle-of-attack for an airfoil with a single baseline protuberance ($h = 0.006$, $\lambda = 0.01$) centered at 0.28c under the baseline test conditions are presented in Figure 5-3 through Figure 5-6.

Figure 5-3 shows that there is an increase in lift generated by the airfoil with the protuberance at low to moderate angles-of-attack and that there is positive lift generated at zero degrees angle-of-attack. Note, the lift curve for the airfoil with the protuberance has a similar shape with a slight upward shift. Figure 5-4 more clearly shows the positive lift increment across a wide range of angles-of-attack and the magnitude of the positive lift generated at zero degrees angle-of-attack. The lift increment washed out at approximately 12 degrees angle-of-attack. The total lift results presented were dominated by the pressure lift. The viscous and pressure components of lift were not presented separately as the viscous component remained essentially constant and was four to five orders of magnitude smaller than the pressure component for all configurations tested.

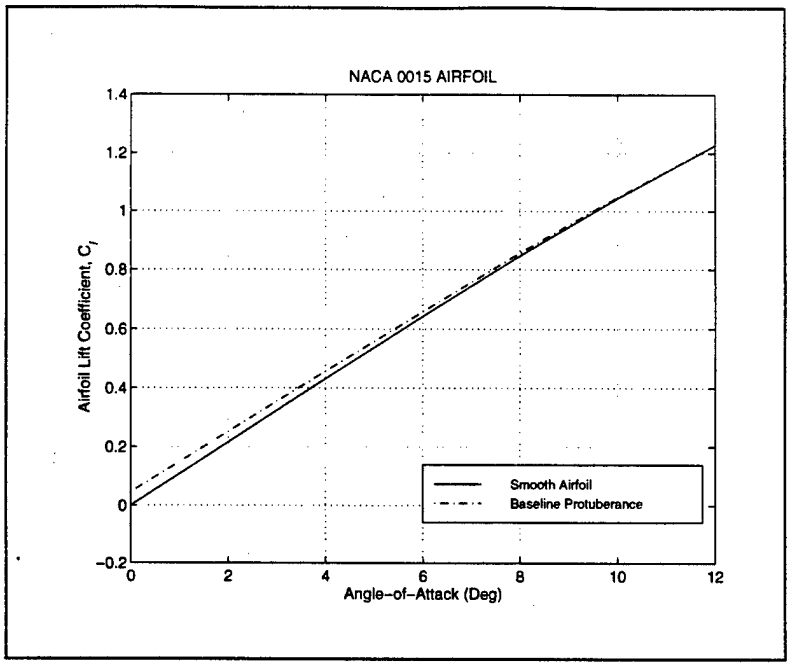

Figure 5-3. Lift as a Function of Angle-of-Attack

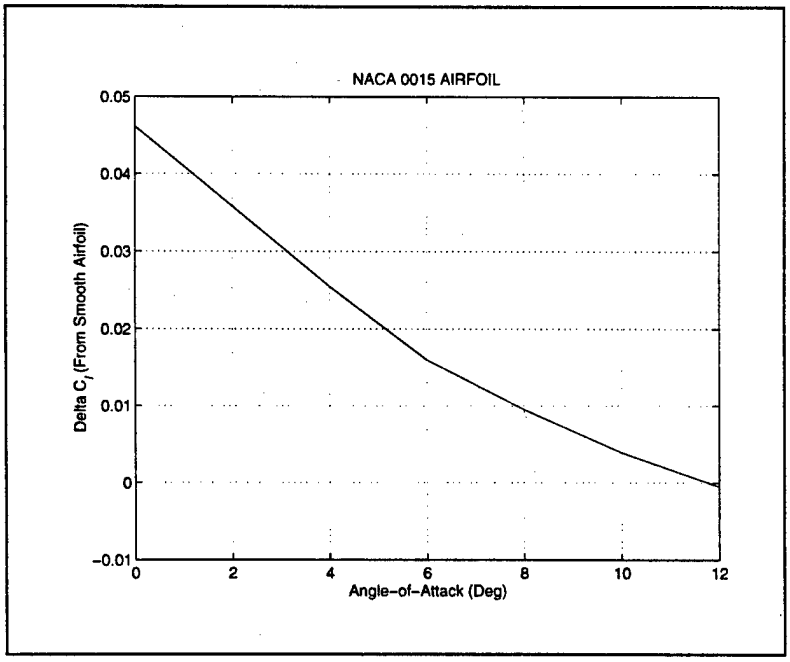

Figure 5-4. Lift Increment as a Function of Angle-of-Attack

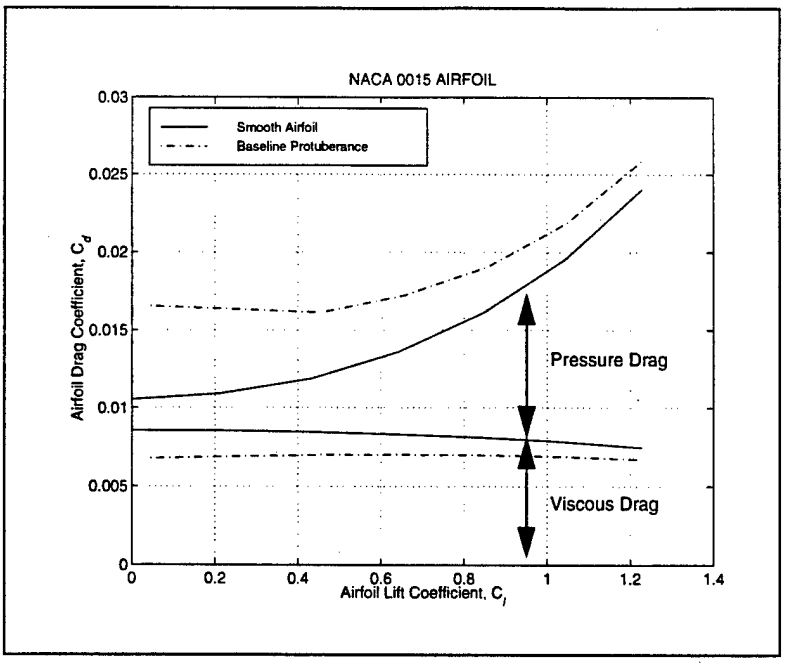

Figure 5-5. Drag as a Function of Lift

The viscous and pressure components of airfoil drag are identified separately in Figure 5-5 as a function of airfoil lift. In general, the drag increased with increased lift, though to a lesser extent with increasingly larger lift. The viscous drag for both the smooth and rough airfoils remained essentially constant over the angle-of-attack range tested. Interestingly, the rough airfoil had a lower viscous drag compared to the smooth airfoil. Figure 5-5 indicates that the performance effects were dominated by the changes in the pressure field as opposed to the viscous forces as evidence by the large increase in pressure drag for the rough airfoil.

For the airfoil attitudes tested, Figure 5-6 shows that the lift-to-drag ratio for the rough airfoil never matched nor exceeded the performance of the smooth airfoil.

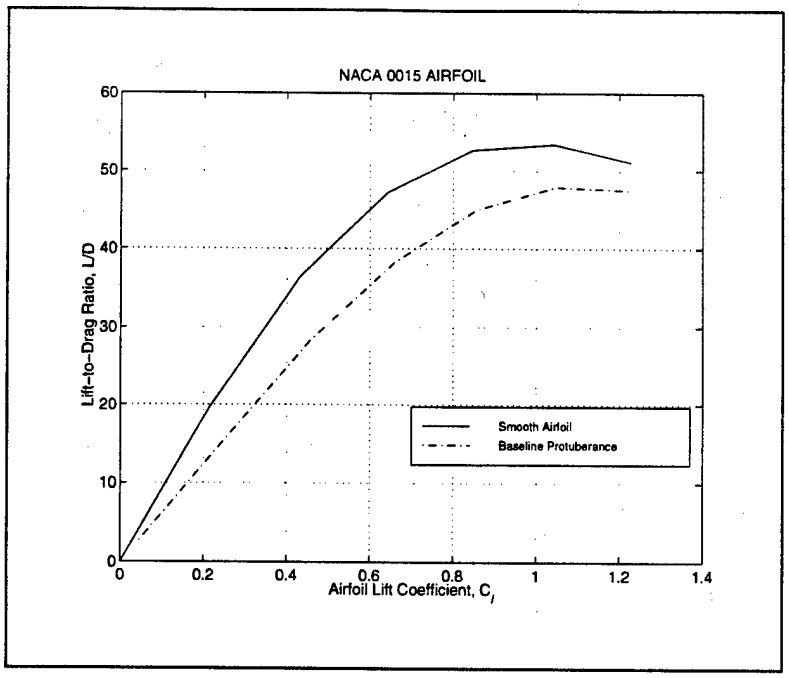

Figure 5-6. Lift-to-Drag Ratio as a Function of Lift

Location. Comparison plots of computational results for a NACA 0015 airfoil at 6 degrees angle-of-attack with a single baseline protuberance at varying chord locations under the baseline test conditions are presented in Figure 5-7 through Figure 5-9.

Figure 5-7 shows that for all chord locations tested for the rough airfoil configuration, there was additional lift generated as compared to the smooth airfoil. There was a correlation between protuberance location and airfoil lift, the lift increment increased as the protuberance moved further aft of the leading edge.

In general, Figure 5-8 indicates that the total drag remained essentially unchanged with varying protuberance location. The viscous drag was reduced over that of the smooth airfoil for all protuberance locations, the same trend noted in the angle-of-attack study.

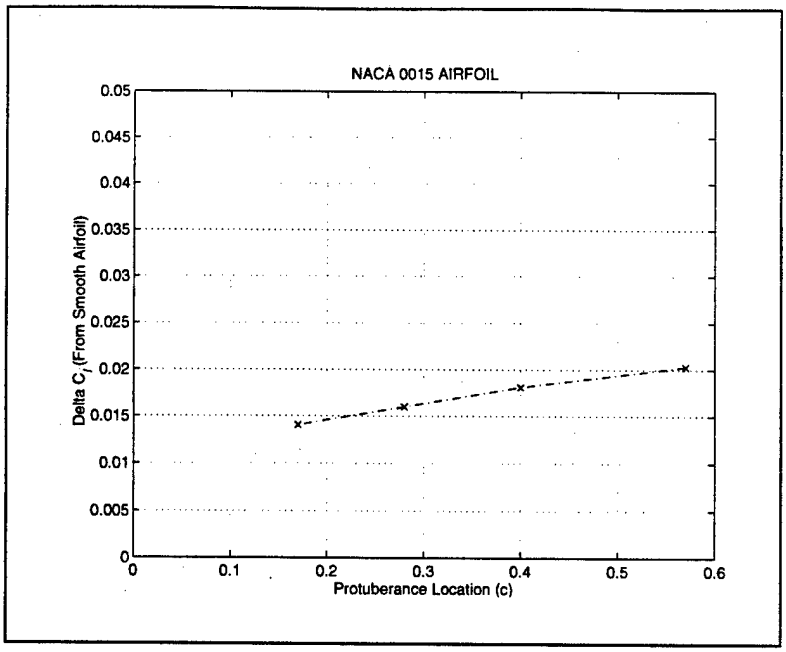

Figure 5-7. Lift Increment as a Function of Protuberance Location

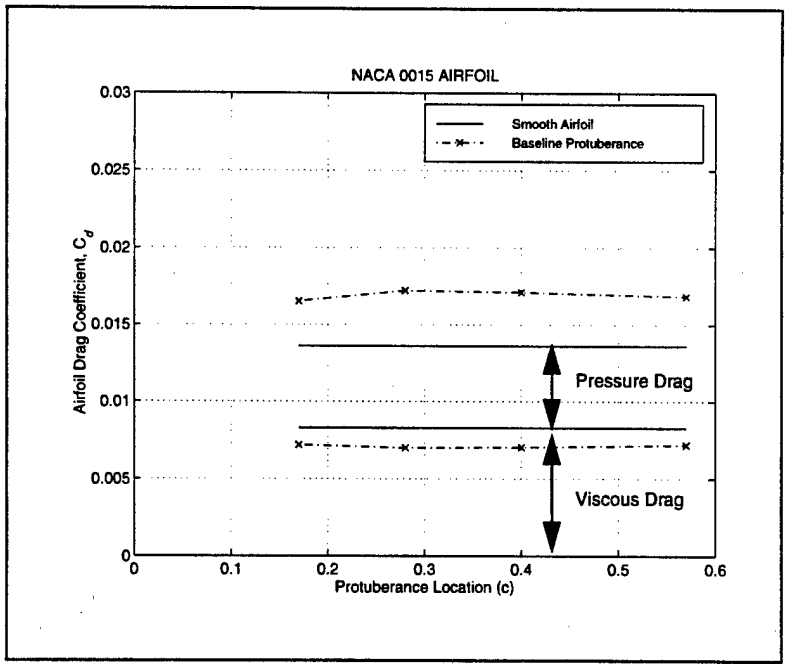

Figure 5-8. Drag as a Function of Protuberance Location

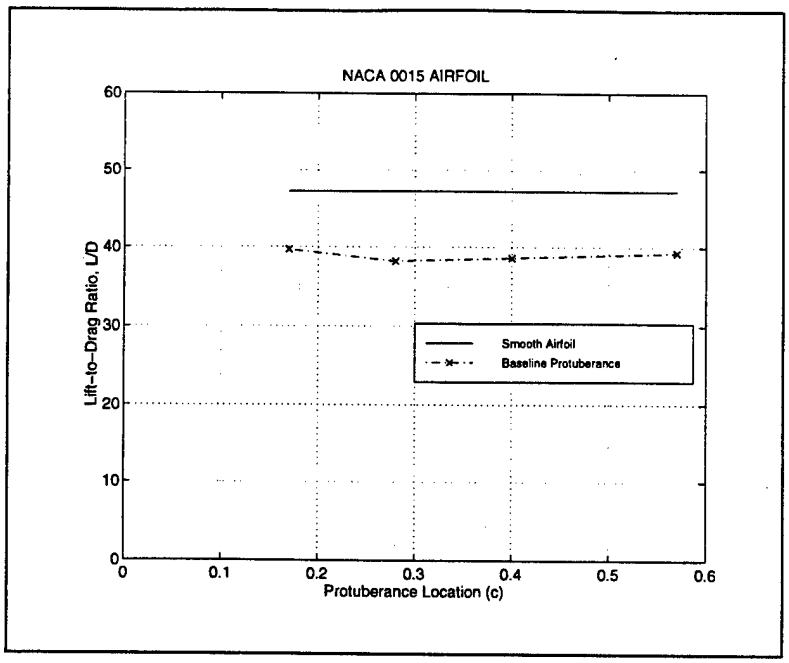

Figure 5-9. Lift-to-Drag Ratio as a Function of Protuberance Location

There was no strong effect of protuberance location on the airfoil lift-to-drag ratio as can be seen in Figure 5-9. Although the airfoil lift increased for aft protuberance locations, the airfoil drag remained constant and its magnitude dominated the much smaller change in lift resulting in the nearly constant lift-to-drag ratio. For all protuberance locations tested, the lift-to-drag ratio of the rough airfoil never matched nor exceeded that of the smooth airfoil.

Geometry. Comparison plots of computational results for a NACA 0015 airfoil at zero degrees angle-of-attack with a single baseline protuberance of independently varying height and width centered at 0.28c under the baseline test conditions are presented in Figure 5-10 through Figure 5-40.

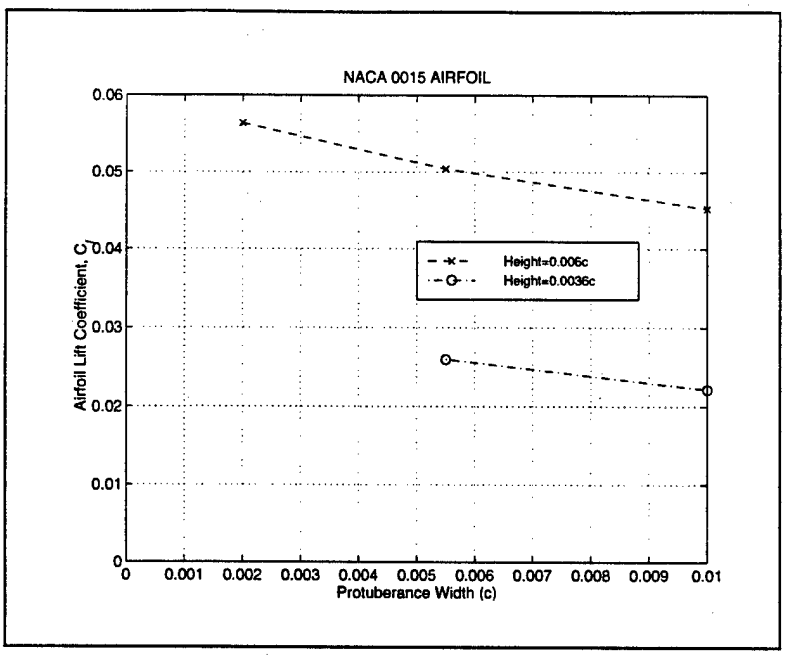

Figure 5-10. Lift as a Function of Protuberance Width

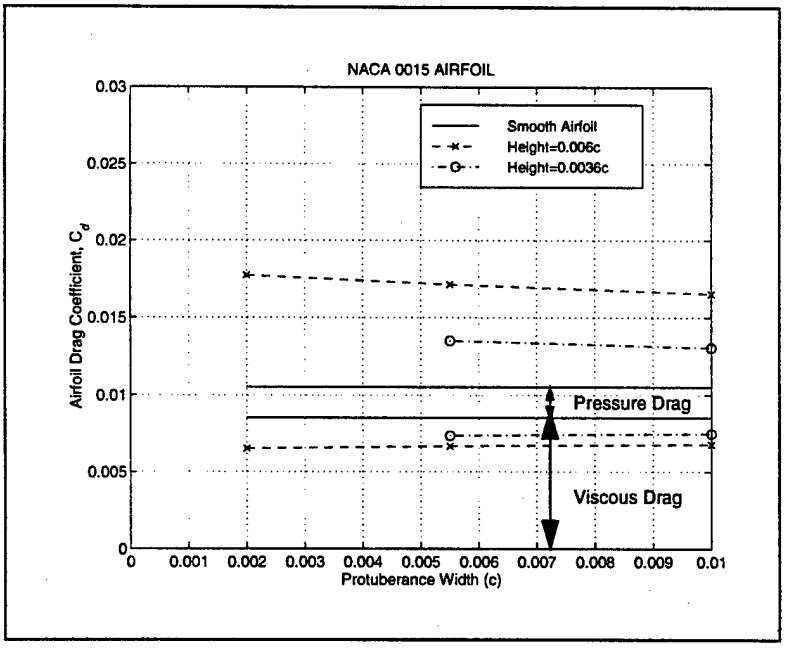

Figure 5-11. Drag as a Function of Protuberance Width

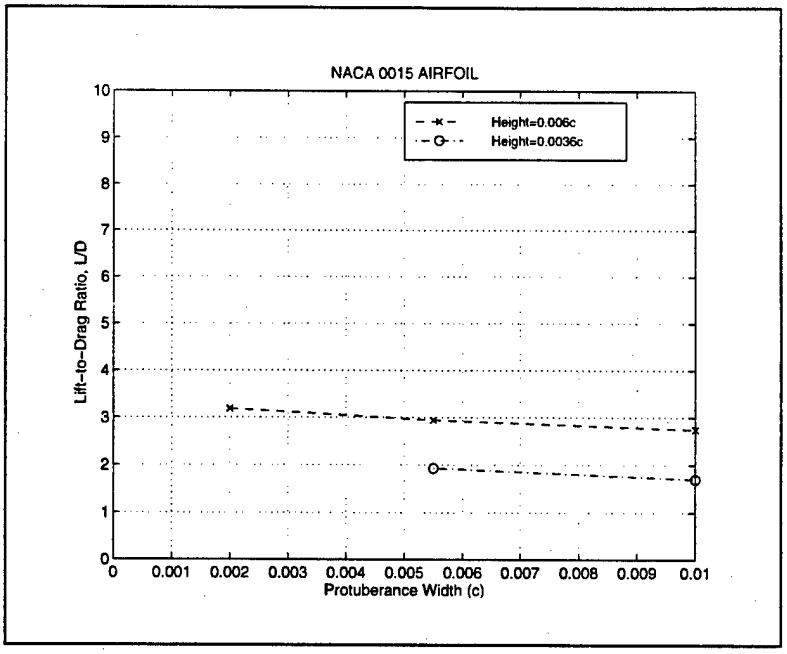

Figure 5-12. Lift-to-Drag Ratio as a Function of Protuberance Width

Figure 5-10 shows the influence of protuberance width on the rough airfoil lift performance. Additional lift was generated for all widths tested and there was a negative relationship between protuberance width and lift, increased protuberance width resulted in reduced lift. Figure 5-11 shows a similar trend with airfoil drag, increased protuberance width resulted in decreased drag. The influence, however, of the protuberance width on drag was not strong. Similarly, varying protuberance width had only a slight effect negative effect on the airfoil lift-to-ratio as seen in Figure 5-12.

Figure 5-13 through Figure 5-15 show that protuberance height was the dominant geometry parameter influencing the airfoil performance. In Figure 5-13, all protuberance heights tested produced positive lift increments, with taller protuberances generating larger increments. Increased protuberance height generated more airfoil drag as seen in Figure 5-14. Note that the viscous drag for the rough

airfoil was essentially constant and again below that of the smooth airfoil. Figure 5-15 shows that there was a positive correlation between protuberance height and the lift-to-drag ratio, as protuberance height increased, the lift-to-drag ratio increased. However, no protuberance geometry tested generated a lift-to-drag ratio that matched or exceeded that of the smooth airfoil.

Note that the weak influence of protuberance width on airfoil performance was demonstrated with the nearly overlaying performance curves for two different widths in Figure 5-13 through Figure 5-15. Additionally, the strong effect of protuberance height can be seen by the large performance differences for the two protuberance heights in Figure 5-10 through Figure 5-12.

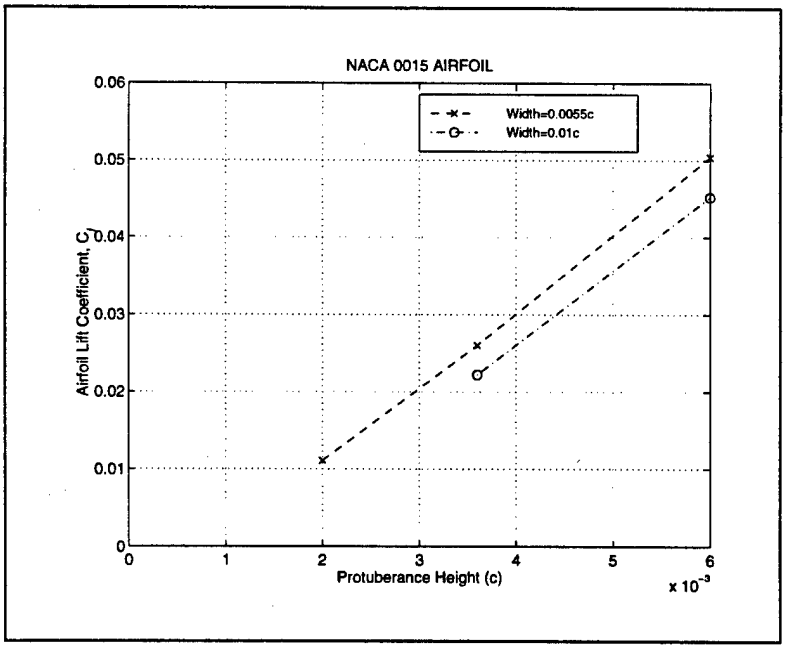

Figure 5-13. Lift as a Function of Protuberance Height

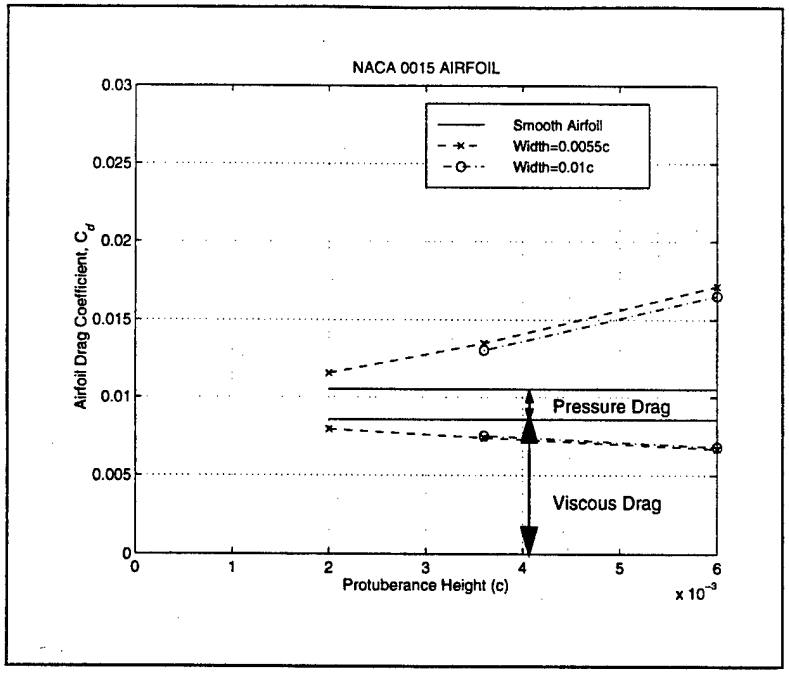

Figure 5-14. Drag as a Function of Protuberance Height

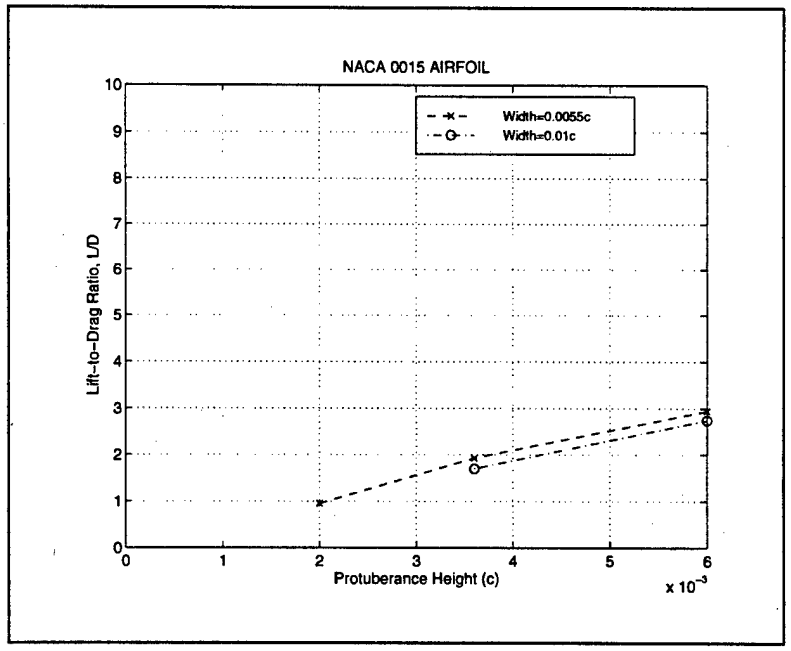

Figure 5-15. Lift-to-Drag Ratio as a Function of Protuberance Height

5.4.2 PRESSURE DATA

Pressure data results from the single protuberance studies were analyzed and are reported based on varying airfoil angle-of-attack, protuberance location, and protuberance geometry.

Angle-of-Attack. The results presented are for a baseline protuberance centered at 0.28c under baseline conditions. The presence of the two-dimensional protuberance created two changes to the pressure coefficient distribution over an airfoil. For 6 degrees angle-of-attack in Figure 5-16, the protuberance created a distinct pressure change in the immediate region of the protuberance and widened the pressure distribution overall, i.e. the pressure decreased over the upper surface and increased over the lower surface on the rough airfoil. The approximate result of the widened pressure distribution would be a greater lift. Near the protuberance, the flow neared stagnation conditions as it approached the forward face and the apex of the protuberance. There was a sudden expansion over the rearward surface and a commensurate decrease in pressure. The flow then recovered and pressure increased. As seen in Figure 5-17, the same trends can clearly be seen for zero degrees angle-of-attack, with the widening of the pressure distribution even more pronounced. These two characteristics persisted in all pressure coefficient contours for all angles-of-attack tested.

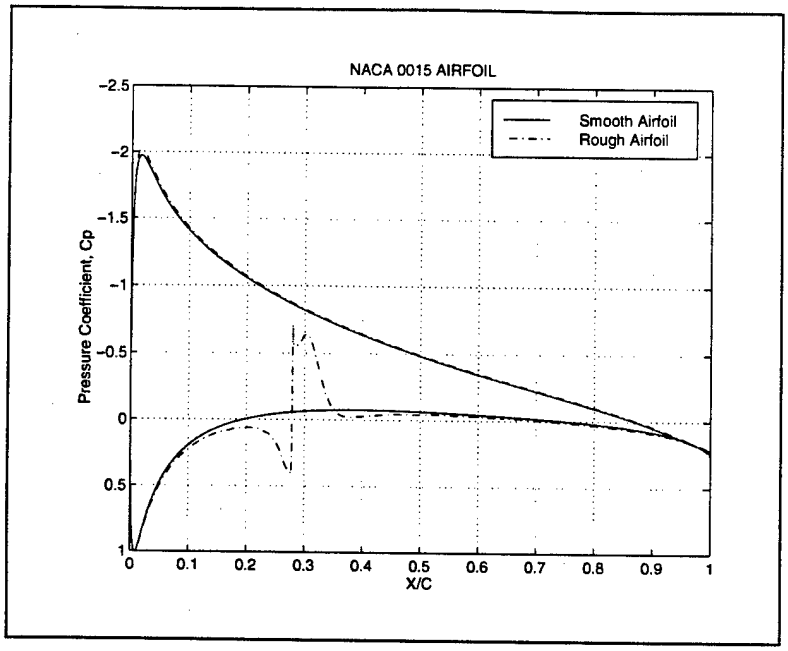

Figure 5-16. Pressure Coefficient Comparison Plot (α=6°)

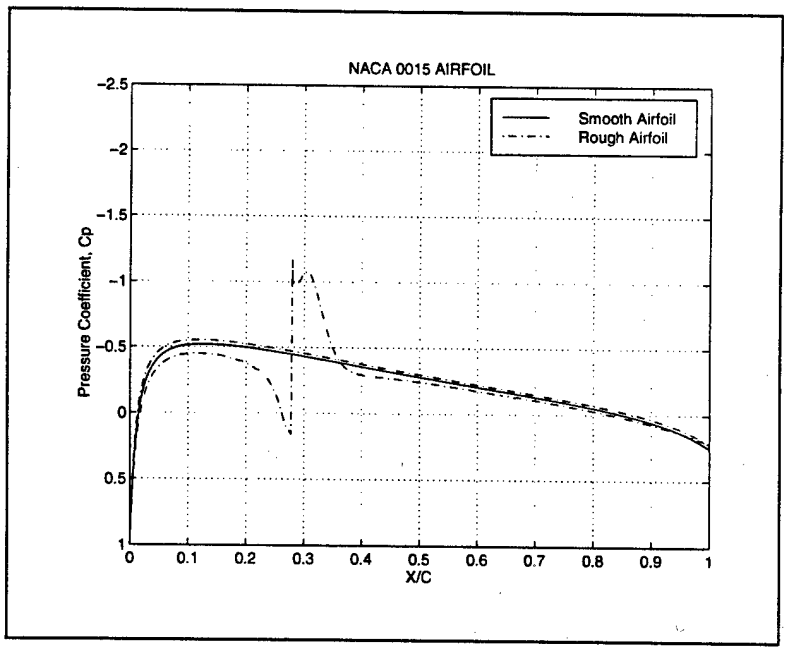

Figure 5-17. Pressure Coefficient Comparison Plot (α=0°)

The pressure data results for this configuration were also analyzed as a function of the ordinate of the symmetrical thickness distribution, or more generally the ordinate of the upper and lower surface. Pressure data plotted in this manner indicates a region of drag when the pressure against the upstream face is greater than the pressure against the downstream face and a region of thrust when the pressure against the upstream face is less than the pressure against the downstream face. In other words, the variation of the pressure distribution with respect to thickness represents the pressure drag generated by a configuration. For the zero degree angle-of-attack case shown in Figure 5-18, there was a unique pressure distribution about the protuberance and the effect of the protuberance was to dramatically increase the pressure drag. Note that there was a stagnation-like point on the upstream face of the protuberance and that the stagnation point of the airfoil moved aft slightly along the lower surface as evidenced by the shift in the rough airfoil pressure distribution. For 6 degrees angle-of-attack, Figure 5-19 shows that the unique pressure distribution about the protuberance persisted and that the protuberance generated a significant increase in the pressure drag.

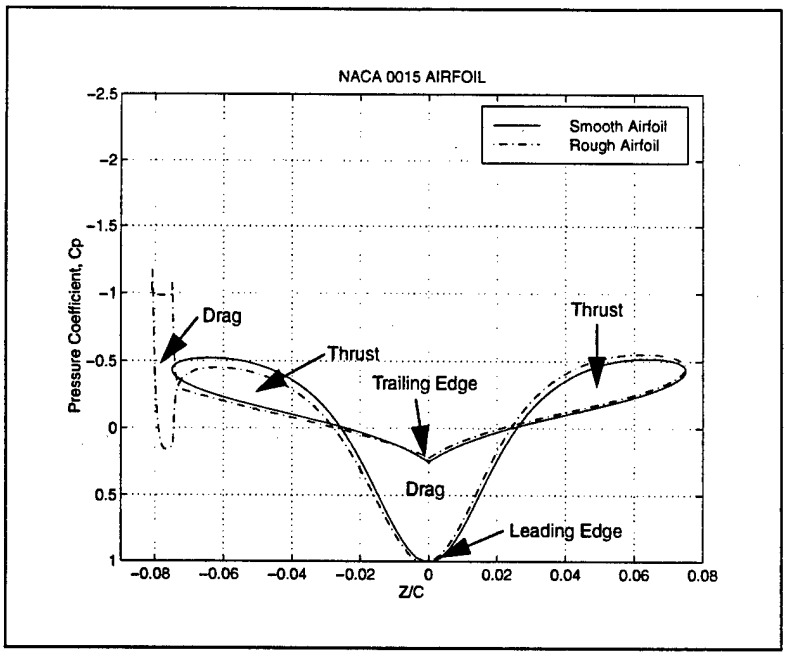

Figure 5-18. Pressure Coefficient Variation with Thickness (α=0°)

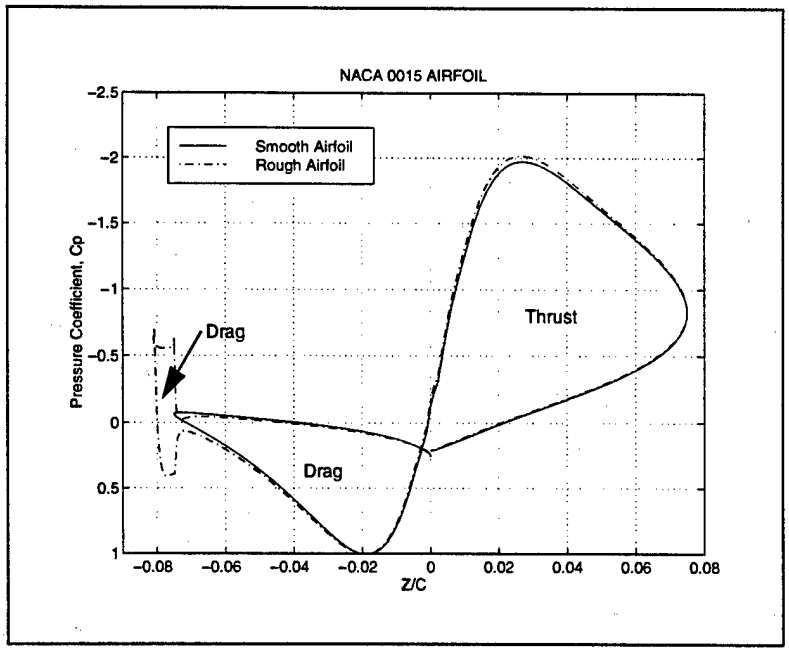

Figure 5-19. Pressure Coefficient Variation with Thickness (α=6°)

Location. The results presented are for a baseline protuberance at 6 degrees angle-of-attack under baseline conditions. The pressure coefficient contours of Figure 5-20 show the same two features described in the angle-of-attack study. In addition, the aft movement of the protuberance changed the shape of the distinct region near the protuberance. As the protuberance moved aft, there was a reduction in the magnitude of the pressure change resulting in a smaller velocity increase and relatively higher pressure along the bottom surface. The persistence of the pressure change increased as the protuberance moved toward the trailing edge. Combined with the pressure change, this resulted in the relatively higher pressure flow affecting the body over a greater surface area.

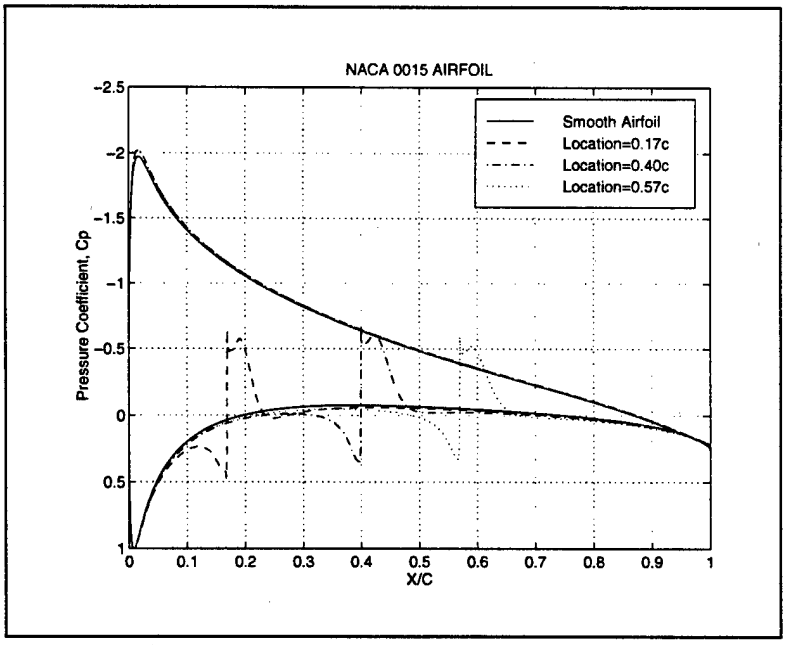

Figure 5-20. Pressure Coefficient Variation with Protuberance Location

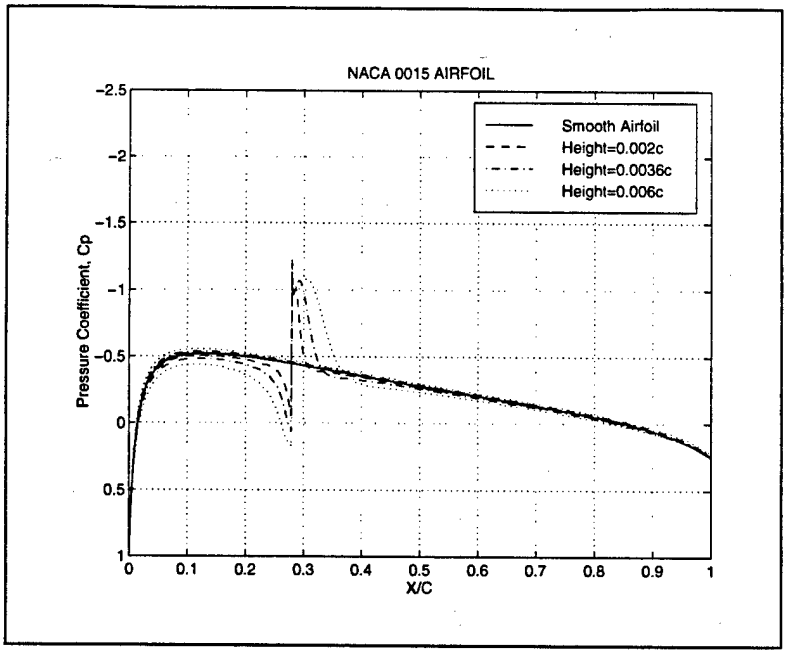

Figure 5-21. Pressure Coefficient Variation with Protuberance Height

Geometry. The results presented are for a single protuberance of varying height with a constant width of 0.0055c at zero degrees angle-of-attack under baseline conditions. Three different effects in Figure 5-21 can be attributed to the variation of protuberance height, the apparent dominant geometry factor. First, there was a clear increase in the pressure differences in the region near the protuberance with increased protuberance height, most notably a pressure increase upstream of the protuberance. Second, there was an increased persistence of the pressure changes near the protuberance as height increased. Last, there was a general increase in the area between the upper and lower surface contours.

The influence of protuberance width was not significant and no results are presented.

5.4.3 FLOW VISUALIZATION

Results from the single protuberance studies were analyzed based on the visualization of the velocity vector field, the pressure field, and the vorticity contours. Results for an airfoil with a baseline protuberance located at 0.28c under baseline conditions at zero degrees angle-of-attack are presented. The vorticity contours represent plot the vorticity magnitude between 7 and 10 at 0.1 intervals. This technique was used to identify the regions of high vorticity in the flow field and, because this level of vorticity approximates that found near the freestream edge of a boundary layer, as a coarse estimate of the edge of the boundary layer.

In the broad view of Figure 5-22, the velocity field is largely undisturbed except in the expected boundary layer and in the region near the protuberance. Figure 5-23 narrows the view to near the protuberance and shows a large recirculation region just downstream of the protuberance. This recirculation region is the primary flow structure created by the protuberance. Figure 5-24 shows the details of the flow in immediate proximity to the protuberance. This view shows three recirculation regions near the protuberance. The first is a small eddy just upstream of the protuberance and close to the airfoil surface. The second is a slightly larger recirculation region just downstream of the protuberance and close to the airfoil surface. The last is the large, primary structure. The extent of this recirculation region was measured based on the distance between the peak of the protuberance and the re-attachment point along the airfoil surface. For the configuration shown, this distance was 0.0929c. The final feature to note is the velocity vector direction of the flow as it moves across the peak of

the protuberance. The direction was influenced by airfoil angle-of-attack, protuberance location, and protuberance geometry.

The presence of the protuberance significantly changed the overall pressure field as shown in Figure 5-25. While the greatest change is noted along the lower surface, the protuberance presumably would effect the entire pressure field given the low-speed property of this flow. Evidence of this influence was already seen in the pressure distribution of Figure 5-17. Figure 5-26 details the larger pressure gradients near the protuberance and the higher, constant pressure region downstream of the protuberance. Comparison of the pressure field of the rough airfoil and the smooth airfoil showed no measurable shift in the stagnation point due to the presence of the protuberance.

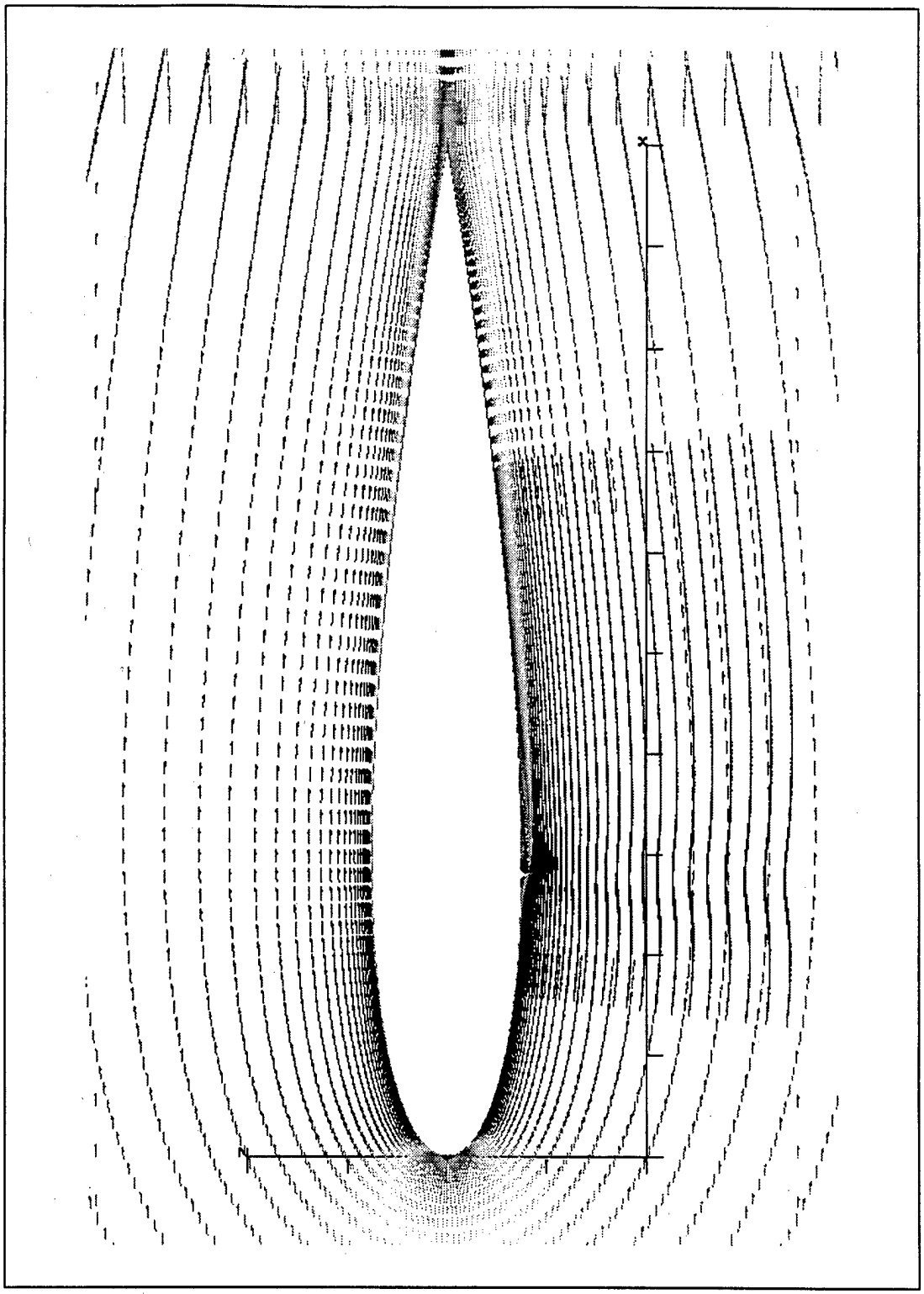

Figure 5-22. Velocity Vector Field About an Airfoil with a Baseline Protuberance

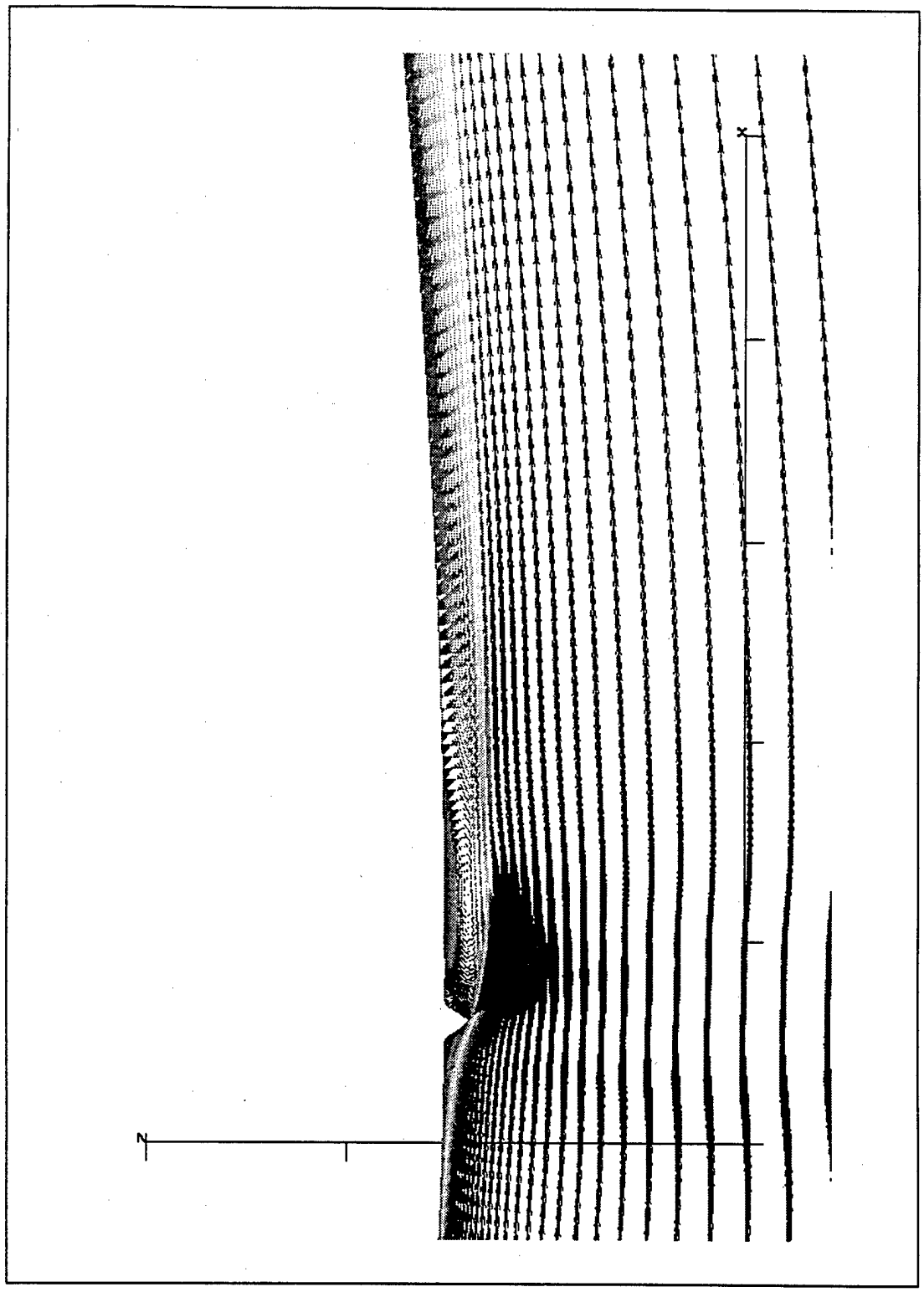

Figure 5-23. Zoom View of Velocity Vector Field About a Baseline Protuberance

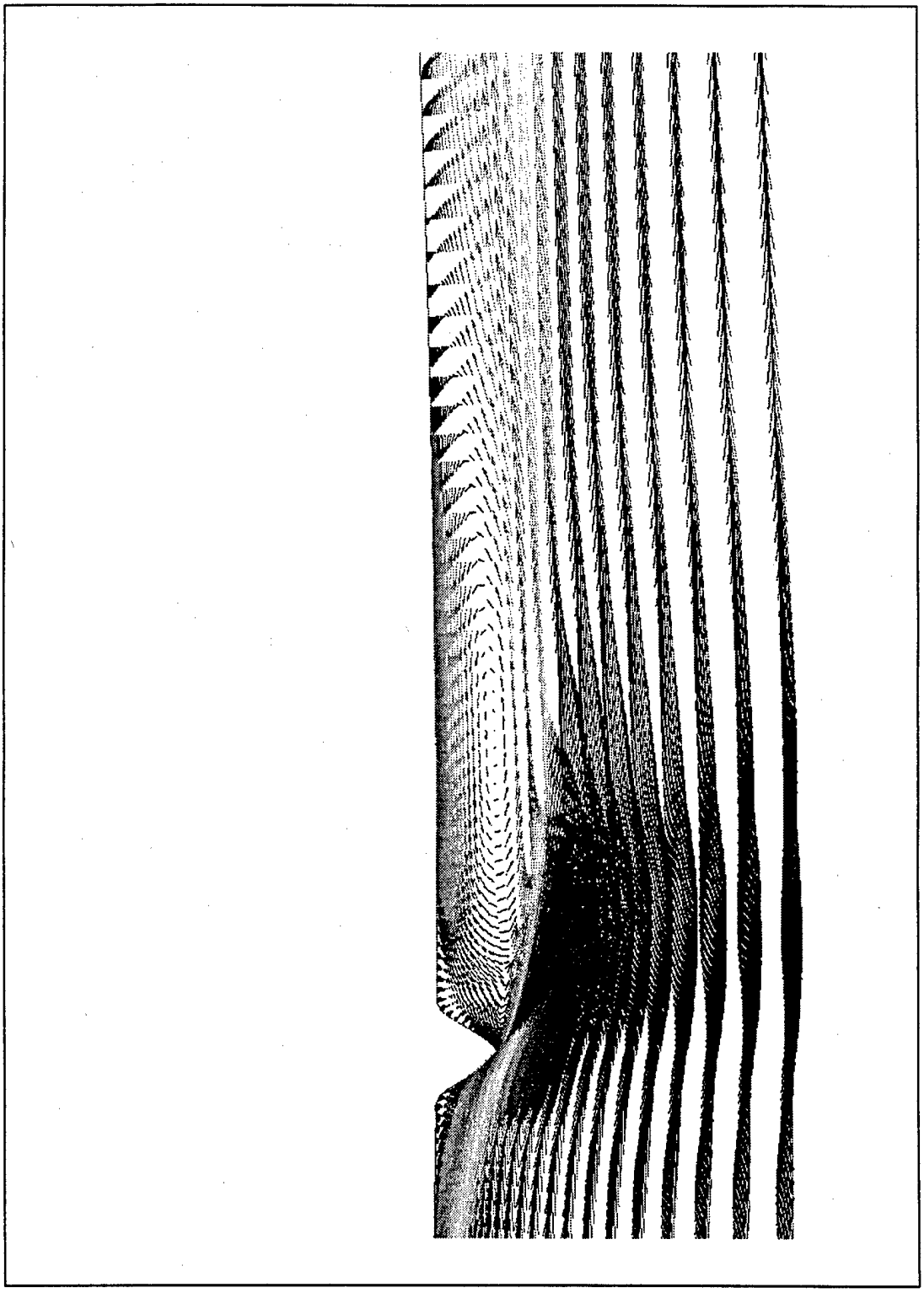

Figure 5-24. Local Velocity Vector Field About a Baseline Protuberance

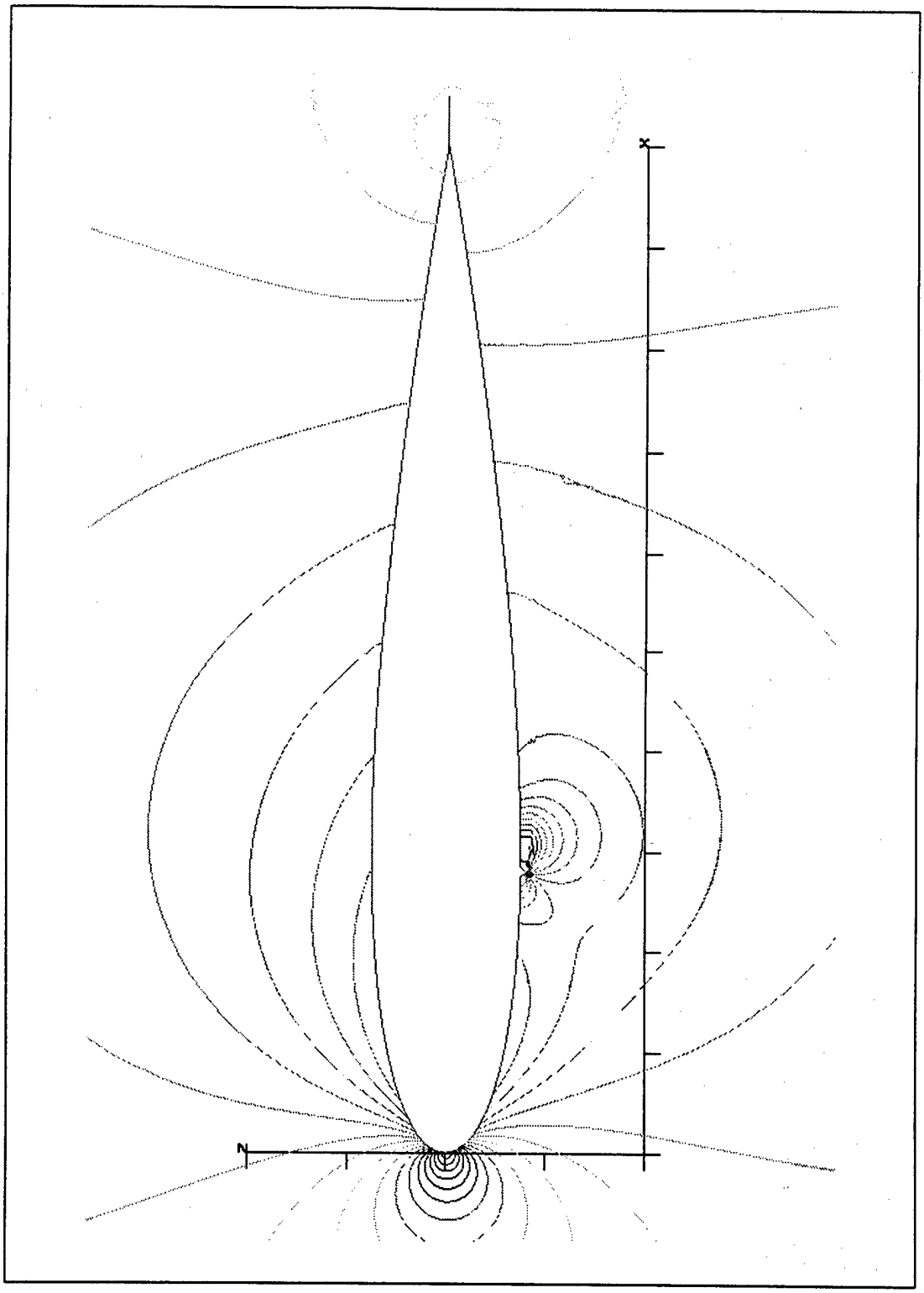

Figure 5-25. Pressure Field About an Airfoil with a Baseline Protuberance

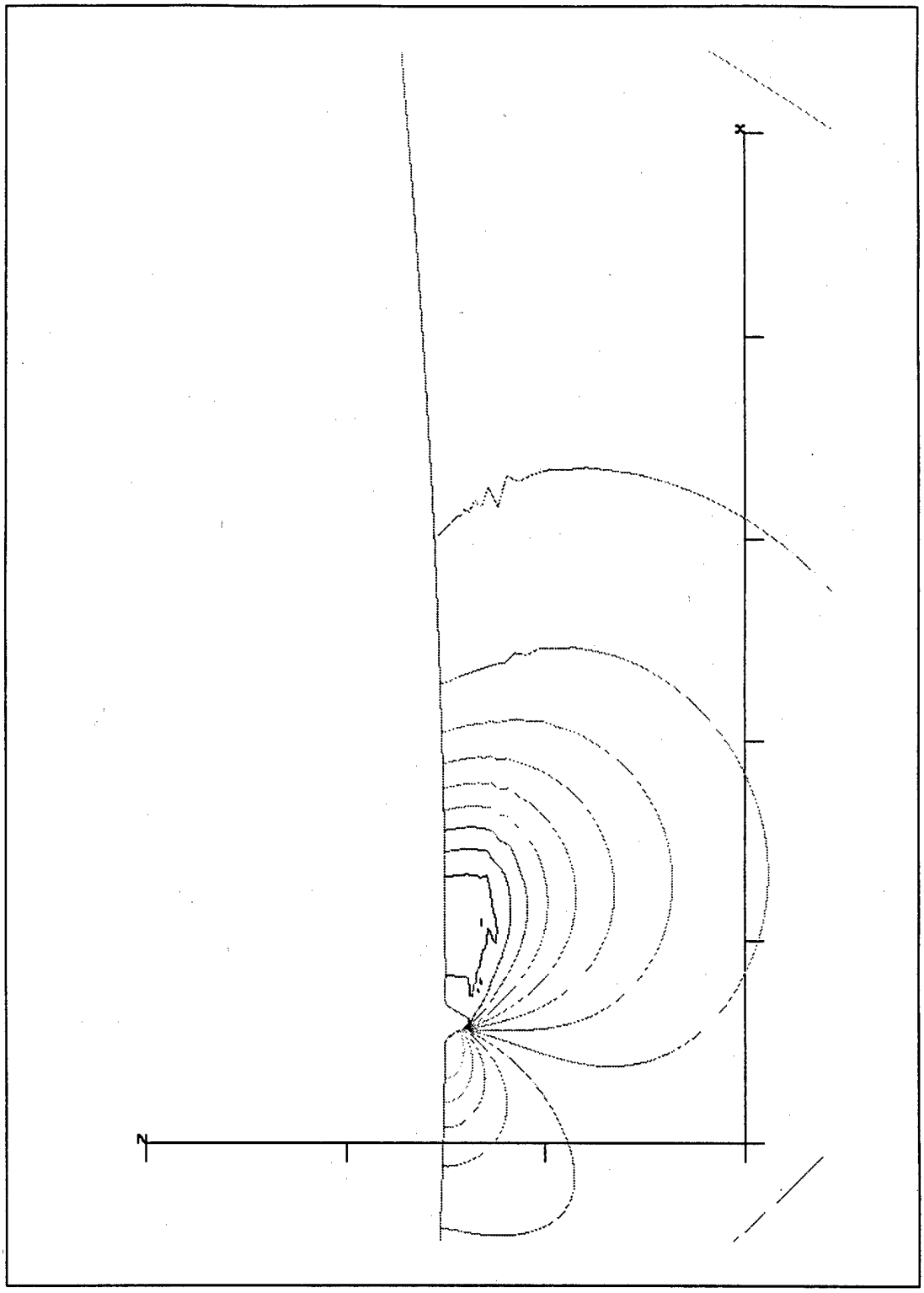

Figure 5-26. Zoom View of Pressure Field About a Baseline Protuberance

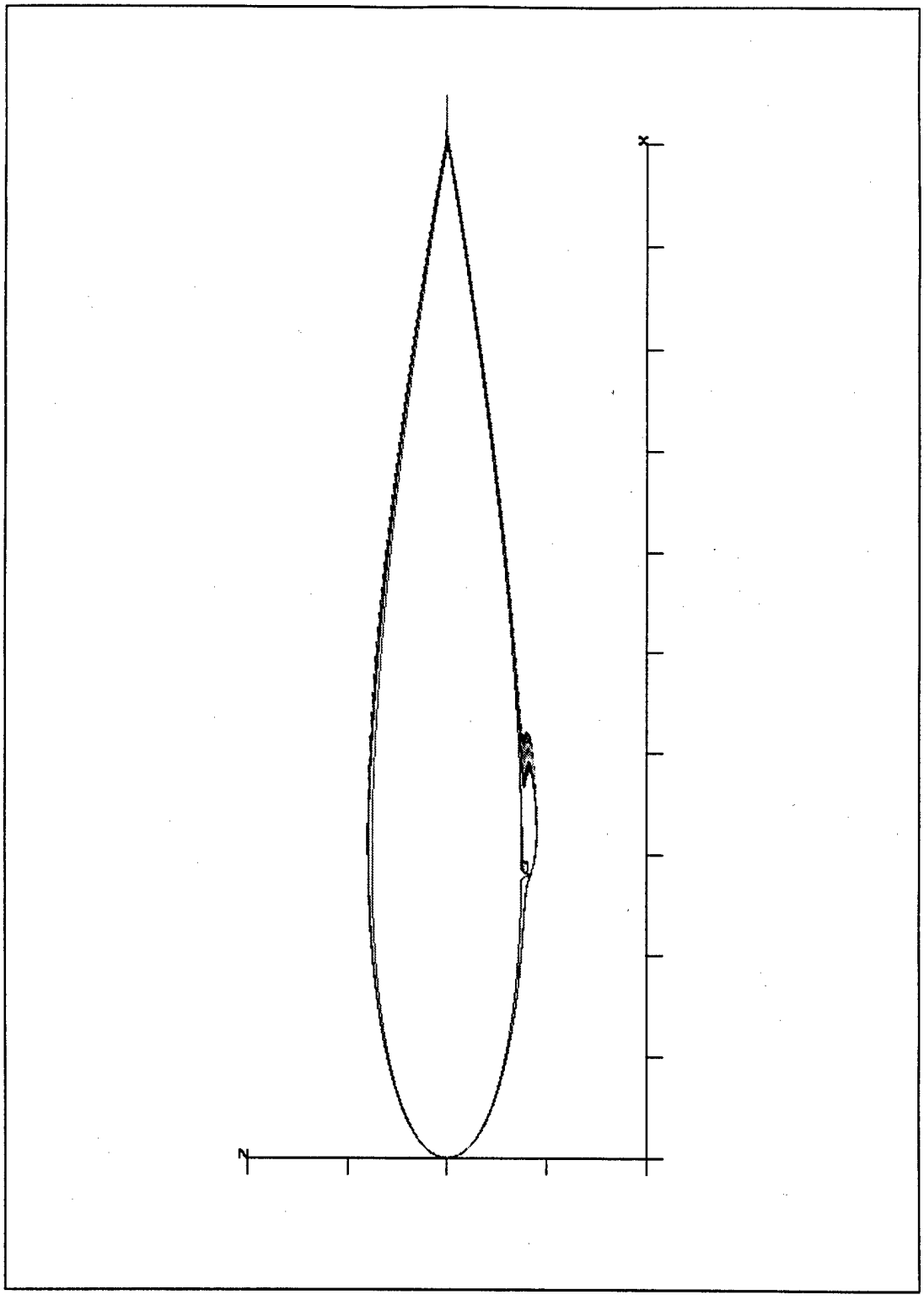

Figure 5-27. Vorticity Contours About an Airfoil with a Baseline Protuberance

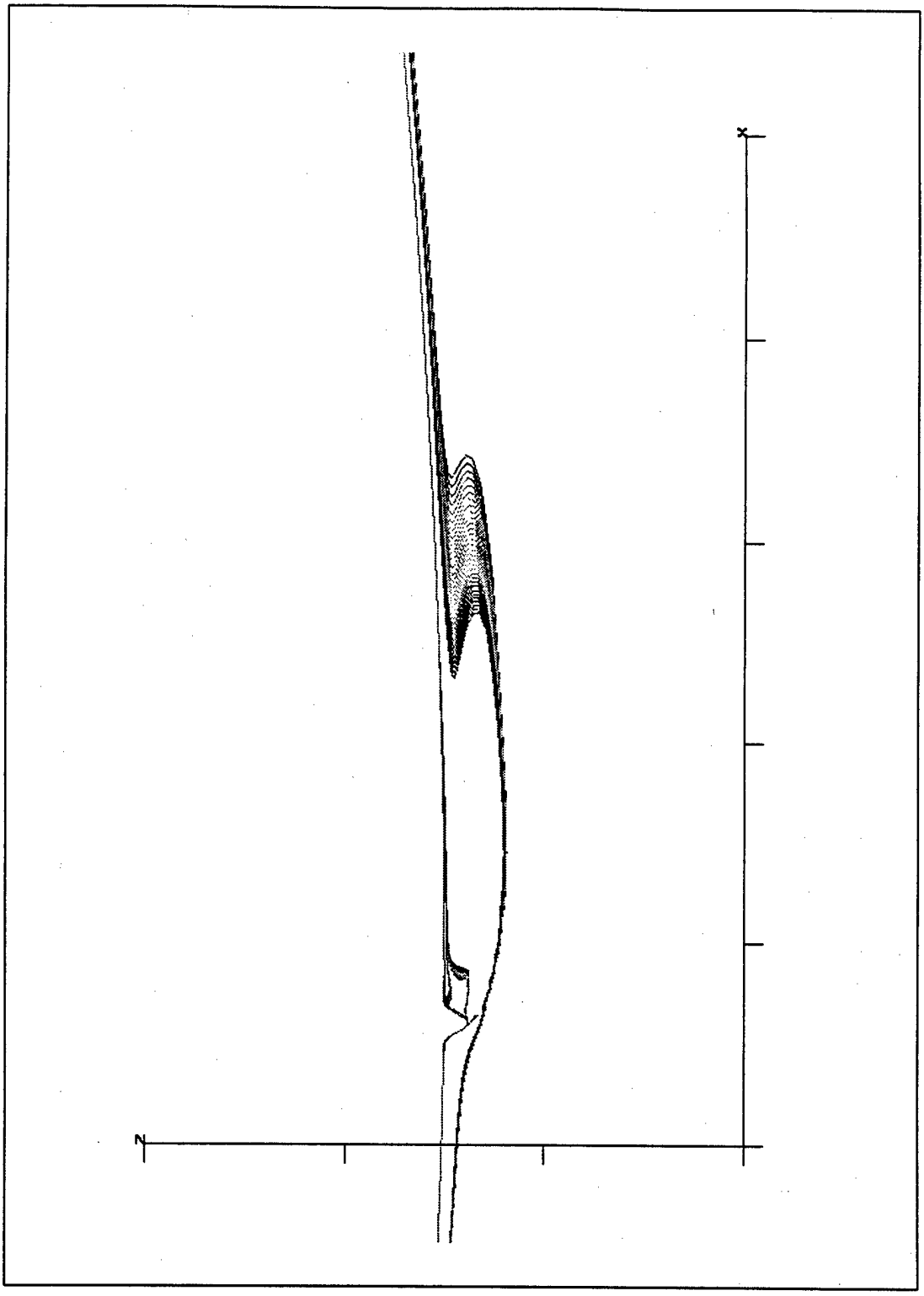

Figure 5-28. Zoom View of Vorticity Contours About a Baseline Protuberance

Figure 5-27 shows that the protuberance is a strong vorticity generator. Detail of the vorticity region is shown in Figure 5-28. The protuberance has a strong influence on vorticity downstream and a moderate influence upstream. Note that the area enveloped by the vorticity contour approximately equals the recirculation region.

For all flow field properties studied, the flow appeared steady with no noticeable fluctuations near convergence.

Structures in the flow fields about all other single protuberance configurations matched the results presented for this particular case and are not included.

5.4.4 FLOW RE-ATTACHMENT DISTANCE

Results from the single protuberance studies were analyzed based on the separated flow re-attachment distance and are reported based on varying airfoil angle-of-attack, protuberance location, and protuberance geometry.

Angle-of-Attack. The results presented are for a baseline protuberance centered at 0.28c under baseline conditions with varying angle-of-attack. Figure 5-29 shows a positive relationship between increasing flow re-attachment distance and increasing lift. The figure also emphasizes the extreme sensitivity of both the re-attachment distance and the lift increment with airfoil angle-of-attack. Figure 5-30 shows a negative correlation between re-attachment distance and airfoil drag, i.e. as re-attachment distance decreases, drag increases. Again, airfoil angle-of-attack is seen to be a dominant factor in determining the flow re-attachment distance and drag. Figure 5-31 shows that the lift-to-drag ratio follows the same dependence with re-attachment distance as airfoil drag.

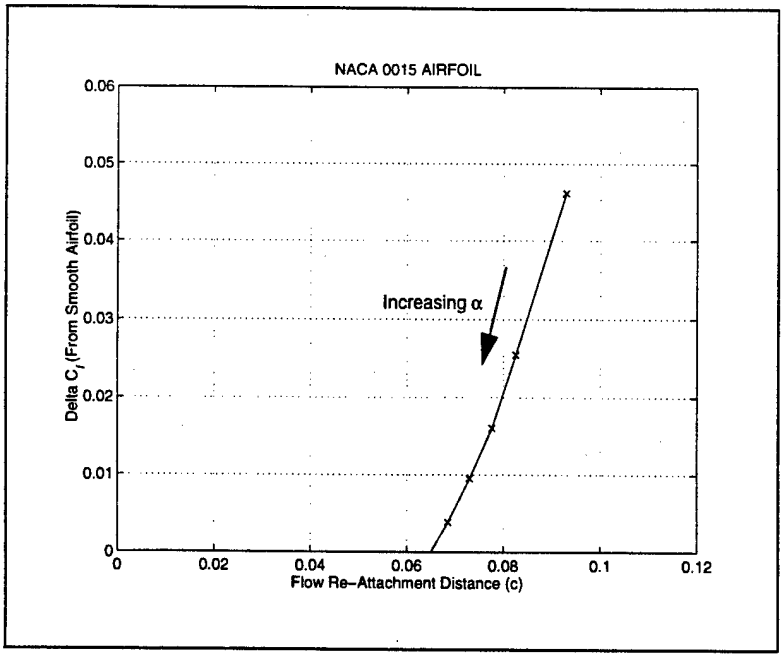

Figure 5-29. Lift Increment as a Function of Flow Re-Attachment Distance for Varying Angle-of-Attack

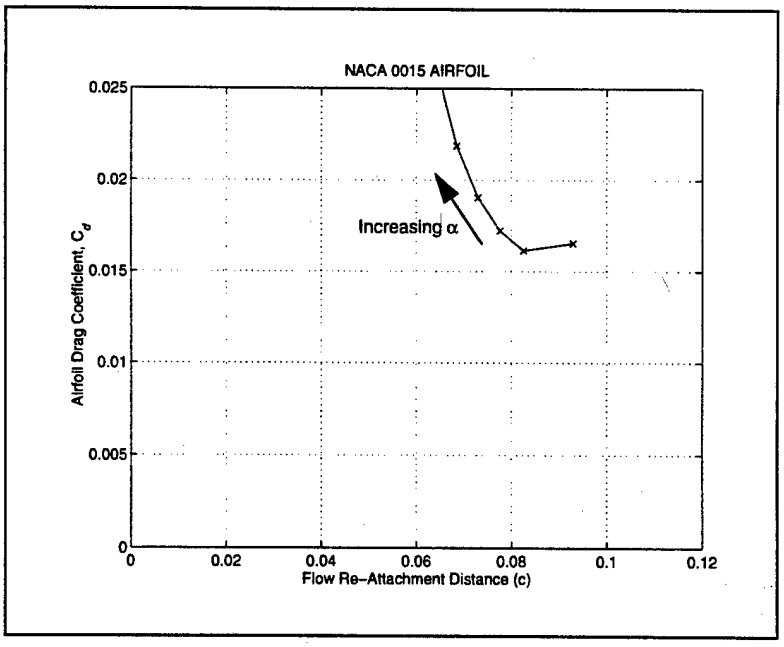

Figure 5-30. Airfoil Drag as a Function of Flow Re-Attachment Distance for Varying Angle-of-Attack

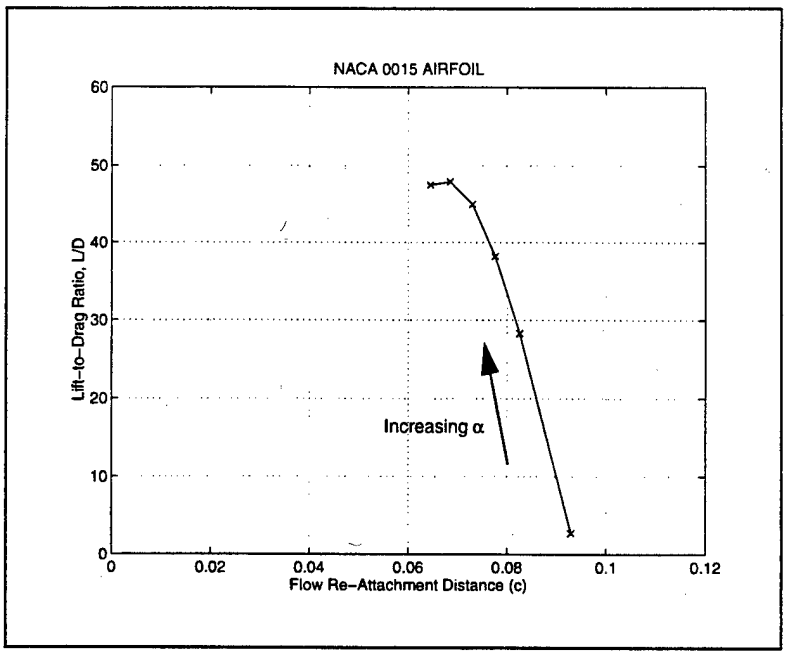

Figure 5-31. Lift-to-Drag Ratio as a Function of Flow Re-Attachment Distance for Varying Angle-of-Attack

Location. The results presented are for a baseline protuberance at 6 degrees angle-of-attack under baseline conditions with varying protuberance location. Figure 5-32 through Figure 5-34 indicate that protuberance location does not strongly effect the flow re-attachment distance and re-emphasizes the weak dependence of the rough airfoil lift increment, drag, and lift-to-drag ratio on varying protuberance location.

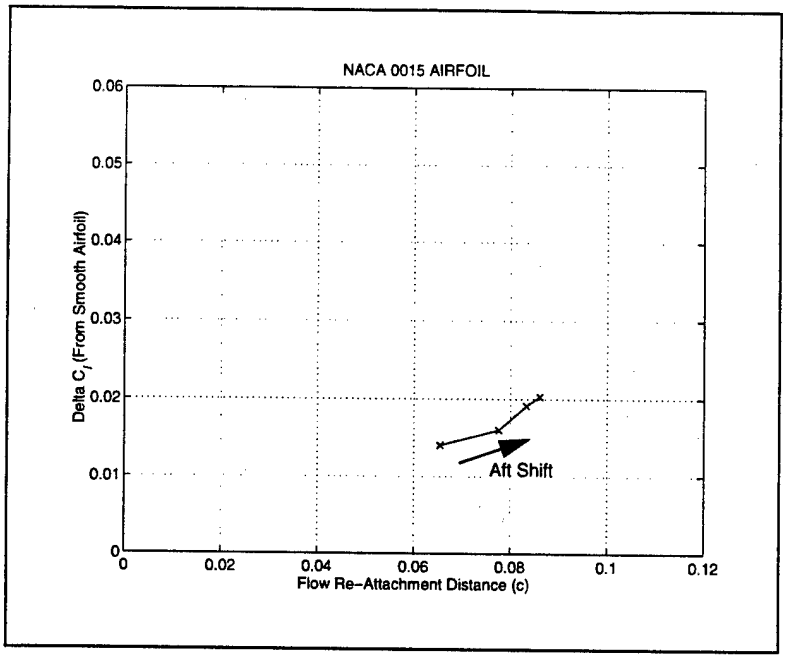

Figure 5-32. Lift Increment as a Function of Flow Re-Attachment Distance for Varying Protuberance Location

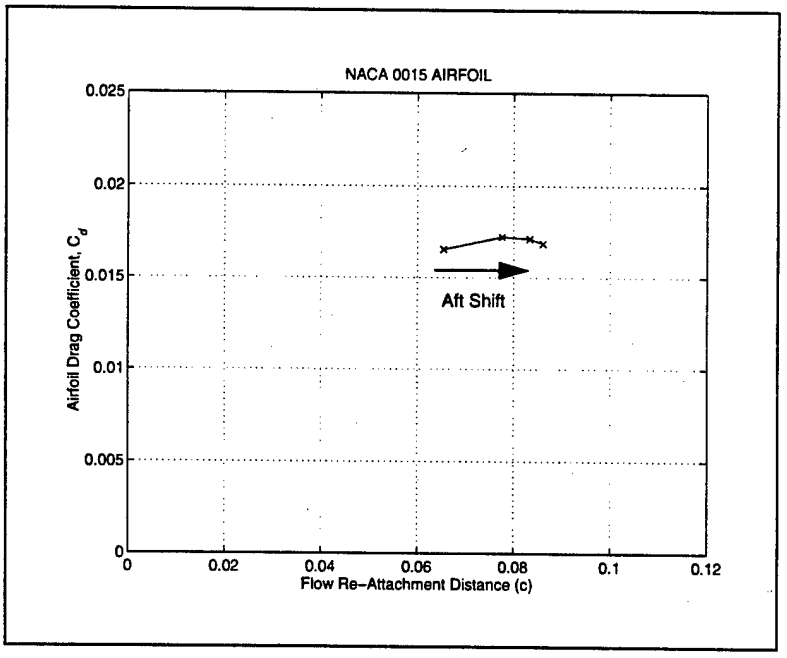

Figure 5-33. Airfoil Drag as a Function of Flow Re-Attachment Distance for Varying Protuberance Location

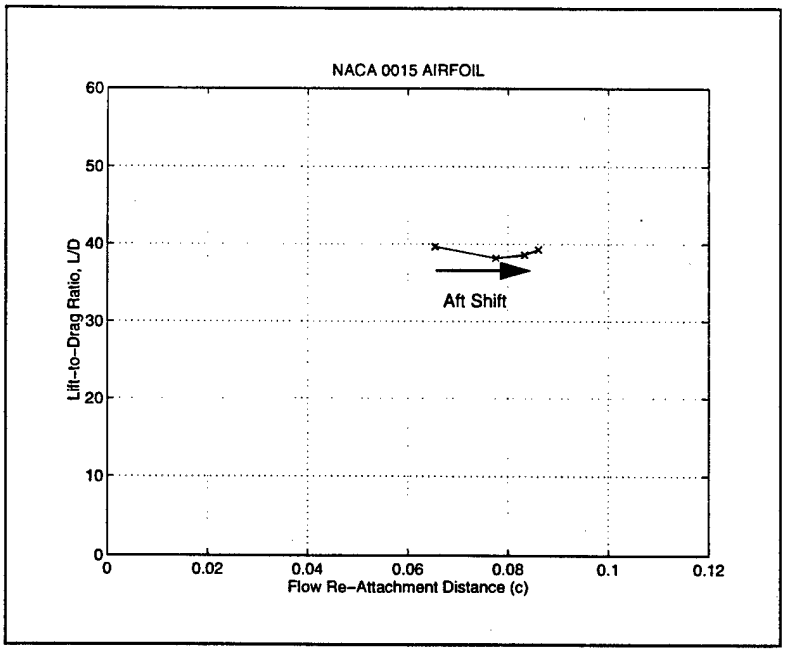

Figure 5-34. Lift-to-Drag Ratio as a Function of Flow Re-Attachment Distance for Varying Protuberance Location

Geometry. The results presented are for a protuberance centered at 0.28c under baseline conditions at 6 degrees angle-of-attack with varying protuberance geometry. Figure 5-35 shows that protuberance height has a strong effect on the magnitude of both the flow re-attachment distance and the lift increment while protuberance width is a secondary factor. Increased protuberance height produced larger lift increments and longer re-attachment distances. The data also suggest an ability to predict relative lift performance at constant angle-of-attack independent of protuberance geometry given flow re-attachment distance. Figure 5-36 shows that protuberance height is the dominant geometric parameter influencing airfoil drag. As protuberance height increased, flow re-attachment distance increased as did airfoil drag. Again, the plot suggests a positive correlation between increased flow re-attachment distance and increased drag independent of protuberance geometry at constant angle-of-attack.

Lastly, Figure 5-37 shows that while protuberance height was the dominant geometrical parameter determining the re-attachment distance, this influence did not result in significant lift-to-drag ratio variations for the conditions tested.

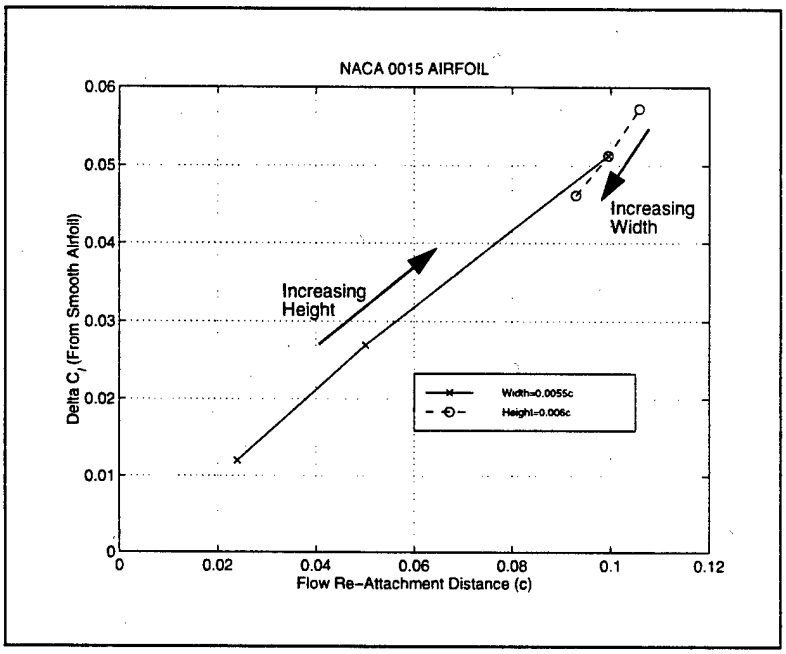

Figure 5-35. Lift Increment as a Function of Flow Re-Attachment Distance for Varying Protuberance Geometry

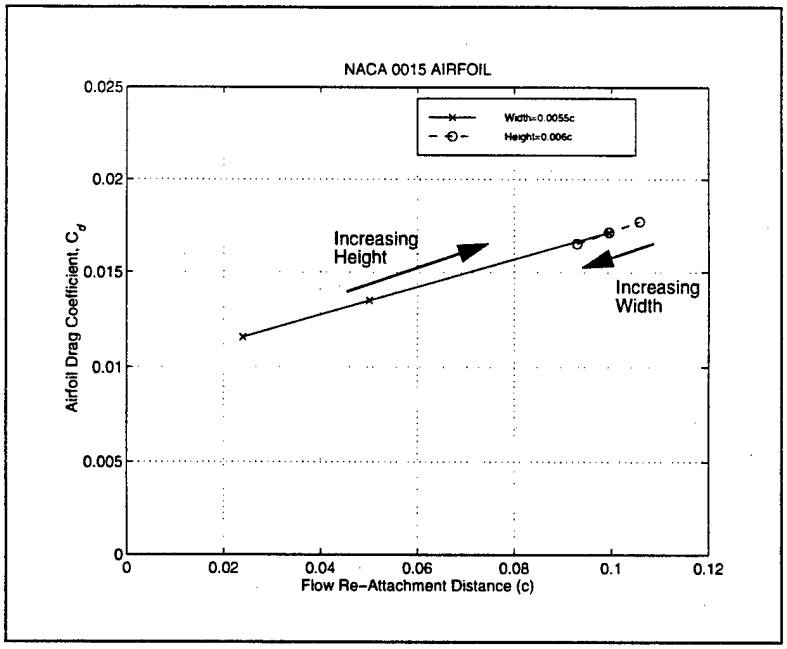

Figure 5-36. Airfoil Drag as a Function of Flow Re-Attachment Distance for Varying Protuberance Geometry

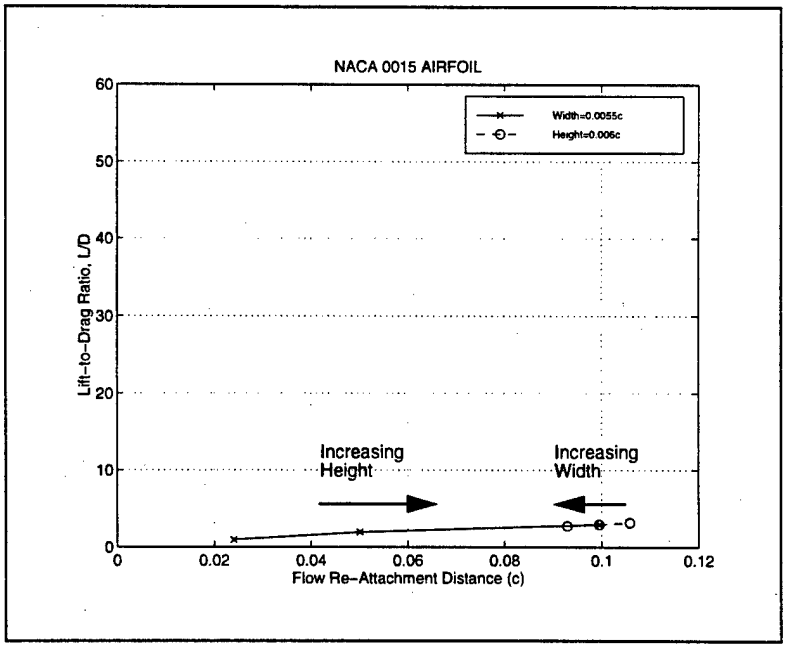

Figure 5-37. Lift-to-Drag Ratio as a Function of Flow Re-Attachment Distance for Varying Protuberance Geometry

5.5 RESULTS: MULTIPLE PROTUBERANCES

Computational experiments using a NACA 0015 airfoil were conducted at the baseline conditions to investigate the effect of a two protuberance configuration on the aerodynamic performance of the airfoil. The results presented were based on an analysis of the force data, the pressure data, and the visualization of the flow field properties.

5.5.1 FORCE DATA

Comparison plots of computational results for an airfoil populated with two baseline protuberances with varying protuberance spacing are presented in Figure 5-38 through Figure 5-40. The spacing of zero equated to a single protuberance centered at 0.28c with any positive spacing value identifying the centered position of the second protuberance aft of 0.28c. The experiments were conducted under the baseline test conditions with the airfoil at 10 degrees angle-of-attack.

Figure 5-38 shows that the introduction of a second protuberance produced a positive lift increment and resulted in the same or more lift compared with a single protuberance configuration. The plot indicates that there was a small positive increase in lift with increased spacing between protuberances.

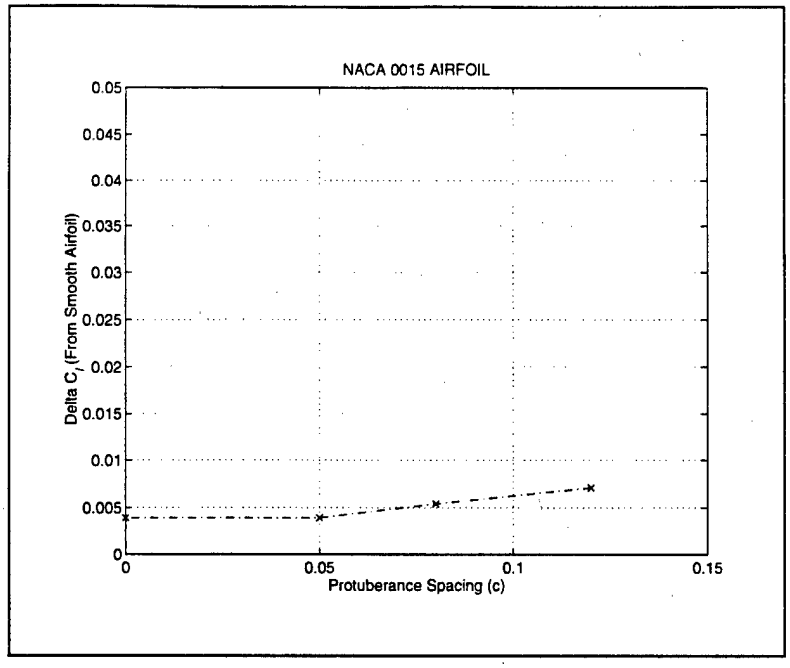

Figure 5-38. Lift Increment as a Function of Protuberance Spacing

Figure 5-39 shows that the total drag for the two protuberance configurations increased over the smooth airfoil and remained the same or increased over the single protuberance configuration. There was a relationship between drag and protuberance spacing where increased spacing resulted in higher drag.

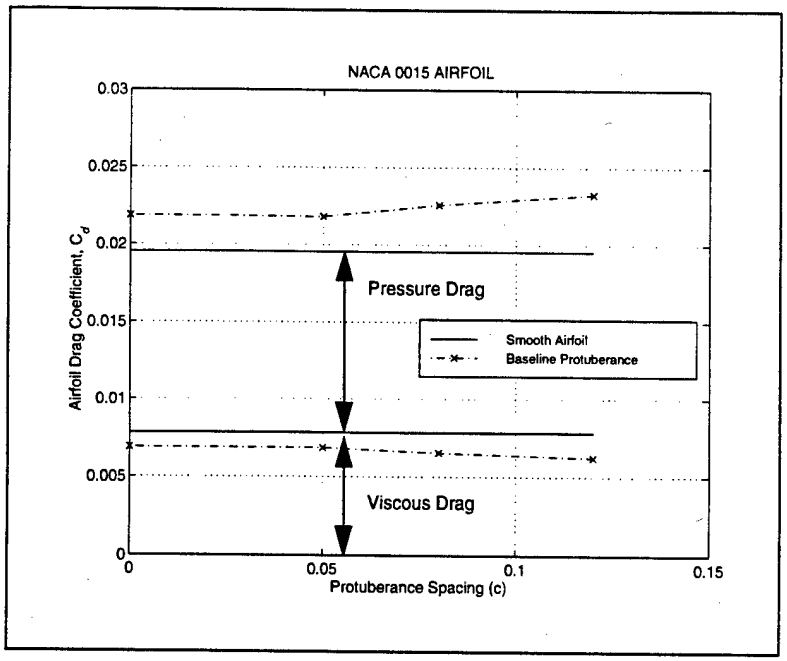

Figure 5-39. Drag as a Function of Protuberance Spacing

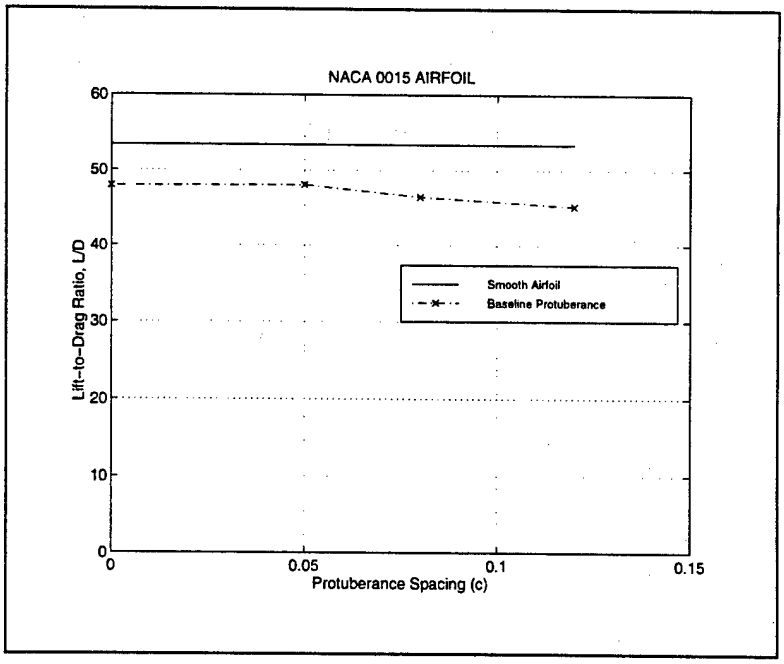

Figure 5-40. Lift-to-Drag Ratio as a Function of Protuberance Spacing

None of the two protuberance configurations tested matched nor exceeded the smooth airfoil lift-to-drag ratio as seen in Figure 5-40. In addition, the two protuberance configurations equalled or fell below the lift-to-drag ratio performance of the single protuberance configuration. There was a slight trend of decreasing lift-to-drag ratio with increased protuberance spacing.

Note that the addition of a second protuberance 0.05c aft of the first protuberance did not seem to alter the aerodynamic performance as measured against the single protuberance performance.

5.5.2 PRESSURE DATA

Pressure data from the multiple protuberance study were analyzed and are reported based on varying protuberance spacing. The results presented are for two baseline protuberances under baseline conditions at 10 degrees angle-of-attack. The first protuberance is centered at 0.28c with the second centered the spacing distance aft of 0.28c. The addition of a second protuberance created no appreciable difference in the overall shape of the pressure coefficient contour beyond the protuberance region. In that area, the second protuberance again had little effect on the characteristic pressure distribution about the first protuberance. The only discernible change in adding the second protuberance was the appearance and growth of a second pressure change similar to that about the first protuberance.

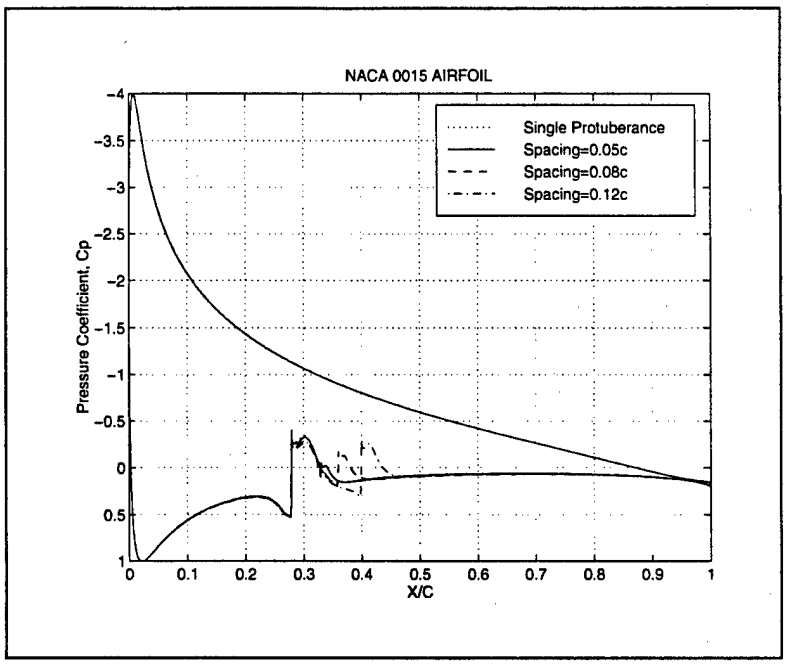

Figure 5-41. Pressure Coefficient Variation with Protuberance Spacing

5.5.3 FLOW VISUALIZATION

Results from the multiple protuberance studies were analyzed based on the visualization of the velocity vector field, the pressure field, and the vorticity contours. Results for an airfoil with a baseline protuberance located at 0.28c and a second baseline protuberance centered a specified spacing distance downstream are presented. The airfoil was at 10 degrees angle-of-attack under baseline conditions.

There was a strong interaction between the two protuberances as evidenced by the velocity vector fields which weakened with increased spacing between the two protuberances. Figure 5-42 through Figure 5-44 show that as spacing increased, the extent of the recirculation region of both protuberances lengthens. For the 0.12c spacing, Figure 5-44 appears to indicate that the protuberances operate on the flow field independently.

The two protuberances have an equally strong effect on the pressure field as seen in Figure 5-45 through Figure 5-47. The second protuberance does not appear to exert any influence over the pressure field of the first protuberance. In contrast, the pressure variation about the second protuberance changes significantly with increased protuberance spacing. Note that for 0.12c spacing, Figure 5-47 indicates that the influence of the second protuberance does not yet equal that of the first on the pressure field.

Figure 5-48 through Figure 5-50 show that the vorticity contours follow the same trends as the pressure field with increased protuberance spacing. Figure 5-48 details the closest spacing of 0.05c. Here the two protuberances created a single region of higher vorticity. With the spacing increased to 0.08c, Figure 5-49 shows that the vortical region created by the two protuberances appears close to separating into two regions. In Figure 5-50, two distinct vortical regions are created at the 0.12c spacing Note that the first protuberance remained the dominant producer of vorticity for all spacing.

For all flow field properties studied, the flow appeared steady with no noticeable fluctuations near convergence.

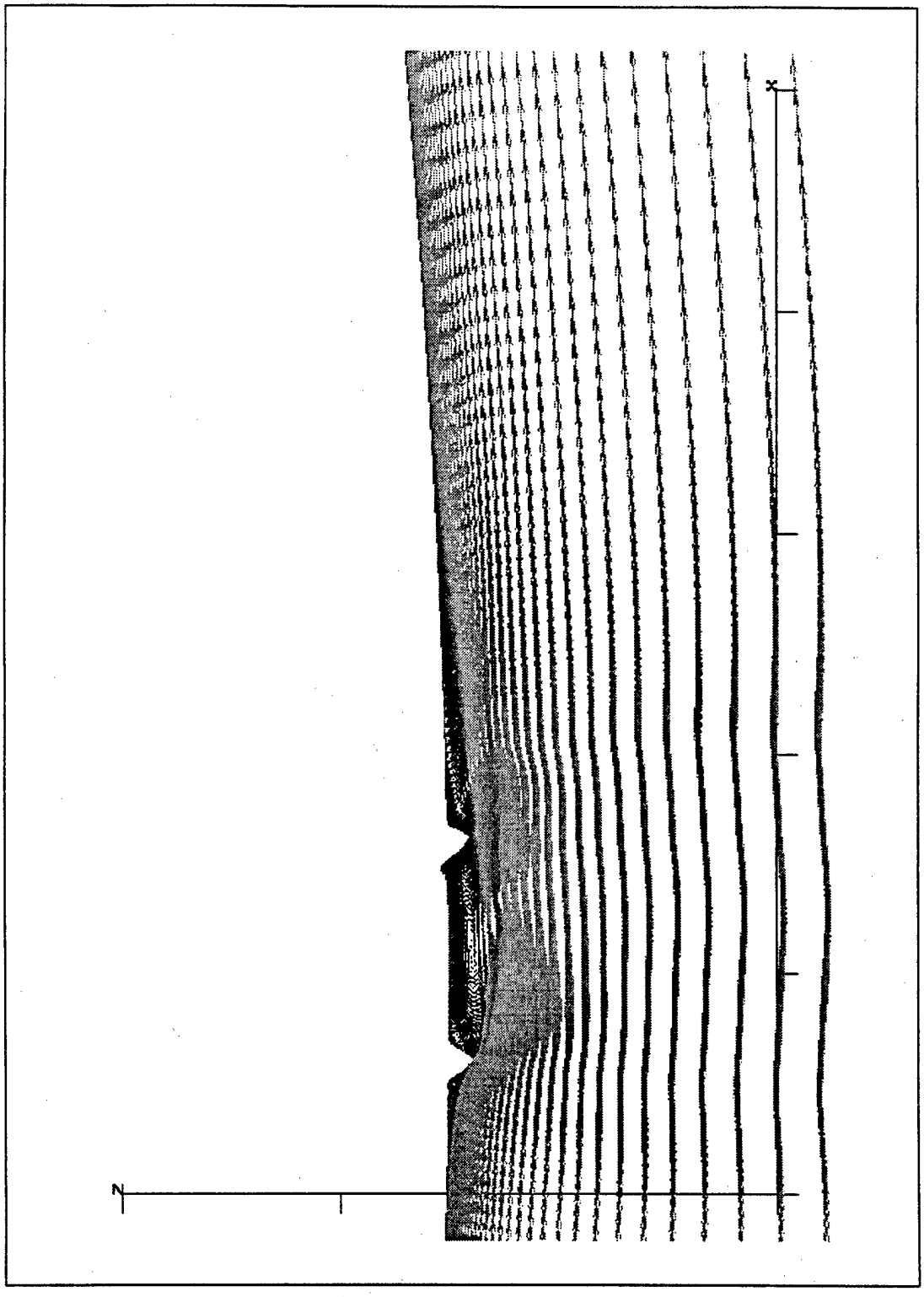

Figure 5-42. Velocity Vector Field About Two Protuberances with 0.05c Spacing

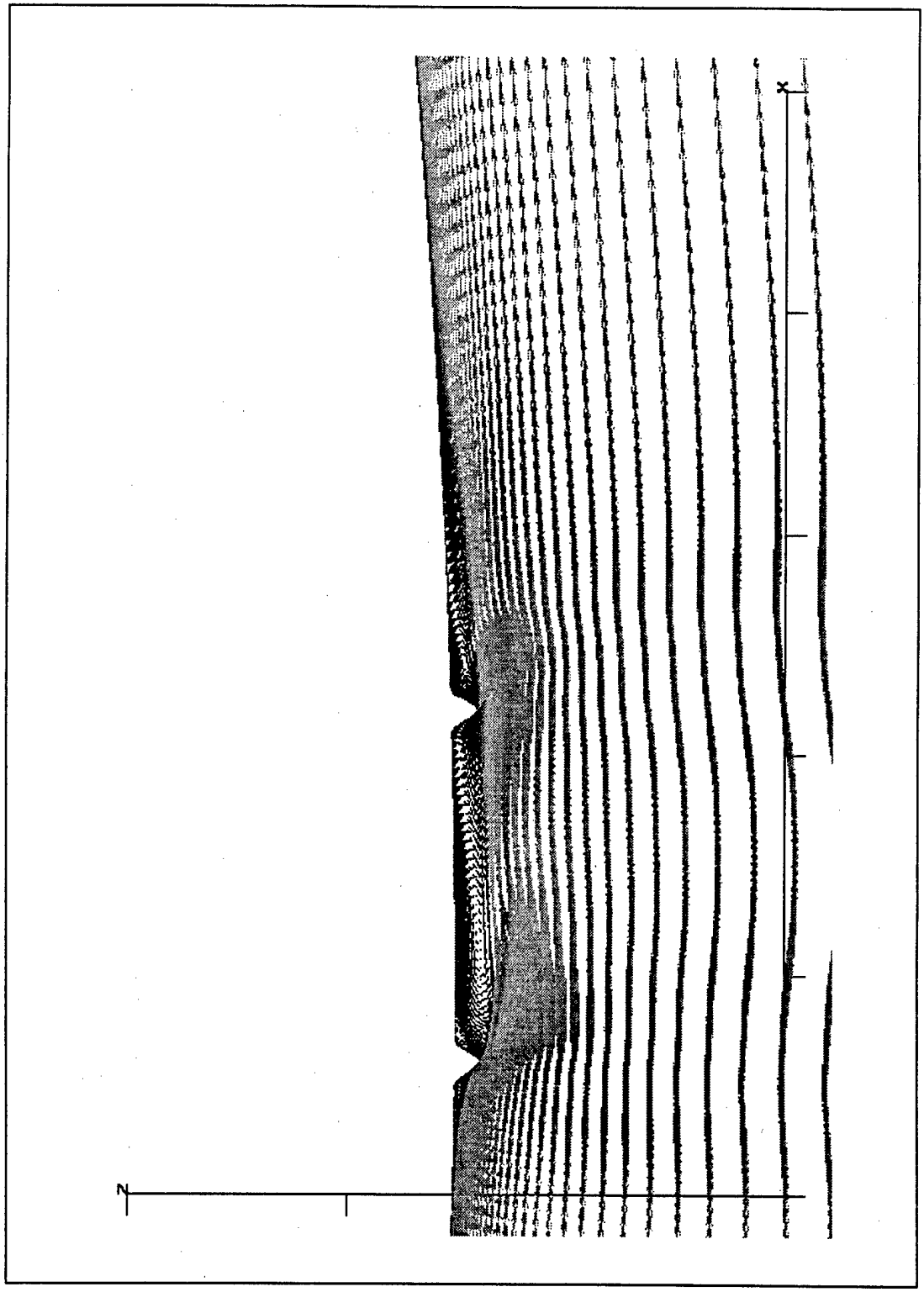

Figure 5-43. Velocity Vector Field About Two Protuberances with 0.08c Spacing

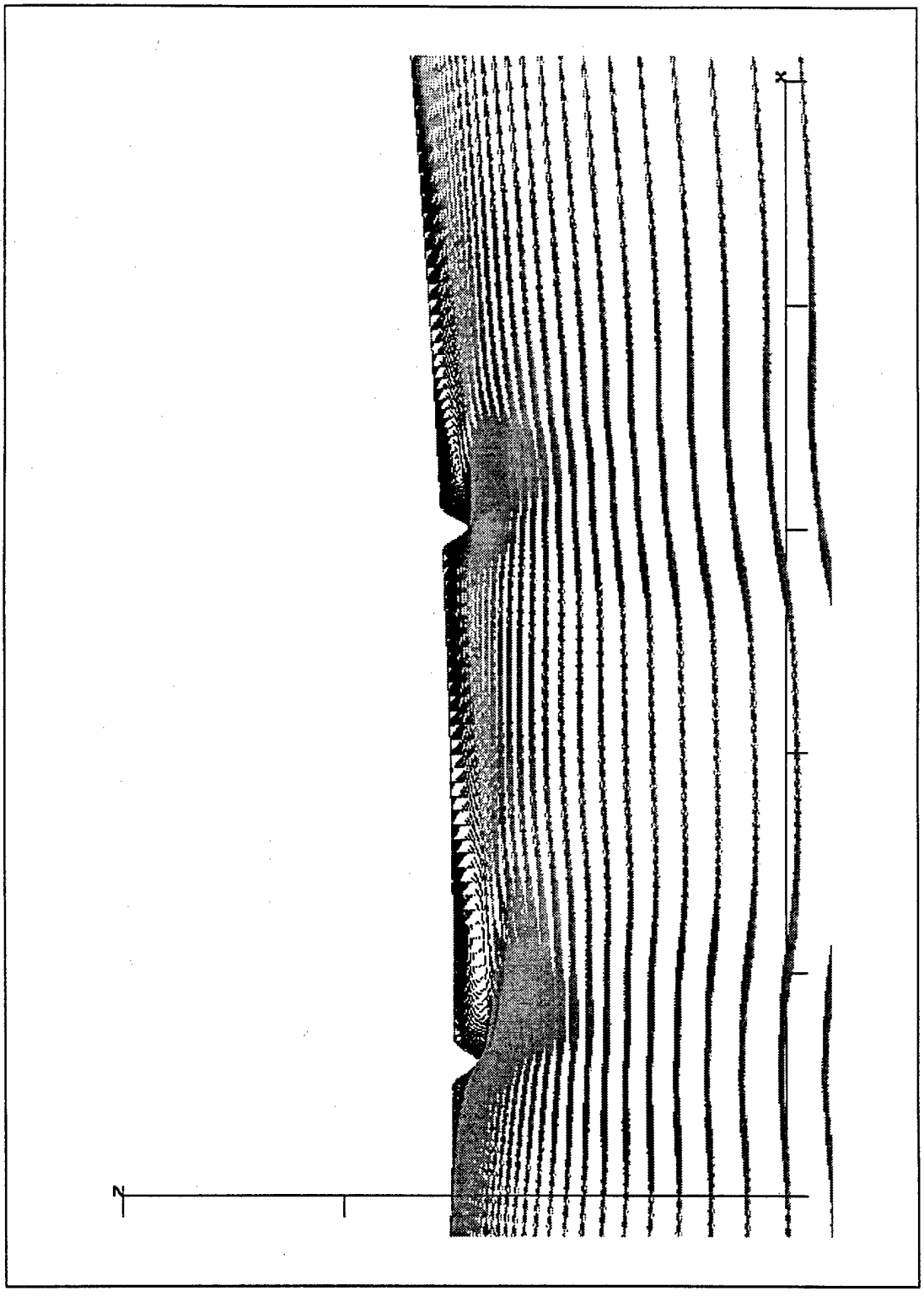

Figure 5-44. Velocity Vector Field About Two Protuberances with 0.012c Spacing

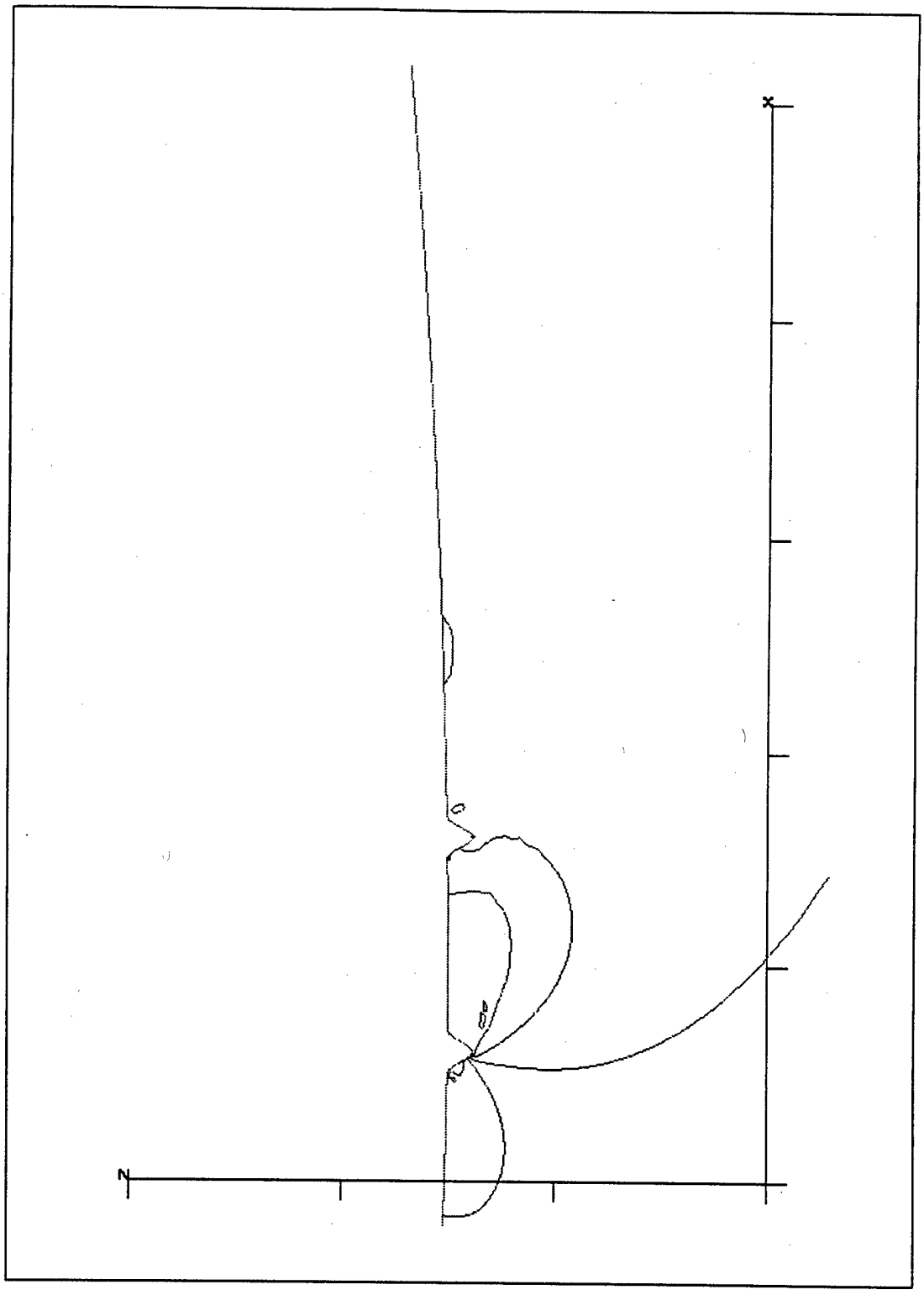

Figure 5-45. Pressure Field About Two Protuberances with 0.05c Spacing

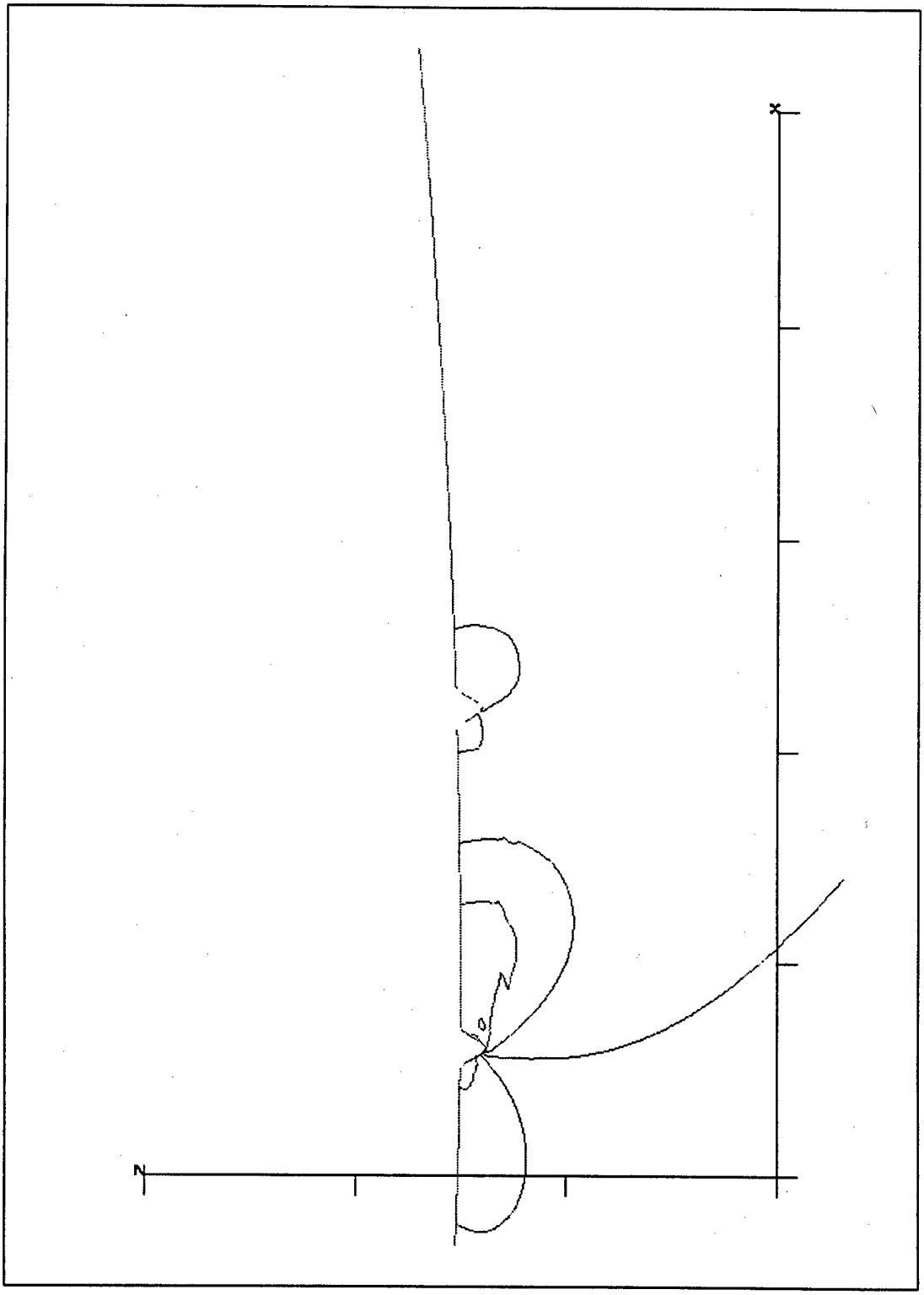

Figure 5-46. Pressure Field About Two Protuberances with 0.08c Spacing

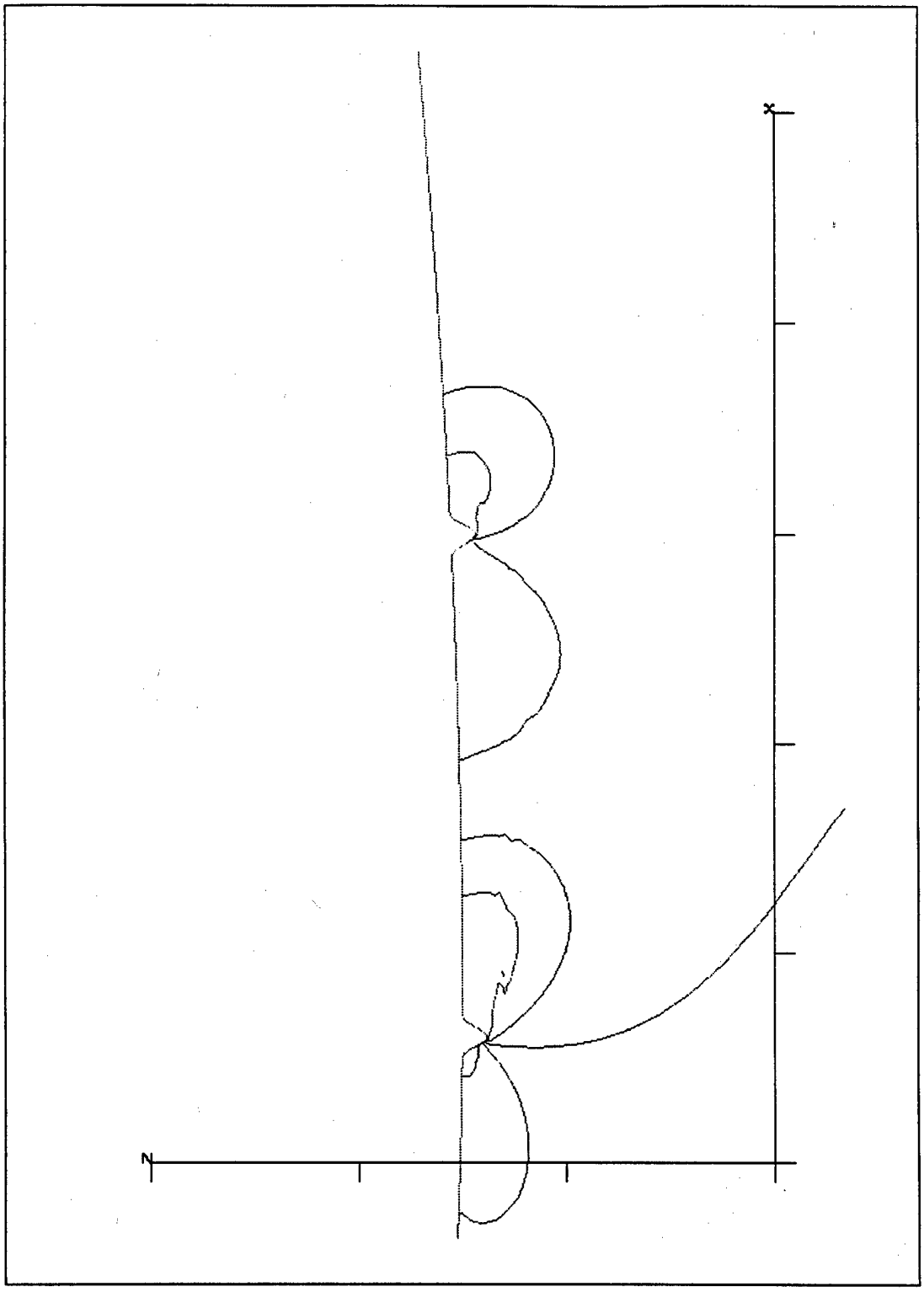

Figure 5-47. Pressure Field About Two Protuberances with 0.12c Spacing

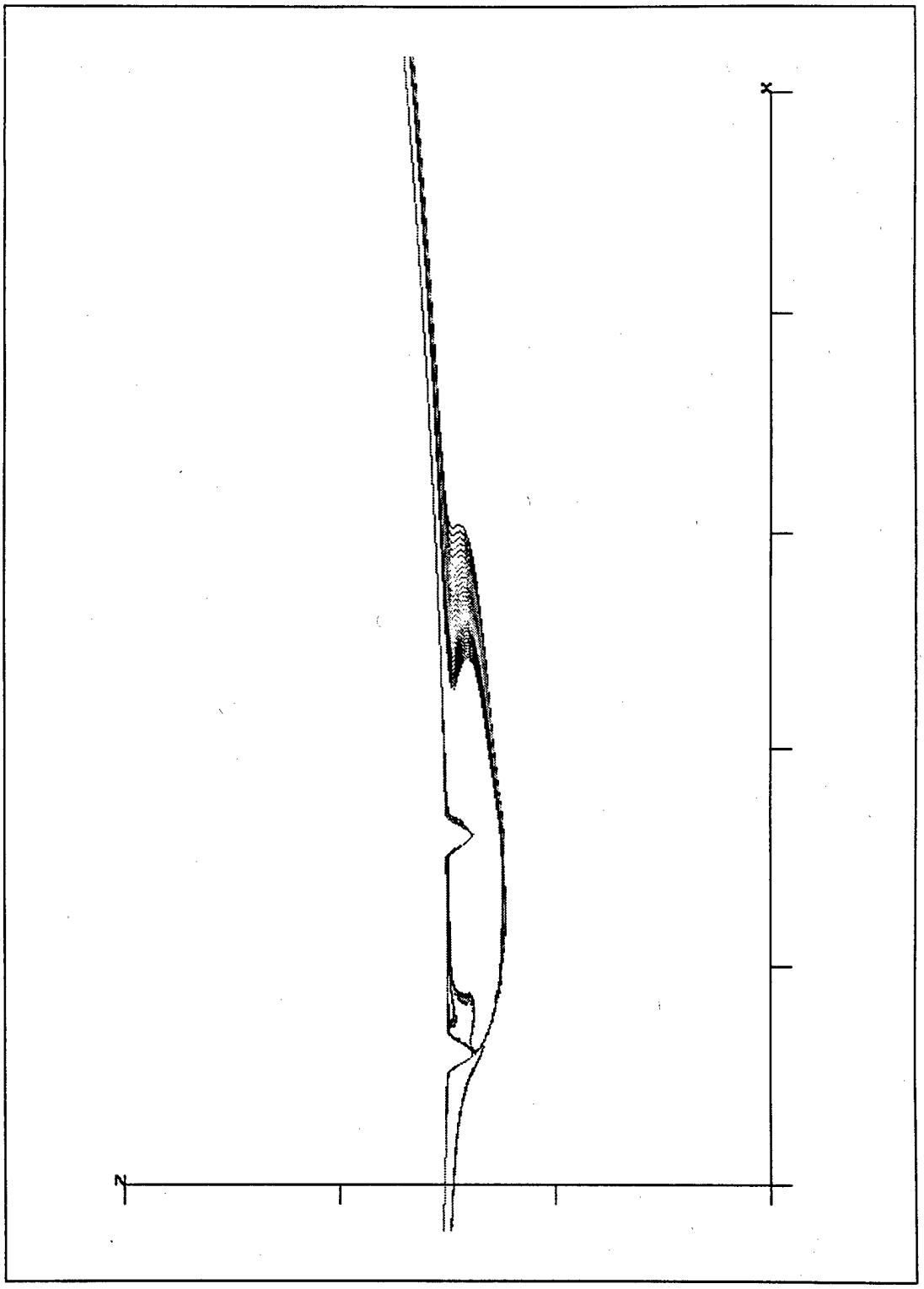

Figure 5-48. Vorticity Contours About Two Protubèrances with 0.05c Spacing

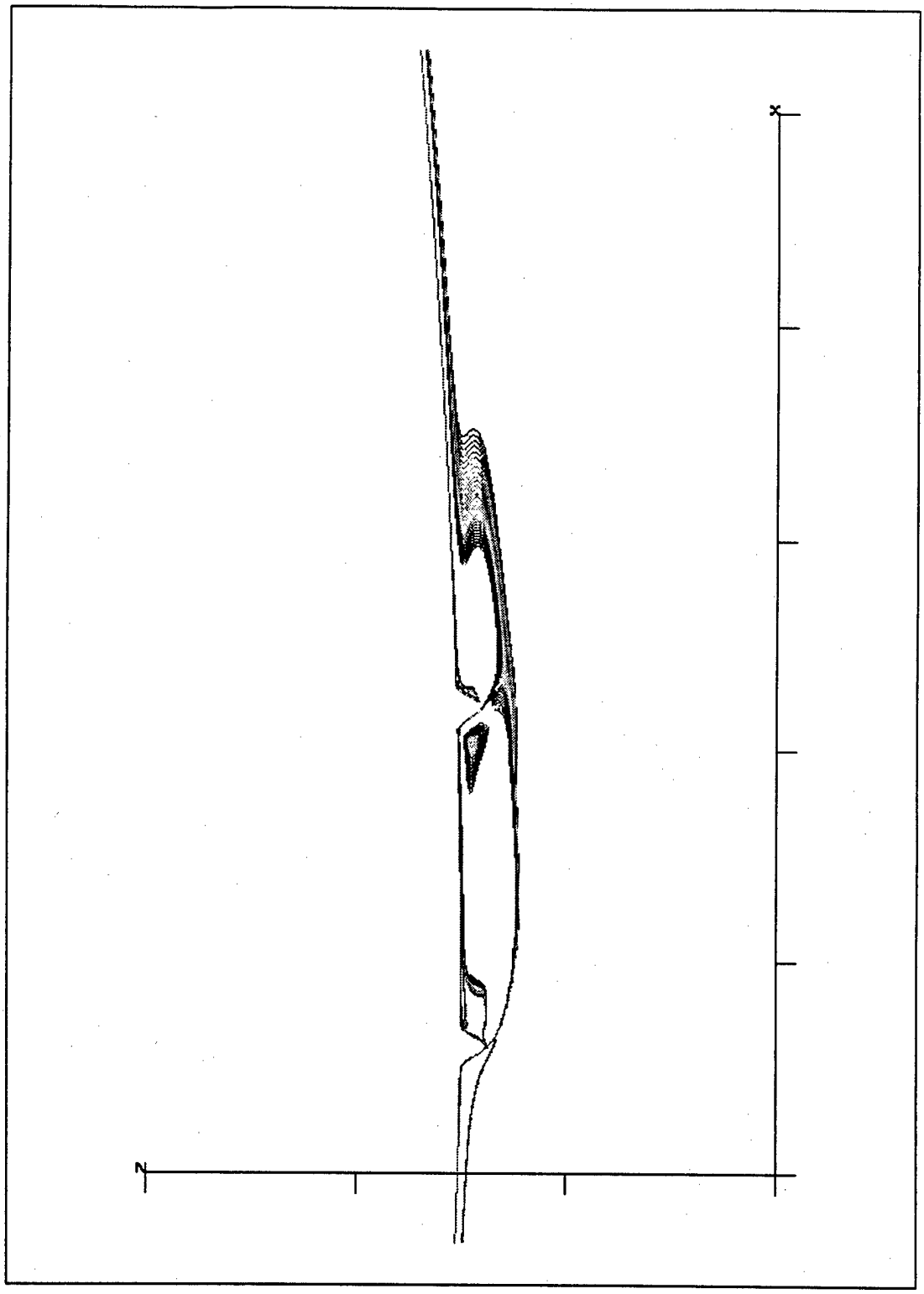

Figure 5-49. Vorticity Contours About Protuberances with 0.08c Spacing

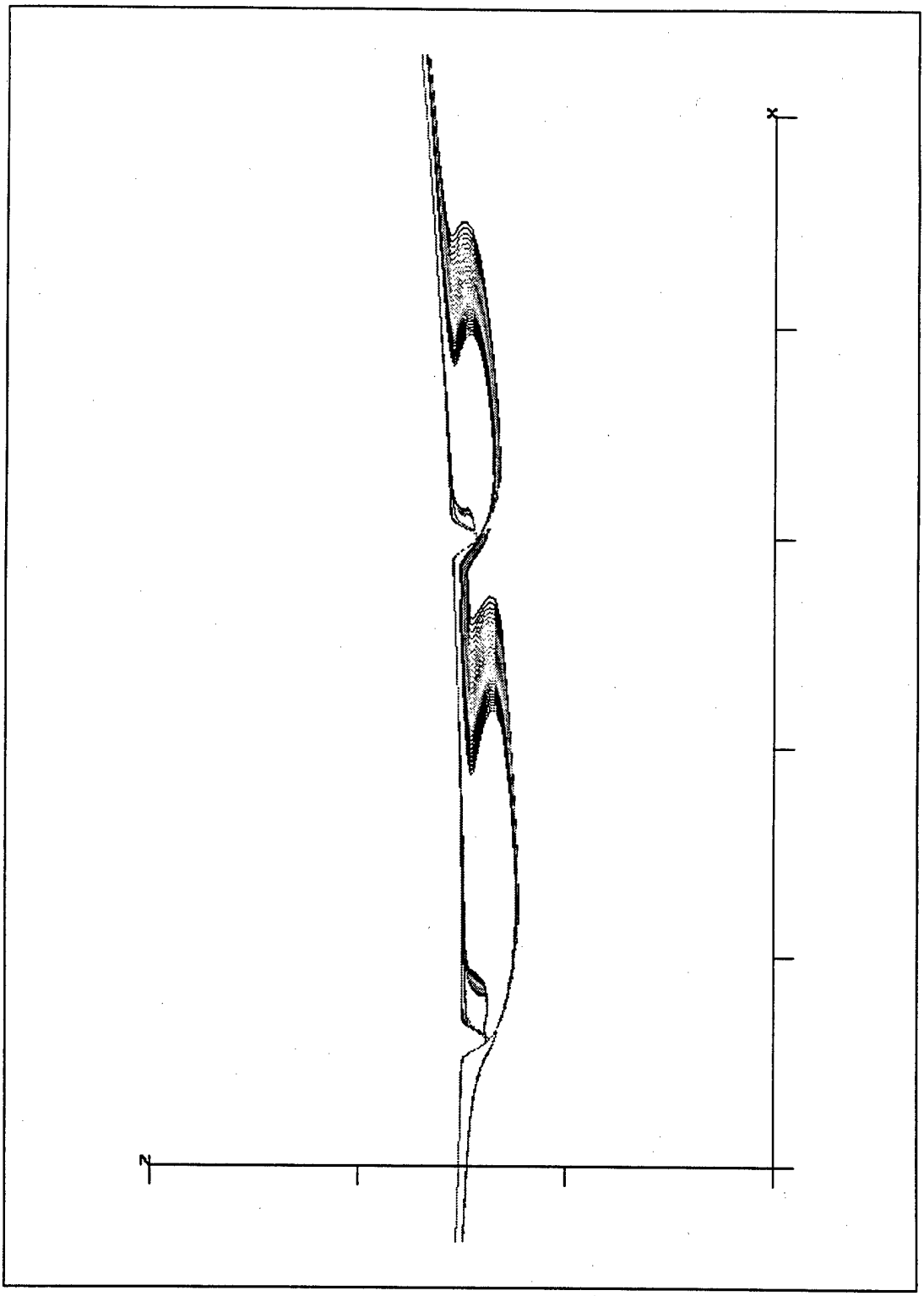

Figure 5-50. Vorticity Contours About Two Protuberances with 0.12c Spacing

5.6 SYNOPSIS

This section summarizes the results of the computational experiments and develops relevant conclusions from these results.

5.6.1 SUMMARY OF COMPUTATIONAL RESULTS

5.6.1.1 Single Protuberance Test

Study of the computational force data for a NACA 0015 airfoil with a single two-dimensional surface protuberance attached on a single side led to the following observations:

- The presence of a protuberance produced an incremental lifting force in a transverse direction to the surface. This effect included the generation of lift at zero degrees angle-of-attack. The effect occurred at low and moderate angles-of-attack and diminished to zero near ten degrees angle-of-attack. The presence of the protuberance also generated increased drag and resulted in a lower lift-to-drag ratio compared to a smooth airfoil.
- Moving the location of the protuberance aft relative to the leading edge increased the lift generated with the drag and the lift-to-drag ratio unchanged with varying location.
- Increasing the height of the protuberance increased the lift, increased the drag, and increased the lift-to-drag ratio. Height was the primary geometry parameter effecting airfoil aerodynamic performance.

- Increasing the width of the protuberance decreased the lift, decreased the drag, and decreased the lift-to-drag ratio. Width was a secondary geometry parameter effecting airfoil aerodynamic performance.
- For all configurations tested, the airfoil with a protuberance generated lower viscous drag and more pressure drag compared to a smooth airfoil.

Study of the pressure distribution over a NACA 0015 airfoil with a single two-dimensional surface protuberance attached on a single side led to the following observations:

- The presence of the protuberance significantly altered the pressure distribution about much of the airfoil by creating a unique pressure variation in the region near the protuberance and by increasing the pressure difference between the upper and lower surfaces.
- The largest portion of the increased pressure drag resulted from the pressure distribution over the surface of the protuberance itself.

Study of the computational flow visualization of a NACA 0015 airfoil with a single two-dimensional surface protuberance attached on a single side led to the following observations:

- The presence of the protuberance created a recirculation region downstream of the protuberance.
- The re-attachment location of the recirculation region relative to the protuberance location varied with airfoil angle-of-attack, protuberance location, and protuberance geometry.

Study of the airfoil test results for a single two-dimensional protuberance compared to the results reported by Vorobiev for cusp-like protuberances led to the following observation:

- All configurations tested produced a similar increase in lift, but none achieved an equal or greater lift-to-drag ratio compared to a smooth, baseline airfoil.

5.6.1.2 Multiple Protuberance Test

Study of the computational force data for a NACA 0015 airfoil with two, two-dimensional surface protuberances attached on a single side led to the following observation:

- Increasing the spacing between the leading and trailing protuberances increased the lift, increased the drag, and decreased the lift-to-drag ratio.

Study of the pressure distribution over a NACA 0015 airfoil with two, two-dimensional surface protuberances attached on a single side led to the following observation:

- The presence of the protuberances significantly altered the pressure distribution about much of the airfoil by creating a unique pressure variation in the region near the protuberances. A second protuberance generates a pressure variation shaped similar to the leading protuberance and whose magnitude varied with spacing.

Study of the computational flow visualization of a NACA 0015 airfoil with two, two-dimensional surface protuberance attached on a single side led to the following observation:

- The presence of the protuberances created a single recirculation region or two separate recirculation regions downstream of the protuberances depending on the protuberance spacing.

Study of the airfoil test results for two, two-dimensional protuberances compared to the results reported by Vorobiev for cusp-like protuberances led to the following observation:

- All configurations tested produced a similar increase in lift, but none achieved an equal or greater lift-to-drag ratio compared to a smooth, baseline airfoil.

5.6.2 CONCLUSIONS FROM COMPUTATIONAL RESULTS

Protuberances on a symmetric airfoil are a mechanism to generate additional lift, specifically at low to moderate angles-of-attack. Based on the results of these computational experiments, the presence of protuberances is not a means to enhance the lift-to-drag ratio of a symmetric airfoil.

The aerodynamic performance changes about an airfoil with protuberances are the result of a pressure related phenomena induced by the presence of surface protuberances. Evidence of this dependence are the significant changes in the pressure field and the independence of lift on viscous effects. In addition, the reduction and

constant magnitude of viscous drag with compared to a smooth airfoil and the accompanying rise in pressure drag are further evidence.

The flow field induced by the protuberances is steady, or nearly steady. There are not unsteady effects such as a shedding vortical structure. Any unsteadiness is manifest as a small magnitude oscillatory perturbation about a larger, well-defined structure exhibiting steady behavior.

The computational experiments identified the importance of several parameters with regards to this phenomena. Airfoil angle-of-attack and protuberance height strongly influence the changes in aerodynamic performance. In contrast, single protuberance location and the presence of a second protuberance appear to have little impact in changing the aerodynamic performance.

The inability of two-dimensional protuberances on a two-dimensional body to produce an increase in the lift-to-drag ratio as reported by Vorobiev suggests that the geometry of the protuberance is critical, a relationship demonstrated based on protuberance height, or that either a three-dimensional protuberance, a three-dimensional body, or both must be present to achieve the enhanced aerodynamic performance.

CHAPTER 6 DISCUSSION OF RESULTS

Having completed three separate investigations into the surface roughness related lift enhancement, this chapter now focuses on the integration and analysis of the results. Specifically, the airfoil wind tunnel results, the wing wind tunnel results, and the airfoil computational results are compared for similarities, inconsistencies, and insight. The entire body of results from the current effort is then compared with key previous work. Additional analysis is presented which, in part, suggests a relationship between the presence of a protuberance and increased effective camber and thickness. In the Synopsis (see Section 6.4), a phenomenological description of the lift enhancement is detailed.

6.1 COMPARISON OF WIND TUNNEL AND COMPUTATIONAL RESULTS

A summary of the results of each experiment and the specific conclusions drawn from the individual experiments were reported at the close of their respective chapters. This section integrates the results from the three individual experiments to develop general observations and specific relationships.

6.1.1 COMPARISON OF FORCE DATA

Based on the results of the wind tunnel and computational experiments, a symmetric airfoil or wing with surface protuberances at zero degrees angle-of-attack produced a positive lift increment on the order of magnitude of 0.05 for the geometries

and conditions tested. This was a consistent finding across wind tunnel and computational results, two-dimensional airfoils and three-dimensional wings, and two-dimensional protuberances and three-dimensional protuberances. Given that a baseline lift does not exist for a symmetric body at zero degrees angle-of-attack, one means to measure the relative increase in performance is by determining the effective change in angle-of-attack represented by the lift increment. Using this criteria, protuberances on two-dimensional airfoils produced a maximum effective angle-of-attack increase of approximately 0.5 degrees and protuberances on three-dimensional wings produced a maximum effective angle-of-attack of approximately 1.0 degree.

From the results of the experiments conducted for this effort, the presence of protuberances on a wing or airfoil resulted in a smaller lift-to-drag ratio compared with a smooth body for all configurations and conditions tested with one exception. The single exception for this finding was identified during the wind tunnel testing of the wavy wing configuration. The absolute magnitude of the lift-to-drag ratio varied widely for the airfoil versus the wing, as expected. Interestingly, the relative decrease in the maximum lift-to-drag ratio for both the wing and the airfoil with surface protuberances compared to a smooth surface body did not exceed 20% for the configurations tested. The wavy wing exception produced a 4% increase in the maximum lift-to-drag ratio. Recall that the wavy wing configuration did not generate a lift increment at zero degrees angle-of-attack. Therefore, the wavy wing did not produce an effective angle-of-attack increase.

The lift increment demonstrated a clear, consistent dependence on angle-of-attack. Increased angle-of-attack resulted in a smaller, positive lift increment and this

effect diminished to zero slightly below the stall angle-of-attack for surface protuberances on both a wing and an airfoil. The opportunity to capture a positive lift increment was only present at low to moderate angles-of-attack for all configurations tested. No similar potential existed for lift-to-drag ratio versus lift coefficient due to its reduced magnitude as noted previously.

Both wind tunnel and computational results suggest that protuberance location was not a strong influence in determining the magnitude of the lift increment nor the lift-to-drag ratio decrease. Results from the wind tunnel testing of the wing for a protuberance field and from the computational experiments for a single protuberance showed that neither combination produced a significant change in the lift increment nor the lift-to-drag ratio with varying location.

The geometry of the protuberance proved to be a critical factor. In the wind tunnel experiments, protuberance height and width were not studied independently. The computational airfoil results showed the strong dependence on height for increased lift and decreased lift-to-drag ratio versus the comparatively weak influence of protuberance width. The wind tunnel testing of the wing with protuberances supports the observation that increased protuberance height increased the lift increment and degraded the lift-to-drag ratio. These results suggest that protuberance height is the critical geometry parameter as no evidence suggests width would become a more significant factor.

Protuberance coverage and the density of the protuberance field were important factors in determining aerodynamic performance during both the wing and airfoil wind tunnel experiments. Increased coverage or increased density resulted in

larger lift increments and smaller lift-to-drag ratios. Based on these results, the addition of a second protuberance on the airfoil during the computational experiments was expected to increase the lift increment and decrease the lift-to-drag ratio. However, the computational results for the two protuberance configurations showed that the lift increment remained the same or decreased and the lift-to-drag ratio remained the same or decreased. This apparent discrepancy between the wind tunnel and computational results is not understood at this time. This finding is especially troubling given that an airfoil baseline was used in both the wind tunnel and computational studies.

The two most similar configurations between the two-dimensional wind tunnel experiment and the two-dimensional computational experiments are compared in Figure 6-1 and Figure 6-2. The GLMWT protuberance configuration consisted of 4 strip protuberances with $h = 0.0044c$ and $\lambda = 0.0088c$ located between 0.10c and 0.35c at 0.05c spacing. The RANS computational configuration consisted of a single baseline protuberance at 0.28c with $h = 0.0060c$ and $\lambda = 0.01c$. Figure 6-1 shows that the magnitude and trend of the lift increment for the experimental and computational results compared favorably. Additionally, a single data point at zero degrees angle-of-attack for one baseline protuberance with $h = 0.0036c$ and $\lambda = 0.01c$ produced a lift increment of 0.0222 from the computational experiment. In Figure 6-2, the lift-to-drag ratio trends appear similar between experimental and the computational results. The maximum lift-to-drag ratio for the rough airfoil was 8% lower than the smooth airfoil based on the experimental results and 11% lower based on the computational results. The distinction in Figure 6-2 is the difference in the magnitude of the lift-to-drag ratio

between the experiments. Figure 3-3 and Figure 5-1 show excellent agreement between the magnitude and variation of the airfoil lift coefficient for the experimental and computational experiments, respectively. The magnitude difference in Figure 6-2 is due to a variation in airfoil drag. The minimum drag coefficient was 0.0117 and 0.0105 for the experimental configuration and the computational configuration, respectively. One possible explanation for this difference was the approximate NACA 0015 section shape of the wind tunnel model (see Section 3.1.2.2 and Section 3.1.3.1) compared to the very precise shape of the computational airfoil model. In addition, the differences in the configurations for each test probably contributed to this difference. The last observation is that the two-dimensional insert used in the GLMWT experiment approximates two-dimensional flow.

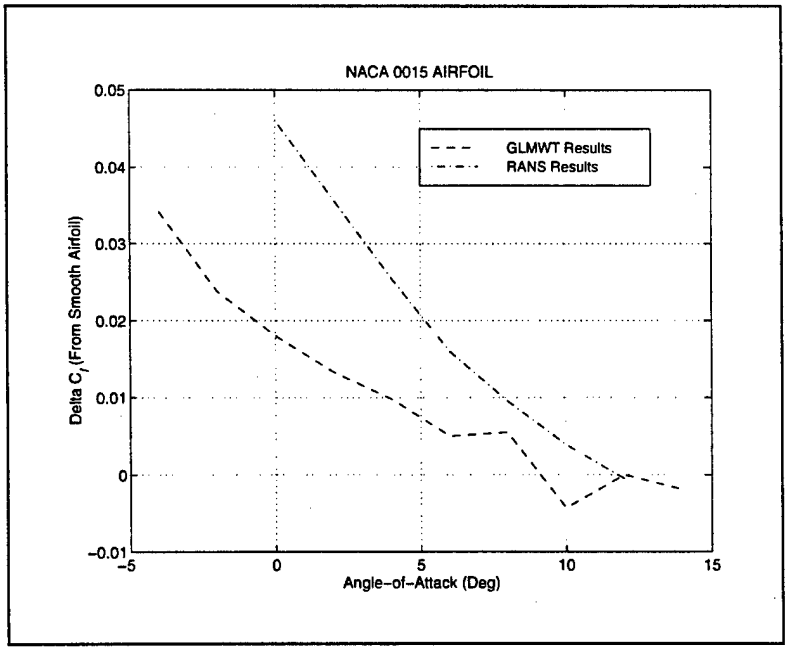

Figure 6-1. Comparison of GLMWT and RANS Lift Increment

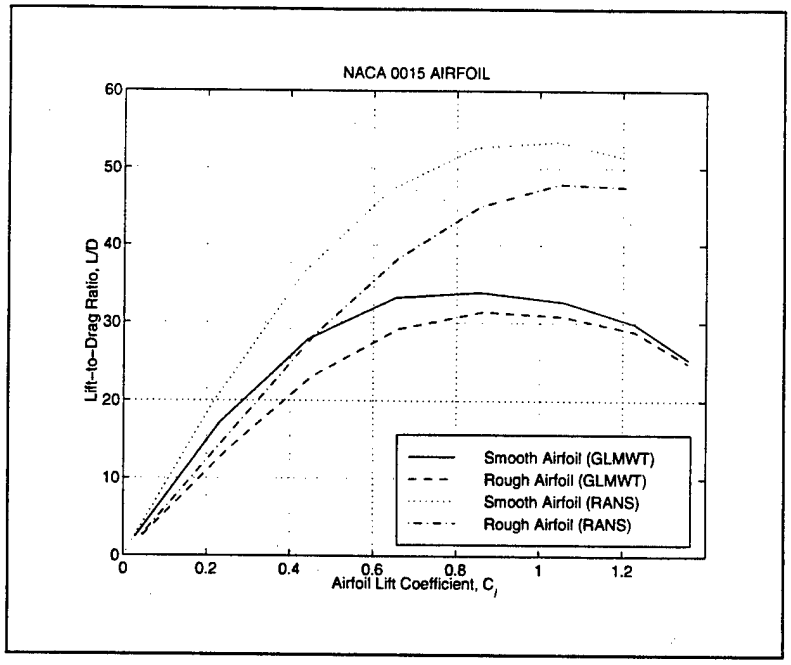

Figure 6-2. Comparison of GLMWT and RANS Lift-to-Drag Ratio

6.1.2 COMPARISON OF PRESSURE DATA

The presence of surface protuberances significantly altered the pressure distributions about the airfoil and the wing as shown in the computational study and the wind tunnel investigation, respectively. Comparison of Figure 5-17 for an airfoil with a single protuberance and Figure 3-22 for a wing with a protuberance field indicate the clear influence of surface protuberances on pressure. For both bodies with protuberances, there was an increase in the area between the pressure curves for the upper and lower surfaces indicating the generation of additional lift. It is not clear from these plots if the effect was the result of an increase in the effective angle-of-attack or a decrease in the zero-lift angle-of-attack.

There are two apparent discrepancies between the pressure distribution about the wing and that about the airfoil. First, the pressure distribution near the

protuberances differed between the airfoil and the wing. The flow appeared to be approaching a stagnation condition as it neared the protuberance on the airfoil while the flow appeared to be accelerating as it approached the protuberance field on the wing. This difference could be the result of the location of the pressure taps on the wing and the location of the pressure measurement on the airfoil. The pressure taps on the wing were located on the airfoil surface, not on the protuberances, and thus captured the venturi effect of the accelerating flow between the initial protuberances. In contrast, the pressure measurements on the airfoil were taken on the surface, including the surface of the protuberance. Near stagnation conditions in the flow as it approached the protuberance is a reasonable result given the blockage effect of the protuberance and might be an expected result on the surface of the protuberances of the wing had it been measured.

Second, the overall pressure about the wing with a protuberance field becomes lower compared to a smooth body while the overall pressure acting on the airfoil with a protuberance does not shift. As will be discussed in Section 6.3.3, the change in the pressure distribution for the wing can be attributed to an increase in the effective section thickness. However, the difference between the wing and pressure distributions cannot be adequately explained based on the results of the current investigation.

6.1.3 OBSERVATIONS BASED ON FLOW VISUALIZATION RESULTS

The lift enhancement observed in the computational experiments is due to the flow recirculation region generated by the presence of the protuberance. This flow field structure induces a change in the pressure field around the airfoil. The velocity vector

fields presented detail the structure of the recirculation region and the pressure field plots show the increased pressure along the lower surface in the vicinity of the protuberance. In addition, the pressure coefficient distributions presented clearly show both a local effect in the region near the protuberance and an overall effect. The lift results from the computational studies strengthen this observation as the variation measured in lift was due solely to changes in the lift due to pressure. The separate drag component results from the computational study also support this observation. While the viscous drag decreases slightly with the presence of the protuberance, the dominant increase in the pressure drag again reinforces the link between pressure and the resultant aerodynamic performance. Last, the strong correlation between increased lift and increased re-attachment distance at a constant angle-of-attack completes the circle and demonstrates the direct relationship between aerodynamic performance and the flow field structure.

The reduced viscous drag for configurations with a protuberance compared with a smooth body is also understood as a direct consequence of the recirculated flow. In this region, the normal velocity gradients near the wall are significantly reduced which reduces the shear stress and the corresponding skin friction.

6.2 COMPARISON WITH PREVIOUS WORK

6.2.1 RUSSIAN RESEARCH

One of the secondary objectives of this research effort was the potential validation of the reported lift and lift-to-drag ratio improvement with surface roughness by Vorobiev.[1] An analysis of the comparative lift increment and lift-to-

drag ratio changes suggest contradictory outcomes between the results of Vorobiev and the present work in two key ways.

First, only the wavy wing configuration in the wind tunnel experiments and no configurations in the computational experiments of the present work achieved a lift-to-drag ratio increase. Given the aerodynamic importance of realizing such an increase, this result is a critical finding. This outcome suggests that this project did not accurately model the necessary protuberance geometry or that the combination of configuration and flow conditions required to realize positive increments to both lift and lift-to-drag ratio exists over a limited parameter range and this study failed to identify the proper parameter set.

Second, the measured lift increment of this project matched that of Vorobiev in absolute magnitude, but not in relative magnitude. Vorobiev reported lift increments ranging from 0.050 to 0.084 for a low aspect wing at zero degrees angle-of-attack. All wind tunnel and computational experiments results from this effort matched in order of magnitude with lift increments on the order of 0.050 at zero degrees angle-of-attack. Using the effective change in angle-of-attack as a means to measure the relative increase in performance, Vorobiev achieved a 3 to 4 degree change in effective angle-of-attack. The wind tunnel results from this study for a wing with surface protuberances achieved a maximum of just a 1 degree change in effective angle-of-attack. The results for the wind tunnel and the computational experiments of an airfoil with surface protuberances showed approximately a 0.5 degree change in effective angle-of-attack. The variance of the relative lift improvement again suggests a variance with the reported Russian results or that the absolute magnitude of the lift

variation is independent of the two- and three-dimensional nature of the protuberance and the two- and three-dimensional nature of the lifting body.

In conclusion, an analysis of the relative lift increment and the lift-to-drag ratio results between those of the current project and those of Vorobiev show that this work did not validate the reported results of Vorobiev.

6.2.2 ZERO-MASS 'SYNTHETIC' JETS

Hassan [16] first reported the similarities between the resultant aerodynamic performance effects of the protuberances studied in this effort and that of a zero-mass jet array. He suggested an equivalence in aerodynamic effect between jet oscillation frequency and protuberance density and between peak jet velocity and protuberance height. The results of this work further the identification of similarities and suggests an even stronger relationship.

First, the flow structures created by a zero-mass jet array and a protuberance are strikingly similar. The zero-mass jet array flow structure from Hassan and JanakiRam [15] in Figure 6-3 contains multiple recirculation regions, caused by the time dependence of the array. The result shown was for a NACA 0012 with an array of zero-mass jets located between 0.13c and 0.23c with a normalized (by the freestream speed of sound) jet peak velocity of 0.2 and a frequency of 1585 Hz. The test conditions were a freestream Mach number of 0.6, an angle-of-attack of zero degrees, and a freestream Reynolds number of 3 million. Note that the recirculation regions created by the zero-mass jet array match the shape and size of the recirculation region generated by a single protuberance as shown in Figure 5-23 and Figure 5-24.

Second, the experimental work from this project supports the equivalences cited by Hassan. The experimental results of this study were the basis for Hassan's observations. The computational results further strengthen the equivalence between peak jet velocity and protuberance height. However, the computational results from the two protuberance study of spacing seems to contradict the equivalence between jet oscillation frequency and protuberance density. The addition of a second protuberance might be considered an increase in protuberance density, yet the results presented show that the lift increment decreased for all two protuberance configurations studied compared with a single protuberance. An explanation of this apparent discrepancy is not yet understood.

Third, the magnitude of the lift increment and drag increment for a freestream Mach number of 0.15 compares very favorably between a zero-mass jet array and a single protuberance. Results from Hassan [16,46] for a zero-mass jet array with a jet oscillation frequency of 1585 Hz are shown in Table 6-1. The array was located between 0.13c to 0.23c on a NACA 0012 airfoil at a freestream Mach number of 0.15, a freestream Reynolds number of 3 million, and an angle-of-attack of zero degrees. For a single, baseline protuberance located at 0.28c under baseline conditions and zero degrees angle-of-attack, the lift increment was 0.0452 (see Figure 5-4) and the total drag coefficient was 0.0165, a 57.1% increase over the smooth airfoil (see Figure 5-5). Given the preference for the lower jet Mach numbers due to the smaller drag, the close agreement in lift and drag performance between a zero-mass jet array and a surface protuberance is striking.

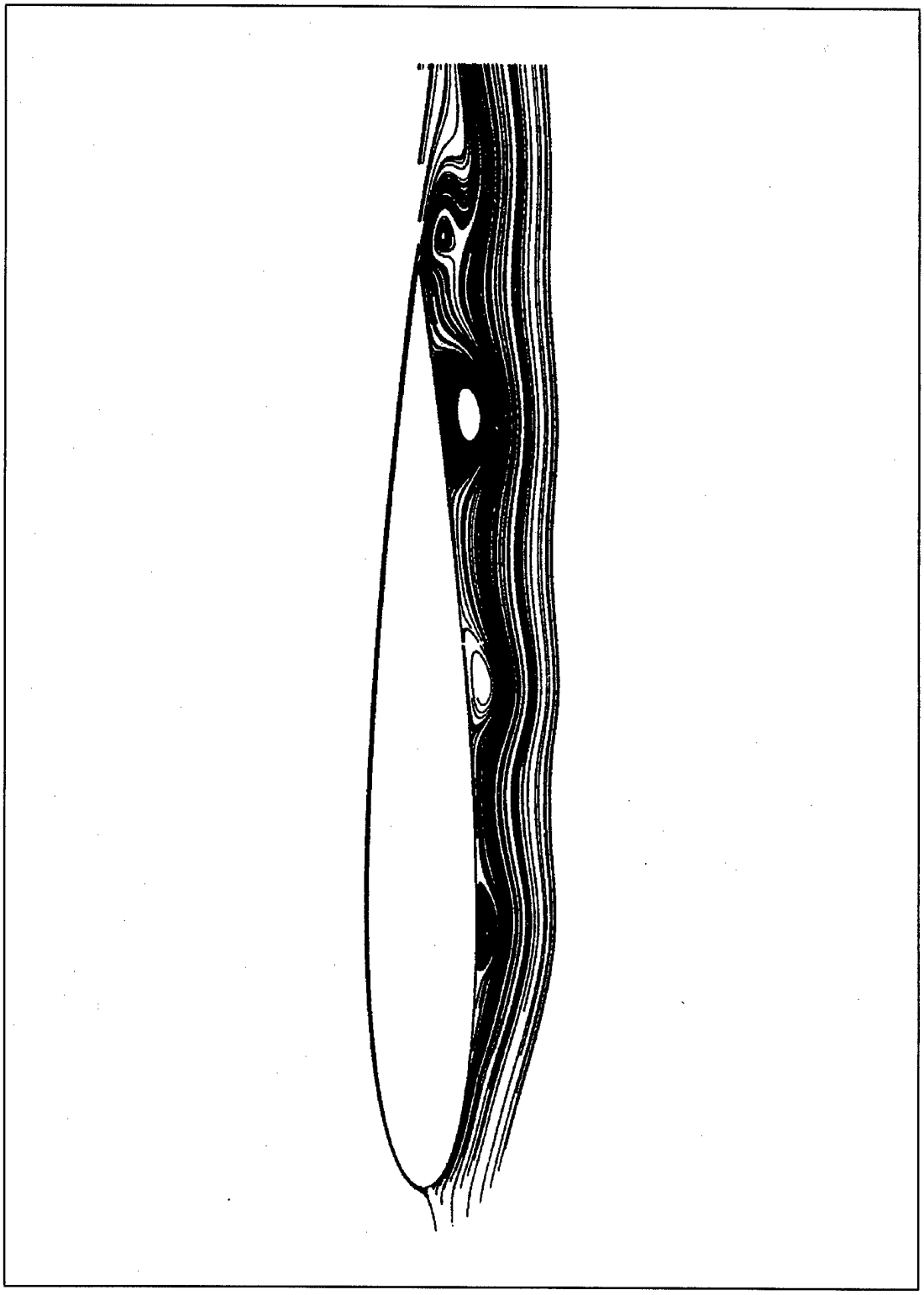

Figure 6-3. Zero-Mass Jet Array Flow Structure Over NACA 0012 Airfoil

Based on the comparisons presented here, it seems quite possible that the flow structures created by a zero-mass jet array and a protuberance of the type studied in this work and the phenomenological basis of their influence on the flow field are identical. Such a conclusion infers that a zero-mass jet array is the unsteady equivalent of a protuberance.

Jet Mach Number	$C_{l,mean}$	$C_{d,mean}$	ΔC_d Off Baseline
0.0 (Baseline)	0.000	0.0098	--
0.05	0.048	0.0138	40.8%
0.10	0.074	0.0213	117%
0.15	0.052	0.0333	240%
0.20	0.008	0.0465	375%
0.25	-0.042	0.0610	522%

Table 6-1. Predicted Mean Force Coefficients for Zero-Mass Jet Array

6.2.3 NACA TECHNICAL REPORT #446

Results of testing by Jacobs [7] compare favorably with the experimental and computational airfoil results. Jacobs experimentally studied the effect of a single protuberance on airfoil lift and drag using an NACA 0012 section. In these tests, the maximum lift increment occurred for a protuberance height of 0.0125c located at 0.65c aft of the leading edge on the lower surface. At zero degrees angle-of-attack and a freestream Reynolds number of 3.1 million, Jacobs measured a lift increment of 0.039 and a total drag coefficient of 0.0244, a 213% increase over a smooth airfoil under the same conditions. The positive lift increment diminished to zero by 6 degrees

angle-of-attack. The lift increment matches the current work in absolute magnitude, in relative magnitude as an effective angle-of-attack change of 0.4 degrees, and in its behavior with increased angle-of-attack. This analysis serves as a limited validation of the current research effort.

6.3 ANALYSIS OF RESULTS

6.3.1 LINEAR COMBINATION OF PROTUBERANCE DRAG

An analysis was performed to determine the contribution of the protuberance to the total drag. Using OVERINT in its stand-alone mode, force coefficients were calculated over the protuberance surface for both a single protuberance and a two protuberance configuration.

The single protuberance configuration used was a baseline protuberance located at 0.28c under baseline conditions with varying angle-of-attack. Figure 6-4 shows the total drag of the protuberance as function of the configuration lift coefficient. The total protuberance drag decreased slightly with increasing lift, or angle-of-attack. From the calculations, the pressure drag and viscous drag coefficients for the protuberance for a zero degree angle-of-attack were 0.00552 and 0.00005, respectively. This dominance of pressure drag was expected given the high pressure recirculation region downstream of the protuberance and existed for all configurations studied in this analysis. The calculated total drag of the protuberance was then added to the total drag of the smooth airfoil. This result is also shown in Figure 6-4. Note that this simple linear drag combination appears to provide correct order of magnitude estimates for the combined configuration at lift coefficients below 0.4, corresponding

to approximately 4 degrees angle-of-attack, but this approach clearly diverges at larger values of lift. Note that the results presented here are consistent with the findings based on the pressure coefficient variation with thickness presented in Section 5.4.2.

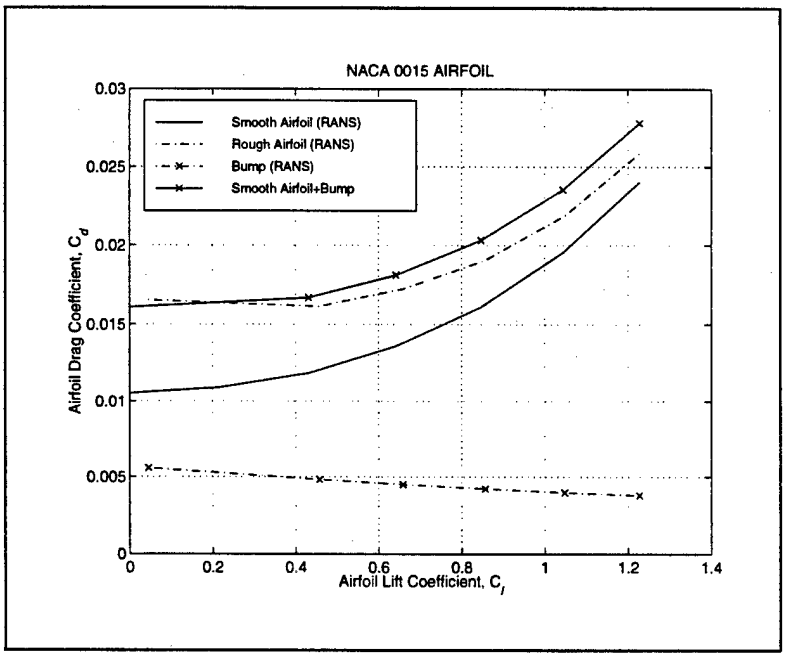

Figure 6-4. Linear Drag Analysis for Single Protuberance as a Function of Lift

The multiple protuberance configuration used included two baseline protuberances under baseline conditions at 10 degrees angle-of-attack with the leading protuberance at 0.28c and the second centered at the specified distance aft of the first. OVERINT was used to calculate the total drag over each individual protuberance. Figure 6-5 shows that the total drag of the leading protuberance remains essentially constant and appears not to be effected by the presence of the second protuberance. The total drag of the second, or trailing, protuberance increased with increased spacing. Note, a protuberance spacing of zero corresponds to a single protuberance. Again, the total drag of both protuberances was added to that for the smooth airfoil.

The results shown in Figure 6-5 indicate that this linear approach to calculating total drag on the combined configuration is not representative of the measured value for the combined configuration. Note that this result might also confirm the previous observation that this approach is inaccurate at larger angles-of-attack as this analysis was for an airfoil at 10 degrees angle-of-attack.

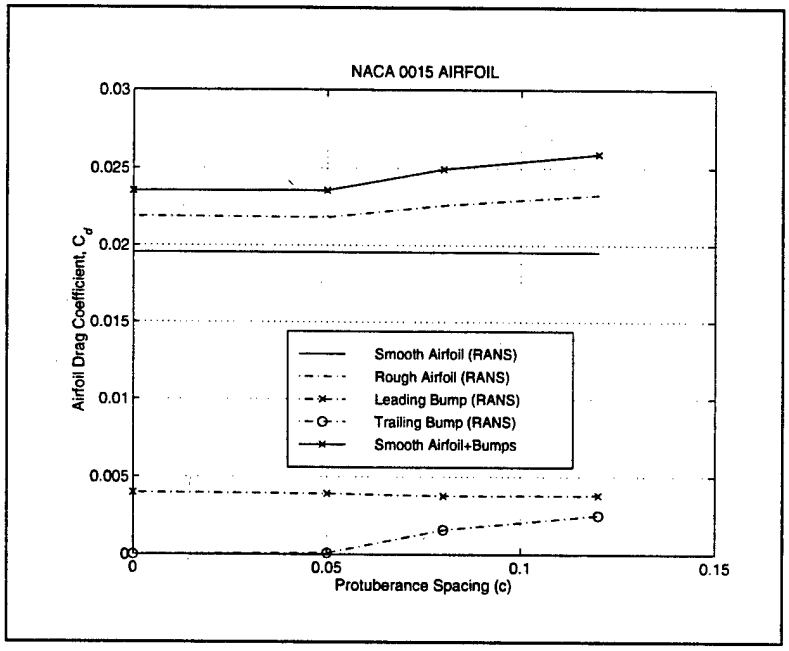

Figure 6-5. Linear Drag Analysis for Two Protuberances as a Function of Spacing

The key finding of this analysis is that the drag increase for an airfoil with a protuberance can be studied based on the drag of the protuberance. This first-order effect is most accurate at low angles-of-attack which is the primary region of interest due to the larger lift increments generated there. However, this observation does not necessarily suggest that studying a protuberance over a simple body, such as a flat plate, will produce accurate total drag predictions.

6.3.2 DISPLACEMENT THICKNESS ANALYSIS

An analysis was performed to determine the effective body surface as defined by the calculated displacement thickness from the computational results for an airfoil with a single protuberance. The configuration selected was a baseline protuberance located at 0.28c under baseline conditions at zero degrees angle-of-attack. The displacement thickness was determined based on the mass flux integrated along a normal to the body surface to a distance consistent with a boundary layer edge defined by 99% of the local freestream velocity. For incompressible flow, the displacement thickness is given by:[8]

$$\delta_1 = \int_0^{\infty} (1 - (u/U_{\infty}))dy \tag{6.1}$$

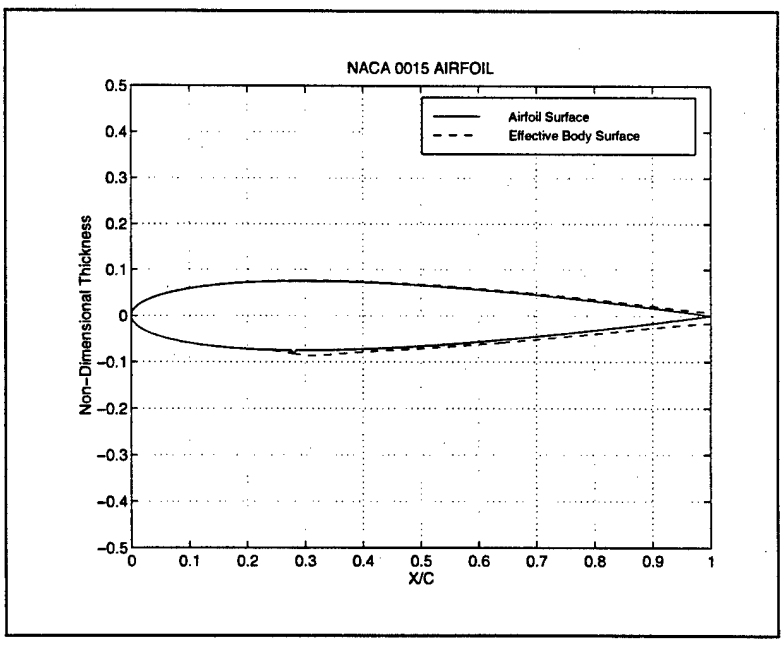

Figure 6-6. Comparison of Effective Body and Airfoil Surfaces for Rough Airfoil

Figure 6-6 compares the resulting effective body surface for an airfoil with a single protuberance versus the airfoil surface. The effect of the protuberance is to increase the displacement thickness along the aft portion of the lower surface. The zoom view in the vicinity of the protuberance depicted in Figure 6-7 shows the sudden increase in the displacement thickness slightly upstream of the protuberance and the increased displacement thickness which persists downstream.

The comparison of the effective body surfaces for a smooth airfoil versus the same for an airfoil with a protuberance in Figure 6-8 isolates the influence of the protuberance. Note that the only apparent change starts near the location of the protuberance and continues downstream. An alternative view for analyzing the effective body is presented in Figure 6-9. In this view, the displacement thickness is increased by a factor of five to dramatically show the effect of the protuberance. The addition of a chord line shows that the protuberance created an effective angle-of-attack of 0.25 degrees, based on the true displacement thickness. Using a lift coefficient curve slope of 0.106/degree from the accepted standard for airfoil characteristics,[43] this equates to a positive lift coefficient increment of 0.0265 for this symmetric airfoil at zero degrees angle-of-attack. The addition of an approximate camber line to Figure 6-9 suggests a change in section camber. The integrated area between the camber line and the chord line, based on the enhanced displacement thickness, was calculated to be 0.0013. This positive value suggests an effective positive camber. The primary effect of increased positive camber is a decrease in the zero-lift angle of attack which results in increased lift at a constant angle-of-attack. The combination of the effective increase in airfoil angle-of-attack and the additional

lift from an effective increase in section camber might sufficiently describe the computationally measured positive lift coefficient increment of 0.0452 for this configuration. Close to the protuberance, Figure 6-8 indicates that the protuberance increases the section thickness of the airfoil. This finding for the airfoil is consistent with the pressure distribution analysis presented in Section 6.3.3 for the wing.

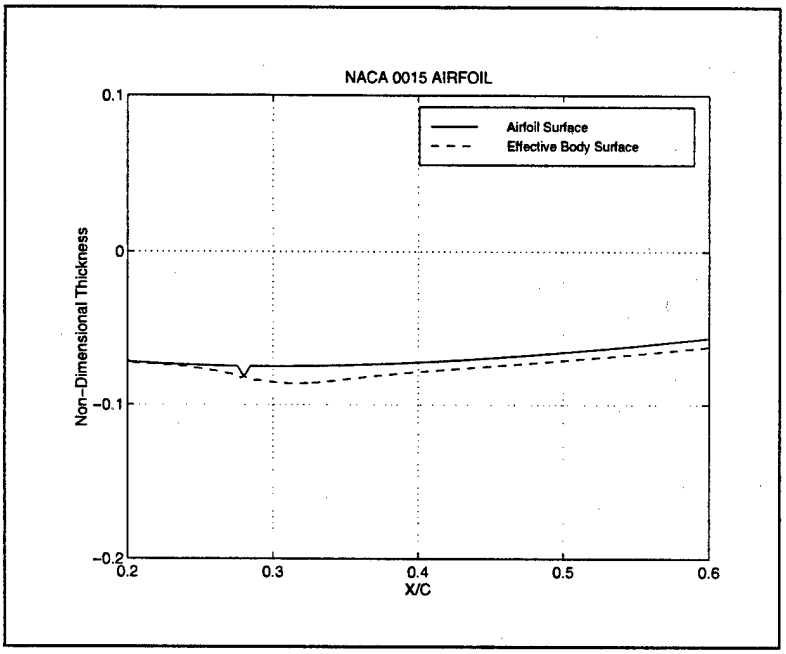

Figure 6-7. Zoom View of Effective Body and Airfoil Surfaces Comparison

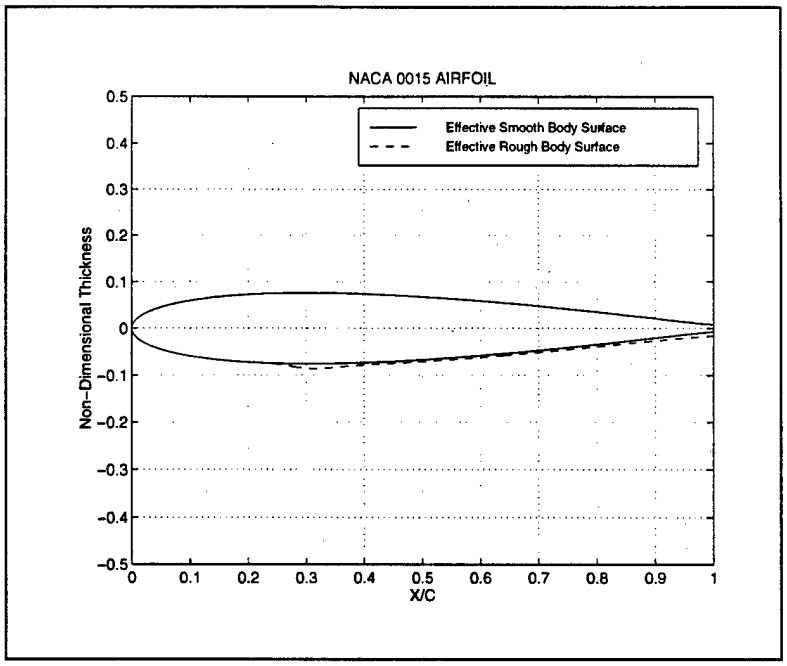

Figure 6-8. Comparison of Smooth and Rough Airfoil Effective Body Surfaces

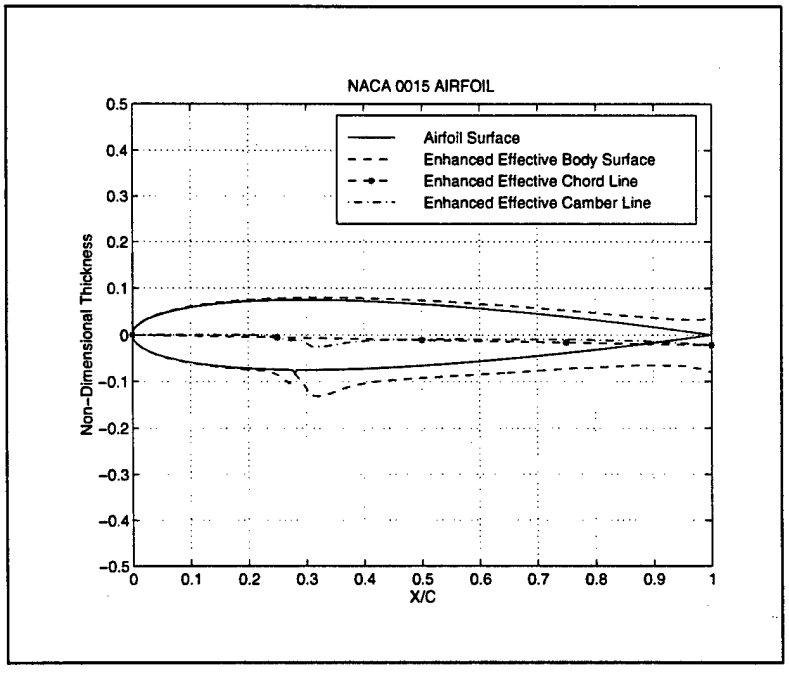

Figure 6-9. Effective Body Surface with Enhanced ($5x\delta_1$) Displacement Thickness

To assess the validity of the proposed prediction method, a computational experiment was conducted on the effective body using OVERFLOW. By using OVERLOW as an Euler solver, an inviscid solution could be generated which would closely approximate a potential flow solution. The blunt trailing edge of the effective body had to be changed to eliminate the possibility of a recirculation region in an Euler solution which would not be expected in a potential flow solution. The blunt trailing edge was smoothed and closed by extending the upper and lower surfaces starting at approximately 0.95c and using the general slope on the aft portion of the respective surface. Figure 6-10 shows the effect of the tapering in creating the Euler body in comparison to the effective body. Based on the limits established by the effective body, the surface integration of the Euler solution calculated a lift coefficient of 0.0303 and the corresponding effective angle-of-attack of approximately 0.3 degrees. These results compare favorably with the RANS calculated lift coefficient of 0.0452 and the effective angle-of-attack of approximately 0.5 degrees. Figure 6-11 compares the pressure distributions of the rough airfoil calculated from a RANS solution with that of the effective body calculated from the Euler solution. The pressure distributions show good overall agreement. While the characteristic shape of the pressure signature remained, the magnitude of the pressure variation about the protuberance was not captured by the effective body solution. In addition, the distributions near the trailing edge did not match. These discrepancies are most likely attributable to the challenges of adequately determining the displacement thickness near the protuberance and of modeling the blunt trailing edge of the effective body.

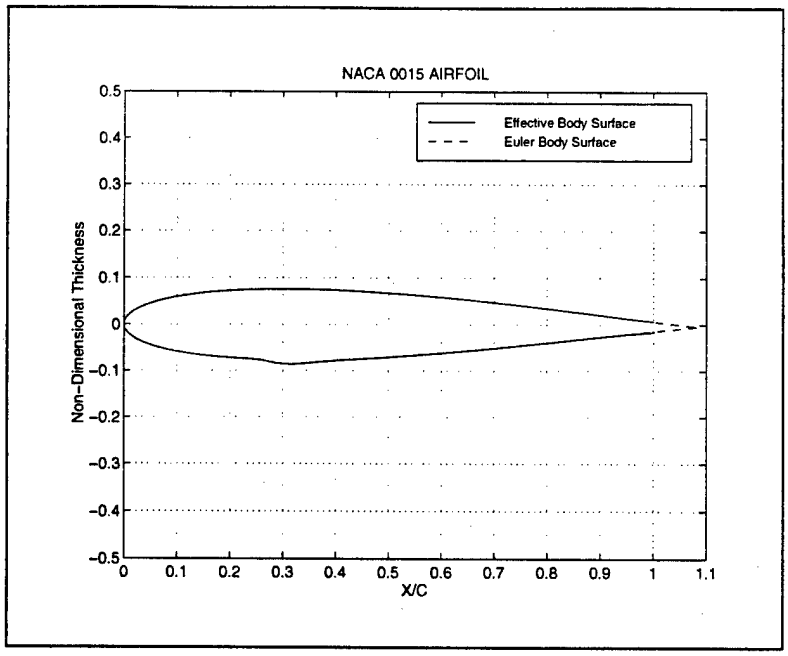

Figure 6-10. Comparison of Effective Body and Euler Body Surfaces

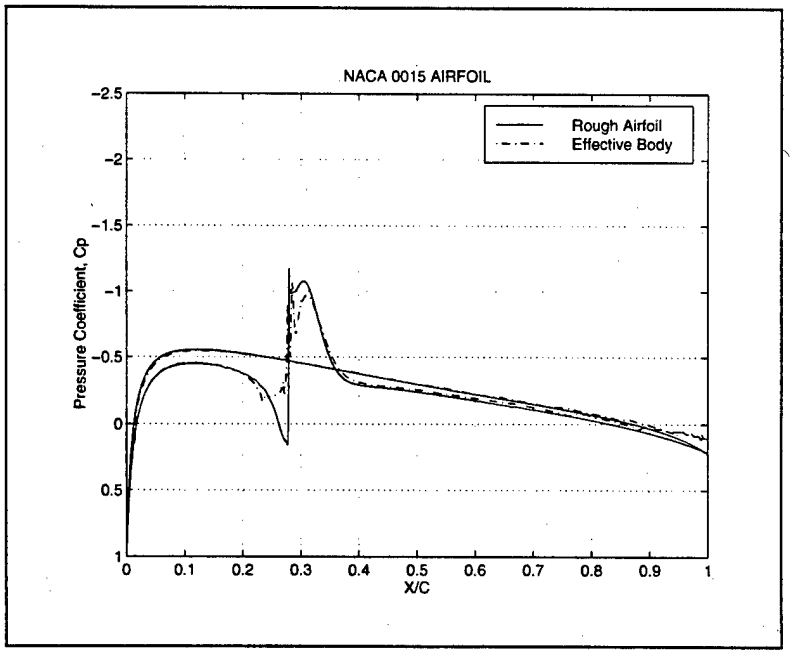

Figure 6-11. Rough Airfoil and Effective Body Pressure Distribution (α=0^o)

In summary, this section detailed a potential means to describe the lift enhancement due to surface roughness based on the effective change in section camber.

6.3.3 AIRFOIL THICKNESS

An analysis was performed to isolate and study the separate effect of airfoil thickness as distinct from that of camber. From the ratio of local velocity to freestream velocity given by Abbott and von Doenhoff [6] for symmetric, basic thickness forms, pressure coefficients for an airfoil at zero degrees angle-of-attack can be calculated using the incompressible relation:[47]

$$C_p = 1 - (u/U_\infty)^2 \tag{6.2}$$

Figure 6-12 shows the difference in the incompressible pressure coefficient at zero degrees angle-of-attack for the NACA 0015 and NACA 0018 sections. Note that the major difference is the overall decrease in the pressure with increasing thickness. The same overall decrease in pressure around the body is seen in the experimental pressure distribution shown in Figure 3-22 for a wing with surface protuberances at zero degrees angle-of-attack. Based on the airfoil effective body results in Section 6.3.2 and assuming equivalence between these results and a similar analysis for a wing with protuberances, the effective thickness of the wing would be 16.1%, a 1.1% increase. From the results shown in Figure 3-22, the pressure coefficient for the upper surface decreased 0.1 at chord position 0.37c between the smooth and rough wings. The pressure decrease was 0.11 at chord position 0.3c and 0.08 at chord position 0.4c

when the thickness increased 3%, from 15% to 18%, based on the airfoil results shown in Figure 6-12. Based on these results, the calculated increase in effective thickness provides only a first order approximation of the shift in the experimental pressure distribution for a wing with surface protuberances.

In addition, Jacobs, Ward, and Pinkerton [42] showed that the maximum lift-to-drag ratio of an airfoil is a function of thickness and is independent of section camber. As the thickness of an airfoil section increases, the maximum lift-to-drag ratio decreases. This result matches the decreased lift-to-drag ratio measured for all configurations with protuberances in this study with the single exception of the wavy wing.

In summary, these combined observations suggest that one result of surface protuberances is an effective increase in the section thickness.

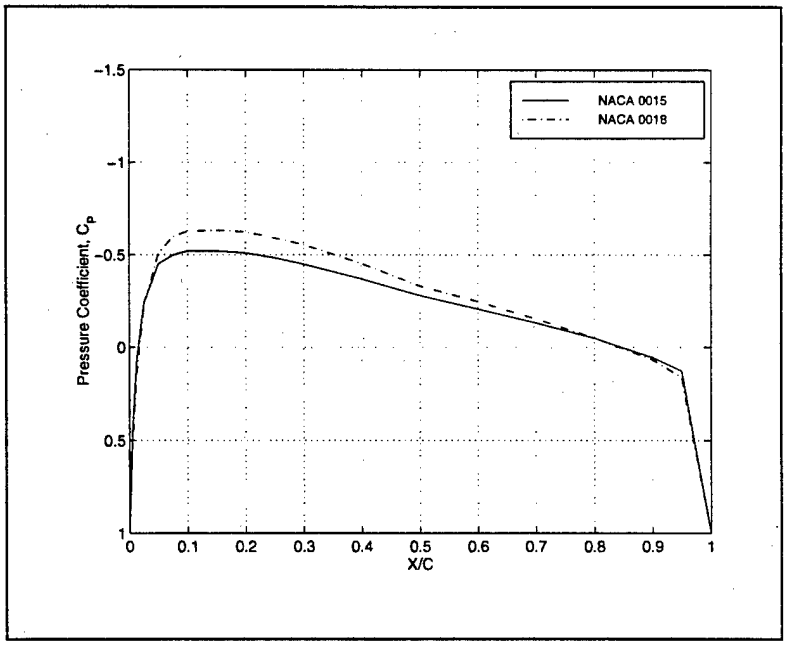

Figure 6-12. Incompressible Pressure Coefficient as a Function of Airfoil Thickness

6.4 SYNOPSIS

The phenomenological basis for the lift enhancement due to surface roughness on a symmetric airfoil is the altered pressure field caused by the presence of the two-dimensional protuberance. Specifically, the pressure variation in the immediate vicinity of the protuberance changed due to the region of recirculating flow downstream of the protuberance. From the perspective of fundamental properties, the recirculation region aft of the protuberance creates a high pressure region along the lower surface which increases the lift generated by the airfoil and increases the drag due to the pressure drag component. In combination, the drag increase dominates and the lift-to-drag ratio decreases in comparison to the smooth body. The recirculation region also induces an overall pressure variation. It is surmised, but not explicitly proven that a similar structure develops around three-dimensional protuberances.

An alternative explanation of this phenomena based on effective changes in section camber and thickness was first considered after the wind tunnel experiments and was detailed in Section 3.3.3. This concept has been shown to be a first order approximation of the measured lift and lift-to-drag ratio changes. This analysis used the effective body surface defined by the calculated displacement thickness to show an increased in effective camber and thickness for the airfoil experiments of the computational testing. An analysis of the pressure distribution of the wing also indicated an increase in the effective section thickness.

The effect of the protuberances can be distinguished as two separate mechanisms. Lift production can be viewed as a global effect evidenced by changes in effective section camber and thickness. In contrast, drag can be seen as a local viscous

effect over the surface of the protuberance itself primarily achieved through pressure effects.

One configuration, the wavy wing, did achieve the lift-to-drag ratio increased reported by the Russian researchers. This configuration was a three-dimensional body combined with a three-dimensional protuberance. This could be an important finding which might influence the protuberance geometry and the integrated configuration of any future research efforts. It is also important to note that only one configuration achieved a lift-to-drag ratio increase and that finding could shift future research efforts away from pursuing lift-to-drag ratio improvements and instead focus on the lift enhancement potential.

CHAPTER 7 CONCLUSION

A low-speed investigation of the aerodynamic effect of surface roughness in the form of protuberances was conducted at a freestream Reynolds number of 1.5 million. The primary parameters studied were lift, drag, lift-to-drag ratio, and pressure. The study was comprised of an experimental investigation of two- and three-dimensional protuberances on an airfoil, an experimental investigation of three-dimensional protuberances on a wing, and a computational investigation of two-dimensional protuberances on an airfoil.

7.1 OBSERVATIONS

During the conduct of this research, the following observations were made about the approach and the project:

1. OVERFLOW was an effective, powerful tool for examining the subject problem. Combined with complementary, integrated software tools, such as Chimera Grid Tools, HYPGEN, and FOMOCO Utilities, this suite of programs created an environment where the researcher could focus on the aerodynamics of the problem and not be distracted by software integration issues.
2. The ability to combine experimental work with computational simulations can greatly enhance the overall research experience for the

researcher. This breadth can also improve the quality of the work. This project provided such an opportunity.

3. The original interest in this project was generated by the apparent contradiction of Vorobiev's experimental results with accepted, aerodynamic predictions for surface roughness. Such work, while sometimes ending with negative conclusions, certainly sparks and maintains the motivation of the researcher.

7.2 CONCLUSIONS

Based on the results of this research and the analysis presented, the following conclusions were formed:

1. The variation of the aerodynamic lift and the lift-to-drag ratio for symmetric airfoils and wings populated with surface protuberances along the lower surface is based on the variation of the pressure field. As demonstrated for an airfoil, the presence of the protuberance creates a recirculation region downstream of the protuberance. This region increases the local pressure along the lower surface resulting in increased lift and increased pressure drag. Though not conclusively demonstrated, a similar phenomenological explanation is expected for a wing populated with surface protuberances.
2. An equivalent understanding of the change in aerodynamic lift and the lift-to-drag ratio based on an increased effective thickness and camber induced by the presence of surface protuberances on an airfoil has been

demonstrated. Though not conclusively proven, a similar relationship is expected for a wing similarly populated with surface protuberances.

3. The results of this research did not validate results reported by Vorobiev. The configurations tested achieved a positive lift increment for a symmetric airfoil, including lift at zero degrees angle-of-attack, but did not produce an increased lift-to-drag ratio.
4. If an increased lift-to-drag ratio is to be achieved, the results of this effort suggest a very strong dependence on protuberance geometry, or a high degree of sensitivity to flow conditions, or both.
5. The effect of a surface protuberance can be viewed as a global effect causing increased lift through variations of effective camber and thickness, and as a local effect causing increased drag through the pressure variations near the protuberance due to viscous induced flow separation.
6. Surface protuberances located on the lower surface of a symmetric airfoil and wing are a lift generating mechanism at low to moderate angles-of-attack. The application of this finding is most appropriate where increased lift is required for short time increments or conditions where significant drag increases are acceptable. The magnitude of the lift increase is strongly dependent on angle-of-attack and protuberance height. There is weak or no dependence on protuberance width and protuberance location. There is apparent, but inconclusive evidence,

that the magnitude of the lift improvement is dependent on protuberance coverage and density.

7. The comparable changes in the measured lift and drag force results and the common flow structure observed in the visualization of the velocity vector field for an airfoil with a single protuberance strengthens the similarity comparison between surface protuberances and an array of zero-mass jets. This suggests a potential common phenomenological basis for both effects.

7.3 RECOMMENDATIONS FOR FUTURE STUDY

The next recommended step in pursuing this research should be a computational study of a three-dimensional surface protuberance on a three-dimensional body. Although often limited in scope due to time and computational considerations, a well-planned test matrix would generate sufficient data for comparison with the existing experimental and computational results. Subsequent paragraphs identify potential paths to be pursued.

The thrust of any future work should further study the effects of protuberance shape and size. The results of the current research suggest that the desired shape and size must reduce the pressure drag while still generating a positive lift increment. A key difference between the present work and that of Vorobiev was the protuberance shapes used in this research and the irregular, cusp-edged shape studied by Vorobiev. The results of this research and a review of Vorobiev's results suggests that the cusp-edged protuberance shape might be critical in controlling the vortical structures of

three-dimensional flow and result in the desired lower pressure drag. Future work should focus specifically on this protuberance shape. Given that the present work did not find an optimum protuberance geometry, the elusive lift-to-drag ratio improvement and even larger lift increments might be achieved should such a configuration be identified.

One area of focus should be the study of the pressure distribution, both along a chordwise line lying along the body surface and along a chordwise line which continues over a protuberance. This area is important because the current results appear to vary depending on two- versus three-dimensional conditions.

The final element of the study should center on protuberance distribution. The results to date appear conflicting for protuberance coverage and density. However, the potential strong effect of these parameters on increased lift and the lift-to-drag ratio suggests that future studies of these factors could be very useful in maximizing the desired aerodynamic effects.

7.4 FINAL THOUGHTS

While not validating the experimental results of Vorobiev by not measuring an increased lift-to-drag ratio, this research effort succeeded in determining a phenomenological understanding of the surface roughness related lift enhancement for a symmetrical airfoil and wing. In addition, the identified change in effective camber and thickness reported provides a physical understanding of this phenomena and suggests at least a qualitative predictive capability.

REFERENCES

1. Vorobiev, N.N., "Appearance of a Transverse Force During Flow Along a Rough Surface," Soviet Physics -- Doklady, Volume 36, Number 5, pp.373-375, 1991.

2. Written Communication, Nikolai Vorobiev, January 1995.

3. Personal Communication, Nikolai Vorobiev, December 1997.

4. Warner, Edward P., Airplane Design Aerodynamics, McGraw-Hill Book Company, Inc., 1927.

5. Wood, D.H., "Tests of Large Airfoils in the Propeller Research Tunnel, Including Two with Corrugated Surfaces," NACA Technical Report Number 336, 1927.

6. Abbott, I.H. and von Doenhoff, A.E., Theory of Wing Sections, Dover Publications, Inc., New York, 1959.

7. Jacobs, E.N., "Airfoil Section Characteristics as Affected by Protuberances," NACA Technical Report Number 446, 1932.

8. Schlichting, H., Boundary-Layer Theory, Seventh Edition, McGraw-Hill, Inc., New York, 1979.

9. Kerho, M.F., and Bragg, M.B, "Airfoil Boundary-Layer Development and Transition with Large Leading-Edge Roughness," AIAA Journal, Volume 35, Number 1, January 1997.

10. Klebanoff, P.S., Schubauer, G.B., and Tidstrom, K.D., "Measurements of the Effect of Two-Dimensional and Three-Dimensional Roughness Elements on Boundary-Layer Transition," Journal of the Aeronautical Sciences, Volume 22, Number 11, 1955.

11. Smith, A.M.O., and Clutter, D.W., "The Smallest Height of Roughness Capable of Affecting Boundary-Layer Transition," Journal of the Aerospace Sciences, Volume 26, Number 4, 1959.

12. Hood, M.J., "The Effects of Surface Waviness and of Rib Stitching on Wing Drag," NACA Technical Note Number 724, 1939.

13. Gulick, B.G., "Effects of a Simulated Ice Formation on the Aerodynamic Characteristics of an Airfoil," NACA Wartime Report L-292, May 1938.

14. Bragg, M.B., Gregorek, G.M., and Lee, J.D., "Airfoil Aerodynamics in Icing Conditions," Journal of Aircraft, Volume 23, Number 1, January 1986.

15. Hassan, AA., and R.D. JanakiRam, "Effects of Zero-Mass 'Synthetic' Jets on the Aerodynamics of the NACA-0012 Airfoil," AIAA Paper 97-2326, June 1997.

16. Hassan, A.A., "Numerical Simulations and Potential Applications of Zero-Mass Jets for Enhanced Rotorcraft Aerodynamic Performance," AIAA Paper 98-0211, January 1998.

17. Ranzenbach, R., and M.T. Beierle, and J.D. Anderson, Jr., "Roughness Related Lift Enhancement to Symmetric Airfoils," AIAA Paper 97-2237, June 1997.

18. Amity, M., Smith, B.L., and Glezer, A., "Aerodynamic Flow Control Using Synthetic Jet Technology," AIAA Paper 98-0208, January 1998.

19. Bragg, M.M, and Gregorek, G.M., "Experimental Study of Airfoil Performance with Vortex Generators," Journal of Aircraft, Volume 24, Number 5, pp. 305-309, May 1987.

20. Vinokur, M., "On One-Dimensional Stretching Functions for Finite-Difference Calculations," Journal of Computational Physics, Volume 50, Number 2, pp. 215-234, May 1983.

21. Ranzenbach, R.C., "Adaptive Gridding Using the Analytic Source Technique," Ph.D. Dissertation, UM-AERO-95-10, University of Maryland, 1995.

22. Masad, J.A., and Iyer, V., "Transition Prediction and Control in Subsonic Flow Over a Hump," Physics of Fluids, Volume 6, Number 1, pp. 313-327, January 1994.

23. Chan, W.M., Rogers, S.E., Nash, S.M., and Buning, P.G., "User's Manual for Chimera Grid Tools," Version 0.3 (Under Construction), December 1997.

24. Chan, W.M., Buning, P.G., and Krist, S.E., "User's Guide for PROGRD," Version 0.4e (In Development), August 1996.

25. Chan, W.M, and Steger, J.L., "Enhancements of a Three-Dimensional Hyperbolic Grid Generation Scheme," Applied Mathematics and Computation, Volume 51, pp. 181-205, 1992.

26. Hoffman, K.A., Computational Fluid Dynamics for Engineers, Engineering Education System, Austin, Texas, 1989.

27. Chan, W.M., Chiu, I.-T., and Buning, P.G., "User's Manual for HYPGEN Hyperbolic Grid Generator and the HGUI Graphical User Interface," NASA TM-108791, October 1993.

28. Buning, P.G., Jespersen, D.C., Pulliam, T.H., Chan, W.M., Slotnick, J.P., Krist, S.E., and Renze, K.J., "OVERFLOW User's Manual," Version 1.7v, June 1997.

29. Chan, W.M., "User Notes for the Program BOXGR (Version 2.0)", October 1997.

30. Suhs, N.E., and Tramel, R.W., "PEGSUS 4.0 User's Manual," AEDC-TR-91-8, Arnold Engineering and Development Center, Arnold AFB, TN, November 1991.

31. Wilcox, D.C., Turbulence Modeling for CFD, DCW Industries, Inc., La Canada, California, 1994.

32. Pulliam, T.H., and Steger, J.L., "Implicit Finite-Difference Simulations of Three-Dimensional Compressible Flow," AIAA Journal, Volume 18, Number 2, February 1980.

33. Personal Communication, Pieter Buning, May 1998.

34. Spalart, P.R., and Allmaras, S.R., "A One-Equation Turbulence Model for Aerodynamic Flows," AIAA Paper 92-0439, January 1992.

35. Beam, R.M., and Warming, R.F., "An Implicit Finite-Difference Algorithm for Hyperbolic Systems in Conservation-Law Form," Journal of Computational Physics, Volume 22, pp. 87-110, September 1976.

36. Beam, R.M., and Warming, R.F., "An Implicit Factored Scheme for the Compressible Navier-Stokes Equations," AIAA Journal, Volume 16, Number 4, April 1978.

37. Steger, J.L., "Implicit Finite-Difference Simulation of Flow about Arbitrary Two-Dimensional Geometries," AIAA Journal, Volume 16, Number 7, July 1978.

38. Pulliam, T.H., "Notes on Solutions Methods in Computational Fluid Dynamics," NASA Ames Research Center, Moffett Field, California, April 1994.

39. Jespersen, D., Pulliam, T., and Buning, P., "Recent Enhancements to OVERFLOW," AIAA Paper 97-0644, January 1997.

40. Chan, W.M, and Buning, P.G., "User's Manual for FOMOCO Utilities -- Force and Moment Computation Tools for Overset Grids," NASA TM-110408, July 1996.

41. Walatka, P.P., Buning, P.G., Pierce, L., and Elson, P.A., "PLOT3D User's Manual," NASA TM-101067, March 1990.

42. Jacobs, E.N., Ward, K.E., and Pinkerton, R.M., "The Characteristics of 78 Related Airfoil Sections from Tests in the Variable-Density Wind Tunnel," NACA Technical Report No. 460, 1932.

43. Abbott, I.H., von Doenhoff, A.E., and Stivers, L.S., "Summary of Airfoil Data," NACA Technical Report No. 824, 1945.

44. Personal Communication, Dennis Bushnell, July 1998.

45. Baldwin, B.S., and Barth, T.J., "A One-Equation Turbulence Transport Model for High Reynolds Number Wall-Bounded Flows," NASA TM-102847, August 1990.

46. Personal Communication, Ahmed Hassan, August 1998.

47. Anderson, J.D., Fundamentals of Aerodynamics, Second Edition, McGraw-Hill, Inc., New York, 1991.

DTIC QUALITY INSPECTED 4